

**ALMA MATER STUDIORUM  
UNIVERSITÀ DI BOLOGNA**

---

**DIPARTIMENTO DI INGEGNERIA CIVILE, CHIMICA,  
AMBIENTALE E DEI MATERIALI**

*CORSO DI LAUREA*

*In*

*CIVIL ENGINEERING*

**TESI DI LAUREA**

*In*

**ADVANCED HYDROSYSTEMS ENGINEERING**

# **MICRO HYDROPOWER IN WATER DISTRIBUTION SYSTEMS**

**CANDIDATO:**  
Mohammad Mashkour

**RELATORE:**  
Prof. Cristiana Bragalli

**CORRELATORE:**  
Prof. Andrea Bolognesi

Anno Accademico 2017/2018

Session III



To my Parents

I am so much of what I  
learned from you. You will  
be with me like a handprint  
on my heart

## To my Wife

Above all I would like to thank my wife, Mirjam Kay, for her love and constant support, for all the late nights and early mornings, and for keeping me sane over the past few months. Thank you for being my muse, editor, proofreader, and sounding board. But most of all, thank you for being my best friend. I owe you everything.

To Professor

CRISTIANA BRAGALLI

I would like to thank Professor  
Cristiana Bragalli for her precious  
teachings, for the great availability  
and courtesy always shown to me,  
and for giving me the possibility  
and the means to elaborate this  
Thesis. Words alone can not  
explain the high level of support I  
have been given by you.

“YOU MUST BE THE CHANGE YOU WISH TO SEE IN  
THE WORLD.”

MAHATMA GANDHI

“LA SAPIENZA È FIGLIOLA DELL'ESPERIENZA.”

LEONARDO DA VINCI

“YOU HAVE YOUR WAY, I HAVE MY WAY. AS FOR  
THE RIGHT WAY, THE CORRECT WAY, AND THE  
ONLY WAY, IT DOES NOT EXIST.”

FRIEDRICH WILHELM NIETZSCHE

“INTELLIGENCE IS THE ABILITY TO ADAPT TO  
CHANGE.”

STEPHEN HAWKING



## Contents

Contents .....	1
Introduction.....	5
1 Hydropower Generation in Water Supply/Distribution Systems.....	7
1.1 Introduction.....	7
1.2 Hydroelectric Power .....	7
1.3 Water Turbines.....	8
1.4 Definitions.....	9
1.4.1 Water pressure.....	9
1.4.2 Excess pressure .....	9
1.4.3 Pressure reducing valves.....	10
1.4.4 Residual pressure .....	10
1.4.5 water turbine .....	10
1.4.6 Cavitation.....	11
1.5 Traditional turbines.....	11
1.5.1 Impulse Turbine .....	11
1.5.1.1 Water wheel.....	11
1.5.1.2 Reverse overshot water-wheel .....	12
1.5.1.3 Pelton .....	13
1.5.1.4 Turgo.....	13
1.5.1.5 Cross-Flow .....	14
1.5.1.6 Jonval .....	14
1.5.1.7 Screw.....	15
1.5.2 Reaction Turbine.....	16
1.5.2.1 Propeller.....	16



1.5.2.2	Francis (radial or mixed flow) .....	17
1.6	Applications and performances.....	18
1.6.1	Wicket gates (or guide vanes).....	18
1.6.2	Runner.....	18
1.6.3	Draft tube .....	18
1.6.4	Power and efficiencies: .....	19
1.7	Design of a Francis Turbine.....	20
1.7.1	Spiral Casing.....	21
1.7.2	Guide or stay vane.....	21
1.7.3	Draft Tube.....	22
1.7.4	Runner of the Francis turbine.....	25
2	Characteristics of Centrifugal Pumps working in direct or reverse Mode.....	30
2.1	Centrifugal Pumps Working Principle.....	30
2.2	Centrifugal Pumps Design .....	32
2.2.1	System analysis for pump selection .....	32
2.2.2	Differential Head required .....	32
2.2.3	NPSHA .....	33
2.2.4	Shape of Head Capacity Curve .....	33
2.2.5	Pump Speed .....	35
2.2.6	Liquid Characteristics .....	35
2.2.7	General Pump Design .....	35
2.3	Energy efficiency optimization in water distribution systems.....	39
2.3.1	Introduction.....	39
2.3.2	Energy Efficiency Indicator for water networks.....	40
3	Micro-Hydro Generators using Pump as Turbine.....	43
3.1	Introduction to Micro-Hydro Generators.....	43
3.2	PATs (Pump as Turbine).....	46

3.3	PATs working principle .....	46
3.4	PAT Applications.....	49
3.5	Components of PATs.....	49
3.5.1	The Volute .....	50
3.5.2	The Impeller.....	51
3.5.3	The Draft Tube.....	51
3.6	A state-of-the-art review on PAT.....	52
3.6.1	Pump-turbine selection .....	54
3.6.2	Pump-turbine performance prediction .....	57
3.6.3	Pump-turbines stability aspects.....	68
4	Selection of PATs .....	74
4.1	Methodology .....	74
4.2	Estimation of Characteristic Curves .....	80
4.3	Performance, Stability and suitable Machinery .....	85
4.3.1	Introduction.....	85
4.3.2	Model Description.....	86
4.3.3	Calculation of the losses model .....	91
4.3.4	Result .....	94
4.3.5	Conclusion .....	108
4.4	Market Obstacles (Interview).....	109
4.4.1	Interview .....	109
4.4.2	Application-Oriented Planning Documents for Pumps as Turbine by KSB [16] .....	111
5	Review of two PAT case studies.....	124
5.1	Pumps as Turbines substituting pressure reducing valves .....	124
5.1.1	Selection and location of Pumps as Turbines substituting pressure reducing valves .....	124
5.1.2	Pump as turbine modeling.....	125
5.1.3	PAT selection and location procedure .....	128

5.1.4	Results and discussion .....	130
5.1.5	Conclusion .....	138
5.2	Environmental impacts of electricity generation .....	139
5.2.1	Introduction.....	139
5.2.2	Methods.....	140
5.2.3	Results & discussion .....	144
5.2.4	Conclusion .....	146
	Conclusion .....	148
6	References.....	151
7	Tables & Figures.....	164
7.1	Figures.....	164
7.2	Tables.....	167
7.3	Equations.....	169

## Introduction

This thesis is an attempt to illustrate the distribution of micro hydro-power by means of investigations of many case studies. It introduces turbines type and design formulation, stage design of centrifugal pumps and quantification of uncertainties. Subsequently, the State-of-the-Art researches followed by theoretical, experimental and numerical analysis, have been carried out. Profound challenges concerning Pump working as Turbine (PAT), will be presented. The thesis tries to cover a variety of settings concerning PAT, such as design and locating, selection of a PAT, performance prediction and environmental impacts. It suggests new areas for further research to be developed.

The most consequential challenge in micro hydro-power is the selection of an appropriate PAT. It has been a growing area of interest for many researchers. Lack of technical information provided by pump manufacturers for pumps working in reverse mode, in addition to absence of a definitive solution to assign a pump working as turbine are of many reasons to focus on in this study. Cutting-edge researches are going to be reported and reviewed comprehensively in order to obtain a clear illustration of the topic. A numerical model to anticipate the performance of PAT will be propounded. The main inputs of the six Pumps, which can be used in “design mode” and in “geometry known mode”, will be modeled. Furthermore, the loss distribution at BEP in percentages in design mode will be reported and forecasting of their efficiency will be predicted with the Williams ellipse plane. Additionally, an interview followed by the KSB (lead pump and turbine manufacturer based in Germany) documentation will represent an overview of market obstacles, marketing problems, production limitations and complications for end users.

Pressure control is one of the most important issues when it comes to optimizing the operation of networks. It is important to reduce leakage volume and avoid pipeline disruption. This shows why using pressure control reducing valves inside the water distribution network is vital. But the potential energy dissipated in high pressure segments can be regenerated by means of PAT substituting the pressure-reducing valve, which has been broadly presented as a case study in Brazil to discuss the performance of single or multi-stage MHP such as PAT. Three fictitious networks with respect to different scenarios, which have been supported by multi-stage computations, will be reported as well as numerical analysis offering an objective function will be

proposed. A Penalty Function that is to be developed by means of further research, will be introduced, so that more accurate results can be obtained subsequently.

Doubtlessly, green energy production is the main concern of miscellaneous scientific publications. Global warming, acidification potential, abiotic resource depletion, human toxicity and fossil resource depletion, among others, are many arguments to have a review on potential harm of hydro power generation, and the positive performance of PAT off or on grid of water distribution infrastructure in the form of case studies.

# I Hydropower Generation in Water Supply/Distribution Systems

## 1.1 Introduction

Hydroelectric power must be one of the oldest methods of generating power. No doubt, the first thinker human stuck some sturdy leaves on a pole and put it in a moving stream. The water would spin the pole that crushed grain to make their delicious, low-fat prehistoric bran muffins. People have used moving water to help them in their work throughout history, and modern people make great use of moving water to produce electricity [173].

## 1.2 Hydroelectric Power

Hydro-electric power, using the potential energy of rivers, now supplies 17.5% of the world's electricity (2.1% in Africa, 1.7% in Middle east & North Africa, 13.2% in Latin America & The Caribbean, 16.1% in North America, 24.4% in Europe, 6% in South & central Asia, 31.6% East Asia and 4.8% South East Asia & Pacific) [174]. Apart from a few countries with an abundance of it, hydro capacity is normally applied to peak-load demand, because it is so readily stopped and started. It is not a major option for the future in the developed countries because most major sites in these countries having potential for harnessing gravity in this way are either being exploited already or are unavailable for other reasons such as environmental considerations. Until 2030, growth is expected mostly in China and Latin America [175].

Hydro energy is available in many forms, potential energy from high heads of water retained in dams, kinetic energy from current flow in rivers and tidal barrages, and kinetic energy also from the movement of waves on relatively static water masses. Many ingenious ways have been developed for harnessing this energy but most involve directing the water flow through a turbine to generate electricity. Those that don't usually involve using the movement of the water to drive some other form of hydraulic or pneumatic mechanism to perform the same task [175].

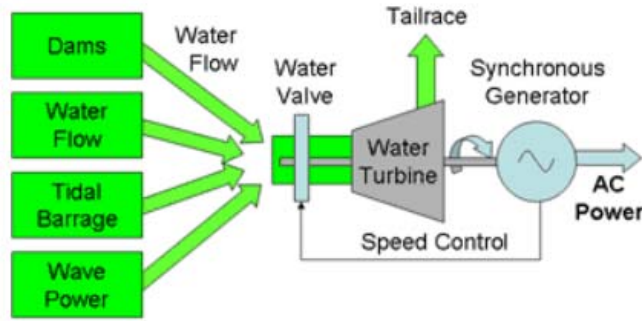


Figure 1-1 Hydro Electric Power Generation[175]

### 1.3 Water Turbines

Like steam turbines, water turbines may depend on the impulse of the working fluid on the turbine blades or the reaction between the working fluid and the blades to turn the turbine shaft which in turn drives the generator. Several different families of turbines have been developed to optimize performance for particular water supply conditions. In general, the turbine converts the kinetic energy of the working fluid, in this case water, into rotational motion of the turbine shaft [175].

Swiss mathematician Leonhard Euler showed in 1754 that the torque on the shaft is equal to the change in angular momentum of the water flow as it is deflected by the turbine blades and the power generated is equal to the torque on the shaft multiplied by the rotational speed of the shaft. See following diagram: [Figure 1-2](#).

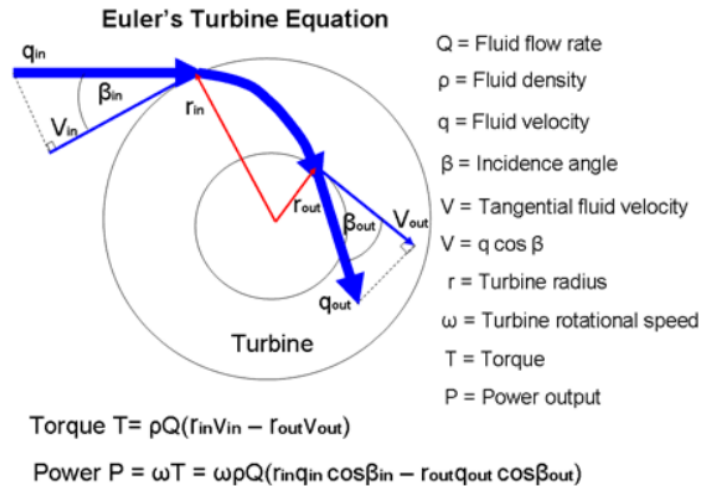


Figure 1-2 Euler Turbine Equation [175]

This result does not depend on the turbine configuration or what happens inside the turbine. All that matters are the change in angular momentum of the fluid between the turbine's input and output[175].

## 1.4 Definitions

### 1.4.1 Water pressure

"Water pressure": the force per unit area exerted by the weight of water. Each 10 meter of sea water exerts a pressure equivalent to one atmosphere, or 14.7 psi.

### 1.4.2 Excess pressure

High water pressure is the major cause of leaks, pipe damage, and wasted water. Symptoms of water pressure induced problems include leaks in multiple fixtures in the home, leaks that only appear intermittently - like at night, and toilets running occasionally without being used. The most common source of excessive water pressure is the municipal water supplier. The water company sets the pressure to meet their own needs, such as delivering water to fire hydrants, high elevation buildings (or tall ones), and for other reasons [176].



### 1.4.3 Pressure reducing valves

There are two types of water pressure reducing valves, direct acting and pilot operated. Both use globe or angle style bodies. Valves used on smaller piping diameter units are cast from brass; larger piping diameter units are made from ductile iron. Direct acting valves, the more popular type of a water pressure reducing valves, consist of globe-type bodies with a spring-loaded, heat-resistant diaphragm connected to the outlet of the valve that acts upon a spring. This spring holds a pre-set tension on the valve seat installed with a pressure equalizing mechanism for precise water pressure control [177].

### 1.4.4 Residual pressure

The pressure available at the fixture or water outlet after allowance is made for pressure drop due to friction loss, head, meter, and other losses in the system during maximum demand periods.

### 1.4.5 water turbine

It is a rotary machine that converts kinetic energy and potential energy of water into mechanical work. Water turbines were developed in the 19th century and were widely used for industrial power prior to electrical grids. Now they are mostly used for electric power generation. Water turbines are often found in dams to generate electric power from water kinetic energy [178]. **Figure 1-3**

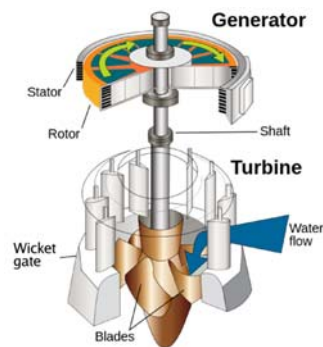


Figure 1-3 Turbine [178]

### 1.4.6 Cavitation

The formation of steam bubbles when the system pressure drops below the vapor pressure of the fluid is called cavitation.

## 1.5 Traditional turbines

There are two main types of hydro turbines: Impulse and Reaction. The type of hydropower turbine selected for a project is based on the height of standing water—referred to as "head"—and the flow, or volume of water, at the site. Other deciding factors include how deep the turbine must be set, efficiency, and cost [179].

### 1.5.1 Impulse Turbine

The impulse turbine generally uses the velocity of the water to move the runner and discharges to atmospheric pressure. The water stream hits each bucket on the runner. There is no suction on the lower side of the turbine, and the water flows out the bottom of the turbine housing after hitting the runner. An impulse turbine is generally suitable for high head, low flow applications [180].

#### 1.5.1.1 Water wheel

A water wheel is a machine for converting the energy of flowing or falling water into useful forms of power, as in a watermill. A water wheel consists of a wheel (usually constructed from wood or metal), with a number of blades or buckets arranged on the outside rim forming the driving surface [181]. Most commonly, the wheel is mounted vertically on a horizontal axle, but can also be mounted horizontally on a vertical shaft, for example the tub or Norse. Vertical wheels can transmit power either through the axle or via a ring gear and typically drive belts or gears; horizontal wheels usually directly drive their load. [Figure 1-4](#).



Figure 1-4 Water wheel

### 1.5.1.2 Reverse overshot water-wheel

Frequently used in mines and probably elsewhere (such as agricultural drainage), the reverse overshot water wheel was a Roman innovation to help remove water from the lowest levels of underground workings. It is described by Vitruvius in his work *De Architectura* published circa 25 BCE. The remains of such systems found in Roman mines by later mining operations show that they were used in sequences so as to lift water a considerable height [182]. [Figure 1-5](#)

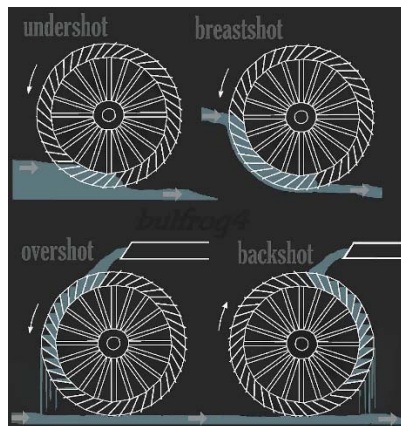


Figure 1-5 Reverse overshot water-wheel

### 1.5.1.3 Pelton

A Pelton wheel has one or more free jets discharging water into an aerated space and impinging on the buckets of a runner. Draft tubes are not required for impulse turbine since the runner must be located above the maximum tail water to permit operation at atmospheric pressure [183]. [Figure 1-6](#)



*Figure 1-6 Pelton [183]*

### 1.5.1.4 Turgo

The Turgo turbine ([Figure 1-7](#)) is an impulse water turbine designed for medium head applications. Operational Turgo Turbines achieve efficiencies of about 87%. In factory and lab tests Turgo Turbines perform with efficiencies of up to 90%. It works with net heads between 15 and 300 m. Developed in 1919 by Gilkes as a modification of the Pelton wheel, the Turgo has some advantages over Francis and Pelton designs for certain applications [184].



*Figure 1-7 Turgo [184]*

### 1.5.1.5 Cross-Flow

A cross-flow turbine (Figure 1-8) is drum-shaped and uses an elongated, rectangular-section nozzle directed against curved vanes on a cylindrically shaped runner. It resembles a "squirrel cage" blower. The cross-flow turbine allows the water to flow through the blades twice. The first pass is when the water flows from the outside of the blades to the inside; the second pass is from the inside back out. A guide vane at the entrance to the turbine directs the flow to a limited portion of the runner. The cross-flow was developed to accommodate larger water flows and lower heads than the Pelton [185].



*Figure 1-8 Cross-Flow[185]*

### 1.5.1.6 Jonval

The Jonval turbine (Figure 1-9) is a water turbine design invented in France in 1843, in which water descends through fixed curved guide vanes which direct the flow sideways onto curved vanes on the runner. It is named after Feu Jonval, who invented it [186].



*Figure 1-9 Jonval [186]*

### 1.5.1.7 Screw

The screw turbine (Figure 1-10) is a water turbine which uses the principle of the Archimedean screw to convert the potential energy of water on an upstream level into work. It may be compared to the water wheel. The turbine consists of a rotor in the shape of an Archimedean screw which rotates in a semicircular trough. Water flows into the turbine and its weight presses down onto the blades of the turbine, which in turn forces the turbine to turn. Water flows freely off the end of the turbine into the river. The upper end of the screw is connected to a generator through a gearbox. [187].



*Figure 1-10 Screw [187]*

## 1.5.2 Reaction Turbine

A reaction turbine develops power from the combined action of pressure and moving water. The runner is placed directly in the water stream flowing over the blades rather than striking each individually. Reaction turbines are generally used for sites with lower head and higher flows than compared with the impulse turbines [188].

### 1.5.2.1 Propeller

A propeller turbine generally has a runner with three to six blades in which the water contacts all of the blades constantly. Picture a boat propeller running in a pipe. Through the pipe, the pressure is constant; if it isn't, the runner would be out of balance. The pitch of the blades may be fixed or adjustable. The major components besides the runner are a scroll case, wicket gates, and a draft tube [188]. There are several different types of propeller turbines:

#### 1.5.2.1.1 *Bulb turbine*

The turbine and generator are a sealed unit placed directly in the water stream. [Figure 1-11](#)



*Figure 1-11 Bulb turbine*

#### 1.5.2.1.2 *Straflo*

The generator is attached directly to the perimeter of the turbine. [Figure 1-12](#)

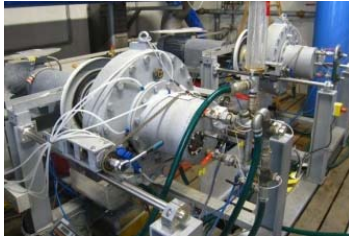


Figure 1-12 Straflo

### 1.5.2.1.3 Tube turbine

The penstock bends just before or after the runner, allowing a straight-line connection to the generator. [Figure 1-13](#)



Figure 1-13 Tube turbine

### 1.5.2.1.4 Kaplan

Both the blades and the wicket gates are adjustable, allowing for a wider range of operation. [Figure 1-14](#)



Figure 1-14 Kaplan

### 1.5.2.2 Francis (radial or mixed flow)

A Francis turbine has a runner with fixed buckets (vanes), usually nine or more. Water is introduced just above the runner and all around it and then falls through, causing it to spin. Besides



the runner, the other major components are the scroll case, wicket gates, and draft tube [189].

Figure 1-15



Figure 1-15 Francis Turbine

## 1.6 Applications and performances

Applications and performances of widely used turbines among both groups of above, impulse and reaction turbines, Francis Turbine (reaction turbine) will be shown as follows. Here are the constitutive elements:

### 1.6.1 Wicket gates (or guide vanes)

Vanes that guide water onto the runner, with appropriate velocity and direction [190].

### 1.6.2 Runner

Connected to the rotating shaft, it extracts energy from the water flow that interacts with its blades [190].

### 1.6.3 Draft tube

If water's kinetic energy is still relatively high at the runner's exit, a draft tube is used to recover part of this kinetic energy [190]. Figure 1-16

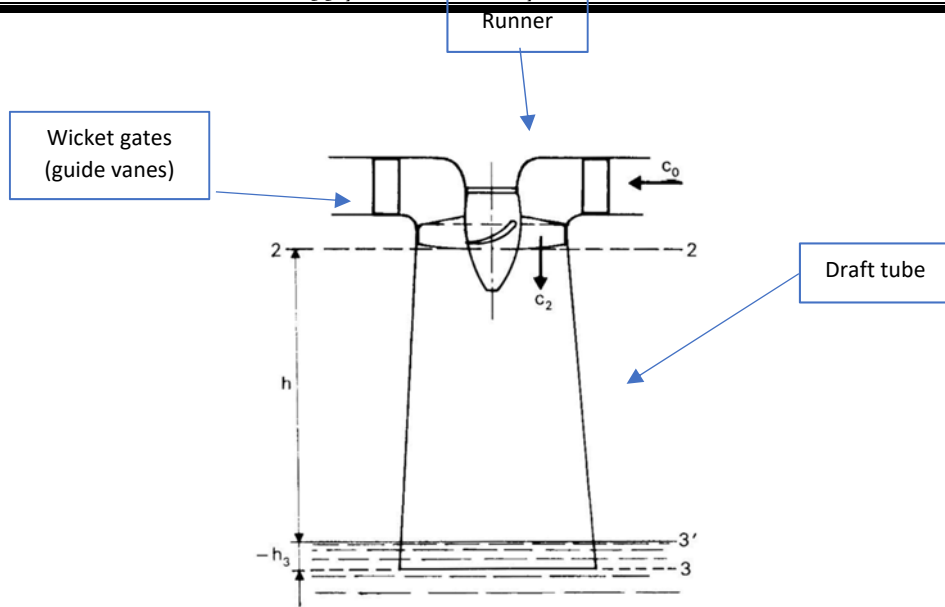


Figure 1-16 Draft Tube [190]

### 1.6.4 Power and efficiencies:

Hydraulic efficiency [190]:

Equation 1-1

$$\eta_h = \frac{\text{Power developed by the runner}}{\text{Power available at the inlet}}$$

Mechanical Efficiency [191]:

Equation 1-2

$$\eta_m = \frac{\text{Power at the shaft of the turbine}}{\text{Power developed by the runner}}$$

Volumetric efficiency [191]:

Equation 1-3

$$\eta_v = \frac{\text{Volume of water striking the bucket}}{\text{Volume of water supplied to the turbine}}$$

Overall turbine efficiency [191]:

$$\eta_t = \eta_h \eta_m \eta_v$$

Equation 1-4

## 1.7 Design of a Francis Turbine

The principal feature of a reaction turbine that distinguishes it from an impulse turbine is that only a part of the total head available at the inlet to the turbine is converted to velocity head, before the runner is reached. Also, in the reaction turbines the working fluid, instead of engaging only one or two blades, completely fills the passages in the runner. The pressure or static head of the fluid changes gradually as it passes through the runner along with the change in its kinetic energy based on absolute velocity due to the impulse action between the fluid and the runner. Therefore, the cross-sectional area of flow through the passages of the fluid. A reaction turbine is usually well suited for low heads. A radial flow hydraulic turbine of reaction type was first developed by an American Engineer, James B. Francis (1815-92) and is named after him as the Francis turbine [192]. The schematic diagram of a Francis turbine is shown in [Figure 1-17](#):

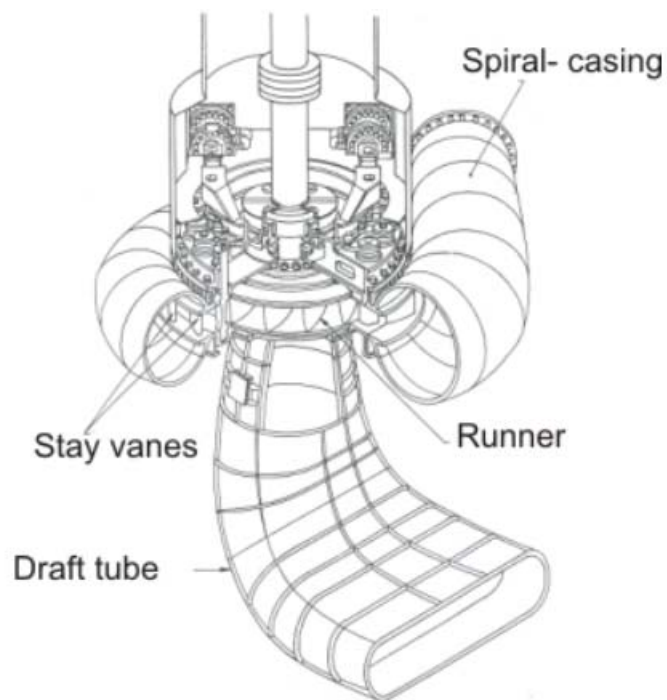


*Figure 1-17 A Francis turbine [192]*

A Francis turbine comprises mainly of four components:

- I. Spiral casing,
- II. Guide on stay vanes,
- III. Runner blades,
- IV. Draft-tube

### 1.7.1 Spiral Casing

Most of these machines have vertical shafts although some smaller machines of this type have horizontal shafts. The fluid enters from the penstock (pipeline leading to the turbine from the reservoir at high altitude) to a spiral casing which completely surrounds the runner. This casing is known as scroll casing or volute. The cross-sectional area of this casing decreases uniformly along the circumference to keep the fluid velocity constant in magnitude along its path towards the guide vane [192].

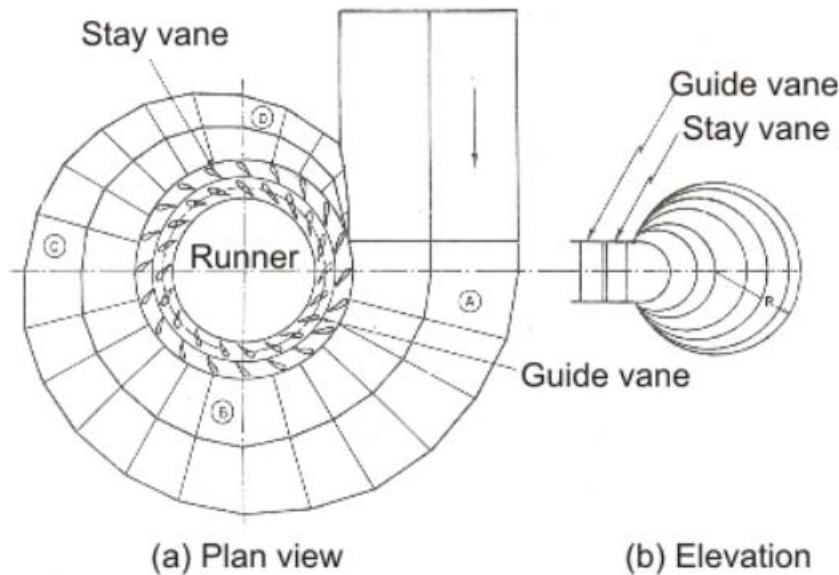


Figure 1-18 Spiral Casing [192]

### 1.7.2 Guide or stay vane

The basic purpose of the guide vanes or stay vanes is to convert a part of pressure energy of the fluid at its entrance to the kinetic energy and then to direct the fluid on to the runner blades at the angle appropriate for the design. Moreover, the guide vanes are pivoted and can be turned by a suitable governing mechanism to regulate the flow while the load changes. The guide vanes are also known as wicket gates. The guide vanes impart a tangential velocity and hence an angular

momentum to the water before its entry to the runner. The flow in the runner of a Francis turbine is not purely radial but a combination of radial and tangential. The flow is inward, i.e. from the periphery towards the center. The height of the runner depends on the specific speed. The height increases with the increases in the specific speed. The main direction of flow changes as water passes through the runner and is finally turned into the axial direction while entering the draft tube [192].



Figure 1-19 Guide vane

### 1.7.3 Draft Tube

The draft tube is a conduit which connects the runner exit to the tail race where the water is being finally discharged from the turbine. The primary function of the draft tube is to reduce the velocity of the discharged water to minimize the loss of kinetic energy at the outlet. This permits the turbine to be set above the tail water without any appreciable drop of available head. A clear understanding of the function of the draft tube in any reaction turbine, in fact, is very important for the purpose of its design. The purpose of providing a draft tube will be better understood if we carefully study the net available head across a reaction turbine [192].



Figure 1-20 Draft tube



Figure 1-21 Complete Assembly (Without draft tube)



Figure 1-22 Spiral casing

The effective head across any turbine is the difference between the head at inlet to the machine and the head at outlet from it. A reaction turbine always runs completely filled with the working fluid. The tube that connects the end of the runner to the tail race is known as a draft tube and should completely be filled with the working fluid flowing through it. The kinetic energy of the fluid finally discharged into the tail race is wasted. A draft tube is made divergent so as to reduce the velocity at outlet to a minimum. Therefore, a draft tube is basically a diffuser and should be designed properly with the angle between the walls of the tube to be limited to about 8 degree so as to prevent the flow separation from the wall and to reduce accordingly the loss of energy in the tube. Figure 1-23 shows a flow diagram from the reservoir via a reaction turbine to the tail race [192].

The total head  $H_1$  at the entrance to the turbine can be found out by applying the Bernoulli's equation between the free surface of the reservoir and the inlet to the turbine as:

$$H_0 = \frac{P_1}{\rho g} + \frac{V_1^2}{2g} + z + h_f$$
$$\text{Or } H_1 = H_0 - h_f = \frac{P_1}{\rho g} + \frac{V_1^2}{2g} + z$$

Equation 1-5

Where:

$h_f$  = the head loss due to friction in the pipeline connecting the reservoir and the turbine.

Since the draft tube is a part of the turbine, the net head across the turbine, for the conversion of mechanical work, is the difference of total head at inlet to the machine and the total head at discharge from the draft tube at tail race and is shown as  $H$  in Figure 1-23:

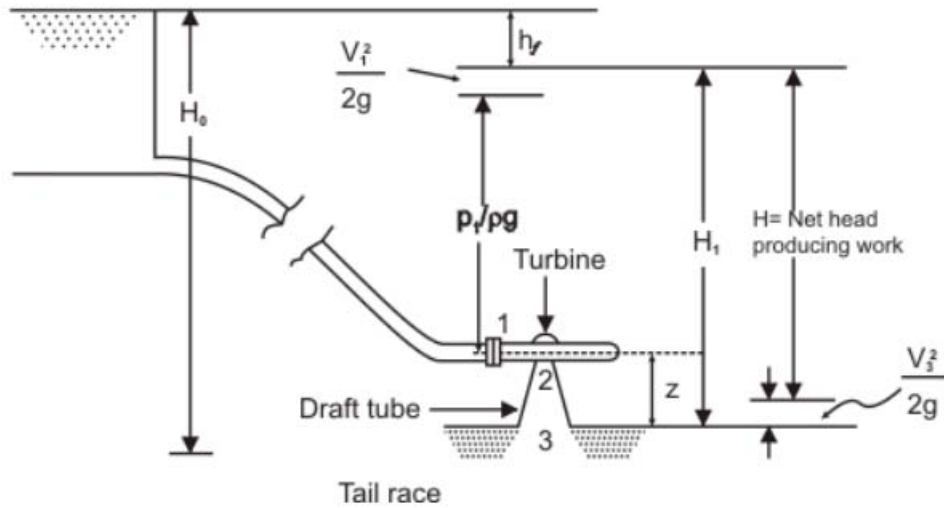


Figure 1-23 Head across a reaction turbine [192]

Therefore,  $H$  = total head at inlet to machine (1) - total head at discharge (3)

$$H = \frac{P_1}{\rho g} + \frac{V_1^2}{2g} + z - \frac{V_3^2}{2g} = H_1 - \frac{V_3^2}{2g} = (H_0 - h_f) - \frac{V_3^2}{2g}$$

Equation 1-6

The pressures are defined in terms of their values above the atmospheric pressure. Section 2 and 3 in Figure 1-23 represent the exits from the runner and the draft tube, respectively. If the losses in the draft tube are neglected, then the total head at 2 becomes equal to that at 3. Therefore, the net head across the machine is either  $(H_1 - H_3)$  or  $(H_1 - H_2)$  [192]. Applying the Bernoulli's equation between 2 and 3 in consideration of flow, without losses, through the draft tube, we can write:

$$\frac{P_2}{\rho g} + \frac{V_2^2}{2g} + z = 0 + \frac{V_3^2}{2g} + 0$$

$$\frac{P_2}{\rho g} = - \left( z + \frac{V_2^2 - V_3^2}{2g} \right)$$

Equation 1-7

Since  $V_1 < V_2$ , both the terms in the bracket are positive and hence  $P_2 < \rho g$  is always negative, which implies that the static pressure at the outlet of the runner is always below the atmospheric pressure. Equation 1-7 also shows that the value of the suction pressure at runner outlet depends

on  $z$ , the height of the runner above the tail race and  $\frac{V_2^2 - V_3^2}{2g}$  the decrease in kinetic energy of the fluid in the draft tube. The value of this minimum pressure  $P_2$  should never fall below the vapor pressure of the liquid at its operating temperature to avoid the problem of cavitation. Therefore, we find that the incorporation of a draft tube allows the turbine runner to be set above the tail race without any drop of available head by maintaining a vacuum pressure at the outlet of the runner [192].

#### 1.7.4 Runner of the Francis turbine

The shape of the blades of a Francis runner is complex. The exact shape depends on its specific speed. It is obvious from the equation of specific speed that higher specific speed means lower head. This requires that the runner should admit a comparatively large quantity of water for a given power output and at the same time the velocity of discharge at runner outlet should be small to avoid cavitation. In a purely radial flow runner, as developed by James B. Francis, the bulk flow is in the radial direction. To be clearer, the flow is tangential and radial at the inlet but is entirely radial with a negligible tangential component at the outlet. The flow, in this situation, has to make a  $90^\circ$  turn after passing through the rotor for its inlet to the draft tube. Since the flow area (area perpendicular to the radial direction) is small, there is a limit to the capacity of this type of runner in keeping a low exit velocity. This leads to the design of a mixed flow runner where water is turned from a radial to an axial direction in the rotor itself. At the outlet of this type of runner, the flow is mostly axial with negligible radial and tangential components. Because of a large discharge area (area perpendicular to the axial direction), this type of runner can pass a large amount of water with a low exit velocity from the runner. The blades for a reaction turbine are always shaped in a way that the tangential or whirling component of velocity at the outlet becomes zero ( $V_{w2} = 0$ ). This is made to keep the kinetic energy at outlet a minimum.

Figure 1-24 shows the velocity triangles at inlet and outlet of a typical blade of a Francis turbine. Usually the flow velocity (velocity perpendicular to the tangential direction) remains constant throughout, i.e.  $V_{f1} = V_{f2}$  and is equal to that at the inlet to the draft tube.



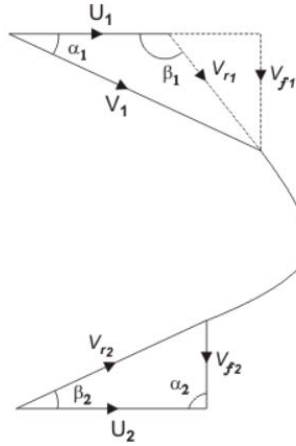


Figure 1-24 Velocity triangle for a Francis runner [192]

The Euler's equation for turbine in this case reduces to:

$$\frac{E}{m} = e = V_{w1} U_1$$

Equation 1-8

where,  $e$  is the energy transfer to the rotor per unit mass of the fluid. From the inlet velocity triangle shown in [Figure 1-24](#):

$$V_{w1} = V_{f1} \cot \alpha_1$$

Equation 1-9

$$U_1 = V_{f1} (\cot \alpha_1 + \cot \beta_1)$$

Equation 1-10

Substituting the values of  $V_{w1}$  and  $U_1$  from [Equation 1-9](#) and [Equation 1-10](#) respectively into [Equation 1-8](#), we have:

$$e = V_{f1}^2 \cot \alpha_1 (\cot \alpha_1 + \cot \beta_1)$$

Equation 1-11

The loss of kinetic energy per unit mass becomes equal to  $V_{f2}^2/2$ . Therefore, neglecting friction, the blade efficiency becomes:

$$\eta_b = \frac{e}{e + \left(\frac{V_{f2}^2}{2}\right)}$$

$$= \frac{2V_{f1}^2 \cot \alpha_1 (\cot \alpha_1 + \cot \beta_1)}{V_{f2}^2 + 2V_{f1}^2 \cot \alpha_1 (\cot \alpha_1 + \cot \beta_1)}$$

Since  $V_{f1} = V_{f2} \cdot \eta_b$  Can be written as

$$\eta_b = 1 - \frac{1}{1 + 2 \cot \alpha_1 (\cot \alpha_1 + \cot \beta_1)}$$

Equation 1-12

The change in pressure energy of the fluid in the rotor can be found out by subtracting the change in its kinetic energy from the total energy released. Therefore, we can write for the degree of reaction:

$$R = \frac{e - \frac{1}{2}(V_1^2 + V_2^2)}{e} = 1 - \frac{\frac{1}{2}V_{f1}^2 \cot^2 \alpha_1}{e}$$

$$[\text{since } V_1^2 - V_2^2 = V_1^2 - V_{f1}^2 = V_{f1}^2 \cot^2 \alpha_1]$$

Equation 1-13

Using the expression of  $e$  from Equation 1-11, we have

$$R = 1 - \frac{\cot \alpha_1}{2(\cot \alpha_1 + \cot \beta_1)}$$

Equation 1-14

The inlet blade angle  $\beta_1$  of a Francis runner varies 45-120° and the guide vane angle  $\alpha_1$  from 10-40°. The ratio of blade width to the diameter of runner B/D, at blade inlet, depends on the required specific speed and varies from 1/20 to 2/3.

Expression for specific speed. The dimensional specific speed of a turbine, can be written as:

$$N_{sT} = \frac{NP^{1/2}}{H^{5/4}}$$

Equation 1-15 [192]

Power generated  $P$  for a turbine can be expressed in terms of available head  $H$  and hydraulic efficiency  $\eta_h$  as:

$$P = \rho Q g H \eta_h$$

Equation 1-16

Hence, it becomes:

$$N_{sT} = N(\rho Q g \eta_h)^{1/2} H^{-3/4}$$

Equation 1-17

$$\text{Again, } N = U_1 / \pi D_1$$

Substituting  $U_1$  from Equation 1-10

$$N = \frac{V_{f1}(\cot \alpha_1 + \cot \beta_1)}{\pi D_1}$$

Equation 1-18

Available head  $H$  equals the head delivered by the turbine plus the head lost at the exit. Thus,

$$gH = e + \left(\frac{V_{f2}^2}{2}\right)$$

Since  $V_{f1} = V_{f2}$

$$gH = e + (V_{f1}^2/2)$$

Equation 1-19

with the help of Equation 1-11 it becomes

$$gH = V_{f1}^2 \cot \alpha_1 (\cot \alpha_1 + \cot \beta_1) + \frac{V_{f1}^2}{2}$$

$$H = \frac{V_{f1}^2}{2g} [1 + 2(\cot \alpha_1 + \cot \beta_1)]$$

Equation 1-20

Substituting the values of  $H$  and  $N$  from Equation 1-20 and Equation 1-18 respectively into the expression  $N_{sT}$  given by Equation 1-17, we get:

$$N_{sT} = 2^{3/4} g^{5/4} (\rho \eta_h Q)^{1/2} \frac{V_{f1}^{-1/2}}{\pi D_1} (\cot \alpha_1 + \cot \beta_1) [1 + 2(\cot \alpha_1 + \cot \beta_1)]^{-3/4}$$

Equation 1-21

Flow velocity at inlet  $V_{f1}$  can be substituted from the equation of continuity as

$$V_{f1} = \frac{Q}{\pi D_1 B}$$

Equation 1-22

where B is the width of the runner at its inlet. Finally, the expression for  $N_{sT}$  becomes:

$$N_{sT} = 2^{3/4} g^{5/4} (\rho \eta_h)^{1/2} \left(\frac{B}{\pi D_1}\right)^{1/2} (\cot \alpha_1 + \cot \beta_1) [1 + 2(\cot \alpha_1 + \cot \beta_1)]^{-3/4}$$

Equation 1-23

For a Francis turbine, the variations of geometrical parameters like  $\alpha_1$ ,  $\beta_1$ ,  $B/D$  have been described earlier. These variations cover a range of specific speed between 50 and 400. Figure 1-25 shows an overview of a Francis Turbine. This figure is shown specifically in order to convey the size and relative dimensions of a typical Francis Turbine to the readers [192].

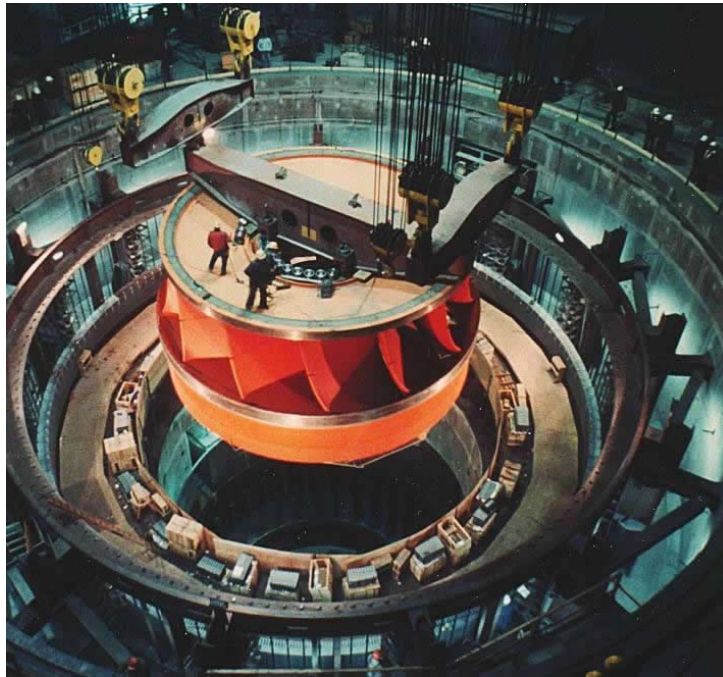


Figure 1-25 instalation of a Francis turbine [192]

## 2 Characteristics of Centrifugal Pumps Working in Direct or Reverse Mode

### 2.1 Centrifugal Pumps Working Principle

One of the most common types of pumps used today is the centrifugal pump. This type of pumps uses one or more impellers to utilize the centrifugal force that pushes the process liquid through the pump. Where centrifugal force is the force that exists, when the object or material moves in a circular motion and pushes the object or material outward from the center of rotation [193]. In centrifugal pump what is moving outward is process liquid. They can be grouped into two basic categories: single stage pumps and multi stages pumps.

The centrifugal pumps contain: Inlet, Casing and Outlet. Inside the casing is an impeller. It has a series of curved veins that extend outfit of center. The pump casing is designed so that the area around the impeller creates a gradually widening spiral channel. This widening channel is known as Volute. If we have one impeller and one volute it is called Single stage pump [193].

During the operation a driver rotates the impeller, creating a centrifugal force that throws the liquid process outward into the volute. The outward movement of liquid causes two things to happen: First, it creates a reduced pressure area at the suction eye of the Impeller. There are of lower pressure, draw more liquid into the pump and provide a constant flow of liquid. Second, it causes the liquid to gain speed. This happens because as the liquid is forced to the outside of the rotating impeller, it must move faster to keep up with the impeller. As the liquid flows away from the impeller, it spreads out to fill the volute. The expansion in the volute causes the liquid to slow down and its pressure to increase. The increased pressure moves the liquid through the discharge of the pump and then on through the piping systems of the process one [193].

One way that centrifugal pumps can be categorized by, is how the liquid flows through them. Three common flow path classifications are Radial flows, Axial flows and Mixed flow. In centrifugal pumps that have radial flow design, the impeller causes the liquid to make a 90-degree turn and flow outward or radially from the suction eye to the tips of the veins. A radial flow pump takes

advantage of the maximum amount of centrifugal force that the impeller develops. Generally, radial flow pumps are capable of higher discharge pressure. But they do not move as much liquid as other types of centrifugal pumps [194].

In centrifugal pumps that have an axial flow design, the impeller moves the liquid through the pump along a path that is parallel to the pump shaft. In this type of pump, the liquid moves mainly by the propeller action of the impeller veins. This impeller uses only a small amount of centrifugal force to move the liquid. As a result, the discharge pressure of an axial flow pump tends to be lower than that of a radial flow pump. However, an axial flow pump may be able to move large quantities of liquid [193].

Mixed flow combines the characteristics of radial flow pumps and axial flow pumps. They use centrifugal force and the propeller action of the impeller veins to move the process liquid. For that reason, a mixed flow pump can develop a relatively high discharge pressure and still move a large quantity of liquid [195].

All centrifugal pumps work by creating a centrifugal force. This force moves the liquid through the pump and increases the liquid's pressure. In applications where large increases in pressure are needed Multistage centrifugal pumps are often being used. A multistage centrifugal pump contains two or more impeller and volutes in a single casing [195].

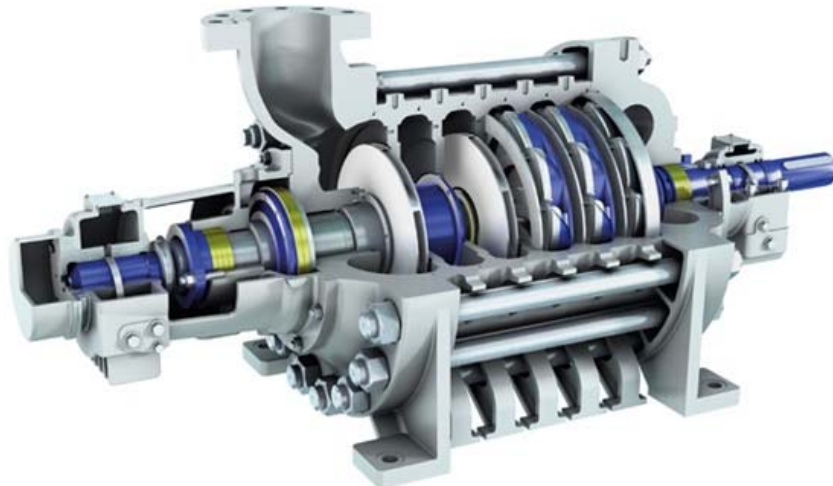


Figure 2-1 Multi stage centrifugal pump[196]

Regardless of how the impellers on a centrifugal pump are arranged, or how many stages a pump has, the liquid's pressure increases as it passes through each stage. This creates a Thrust across the impeller in each stage. This thrust known as Axial Thrust is caused by the difference in pressure between the suction eye and the volute. Because there is a difference across the impeller's axial thrust is created and it tries to push the pump shaft toward the suction eyes. In order for the pumps to operate properly, the thrust must be offset. On some pumps the thrust is offset by using a thrust bearing or a device known as a balanced piston or balance drum. On other pumps the thrust is offset by the arrangement of the impellers [196].

## 2.2 Centrifugal Pumps Design

### 2.2.1 System analysis for pump selection

Before a pump can be selected, the application must be clearly defined. The common requirement of all application is to move liquid from one point to another. As pump requirements must match system characteristics, analysis of the overall system is necessary to establish the pump condition. From the information given, the following will ultimately determine pump selection [3].

- Capacity range of liquid to be moved
- Differential head required
- NPSHA
- Shape of head capacity curve
- Pump speed
- Liquid characteristics
- Construction

### 2.2.2 Differential Head required

The head to be generated by the pump is determined from the system head curve. This is graphical plot of the total static head and friction losses for various flow rates. For any desired flow rate, the head to be generated by the pump or pumps, can be read directly (Figure 2-22 and Figure 2-33) [3].

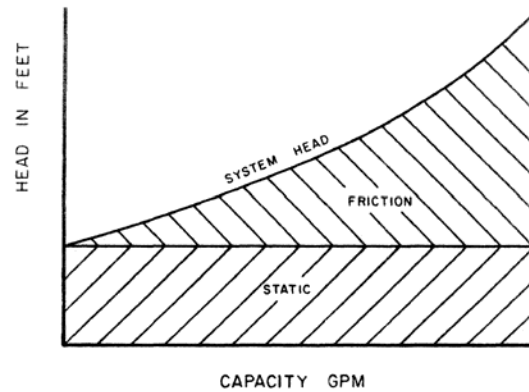


Figure 2-2 System head curve[3]

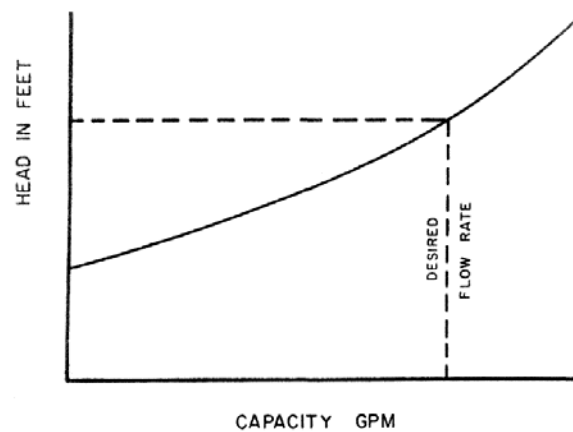


Figure 2-3 The system head curve establishes pump conditions[3]

### 2.2.3 NPSHA

Net positive suction head available (NPSHA) is of extreme importance for reliable operation. It is the total suction head in feet of liquid absolute, determined at the suction nozzle and referred to datum, less the vapor pressure of the liquid in feet absolute[3].

### 2.2.4 Shape of Head Capacity Curve

The desired shape of the head capacity (H-Q) curve is determined during analysis of the system. Most specifications call for a continuously rising curve (Figure 2-44) with the percentage rise from the best efficiency point (BEP) determined by system limits and mode of operation. Unstable or hooked curves (Figure 2-5) where the maximum developed head is at some flows greater than zero



are undesirable in applications where multiple pumps operate in parallel. In such applications, zero flow head may be less than system head, making it impossible to bring a second pump on line. It is also possible for pumps to deliver unequal flow rate from another. these legitimate reasons have resulted in many specifications forbidding the use of unstable curves for any application. This is most unfortunate as in many instances such curves are perfectly suitable. More importantly, pumps with unstable curves will develop more head and be more efficient than their continuously rising counterparts. It should be noted that this tendency of instability is normally confined to the lower range of specific speeds. As specific speed increases, the H-Q curve becomes more stable [3].

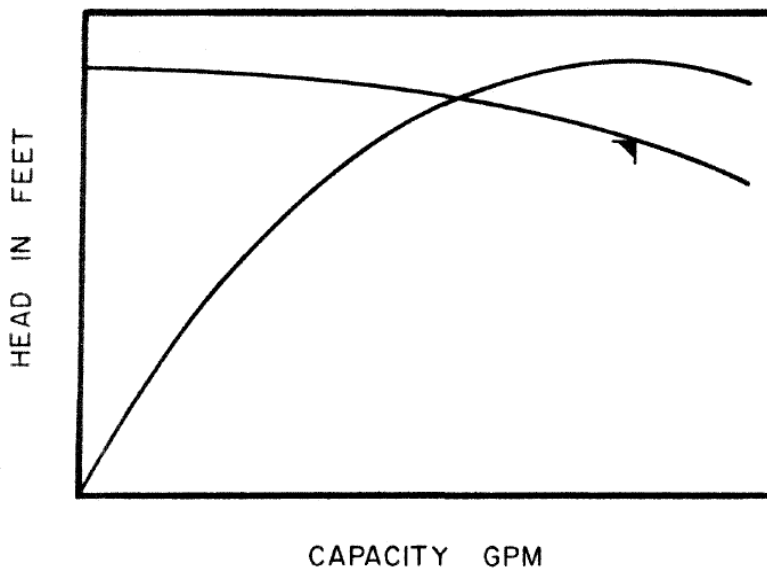
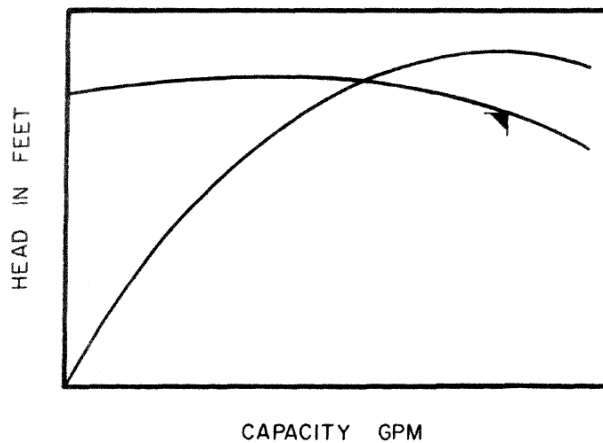


Figure 2-4 Continuously rising head capacity curve[3]



*Figure 2-5 Unstable or hooked head capacity curve.[3]*

### 2.2.5 Pump Speed

Pump speed may be suggested by the user to match electric frequency or available driver speed. However, the pump manufacturer has the ultimate responsibility and must confirm that the desired speed is compatible with NPSHA and satisfies optimum efficiency selection [3].

### 2.2.6 Liquid Characteristics

To have responsible life expectancy, pump materials must be compatible with the liquid. Since liquids range from clear to those that contain gases, vapors, and solid materials, essential information includes temperature, specific gravity, pH level, solid content, amount of entrained air and/or dissolved gas, and whether the liquid is corrosive. In determining final material selection, the pump manufacturer must also consider operation stresses and effects of corrosion, erosion, and abrasion [3].

### 2.2.7 General Pump Design

It is not a difficult task to design a centrifugal pump; however, designing the right pump for a specific application related to specific industry and service requires an extensive knowledge of hydraulics. Also, experience with industrial specifications, end users' and contractors' special requirements is necessary, as well as many years of practical experience in engineering and marketing [3].

The variables that exist for pump requirements are so numerous that the design of the right pump in the right service is a complex project. There is no such product as the "Universal pump" [3].

As an example, let us take a pump that is required to produce 500 GPM and 200-ft head, rotating at 2 or 4 pole speed. In all industries this hydraulic requirement exists; however, the mechanical specifications are entirely different for each and every industry. For instance, the type of pumps used in publications and papers industry are entirely different from pumps used in the petroleum industry, petrochemical industry, or chemical industry [3]. Thus, the pump required to deliver 500GPM and 200-ft head, will be different for each of the following applications:

- Slurry
- Boiler feed

- Pipeline
- Nuclear
- Municipal
- Agricultural
- Marine
- Cargo

Mechanical variables include [3]:

- Open or closed or semi-open impellers.
- Single-stage or multi-stage.
- Vertical or horizontal.
- With water jacket or without.
- Overhung or two-bearings design.
- Close-coupled or coupled units.
- Stiff shaft or flexible shaft design.
- Single volute, double volute, quad volute
- Short elbow-type or turbine-type diffusers.
- Mechanical seals or packing.
- Stuffing boxes with bleed-offs or with clean flush injection.
- Ball, sleeve, or Kingsbury-type bearing.
- Oil rings, forced feed, oil mist, submerged or grease paycheck lubrication.

It can be seen from the variables listed that it is a complex job for a pump designer to design the right pump for the right environment [3].

After complete hydraulic and mechanical specifications have been established, the designer should be ready for pump layout documents [3].

General pump design can be classified in the following categories:

1. Design a new pump to satisfy basics engineering requirements such as shape of H-Q curve, NPSHA, efficiency, etc.

2. Design a new pump to satisfy special applications such as boiler-feed, nuclear coolant, pipeline, large circulator, condensate, secondary recovery, etc.
3. Design a new pump, pulp and paper pumps, building trade pumps, boiler feed pumps, etc.

For pumps in any category, an overall performance chart should be prepared (if not available) as a first step in design study. This chart will establish the flow and head for each pump, establish the number and size of pumps required to satisfy the range chart, and avoid overlap or gaps between pump sizes. Even if only one pump is required, the range chart should be confronted to be sure that the new pump fits into the overall planning [3].

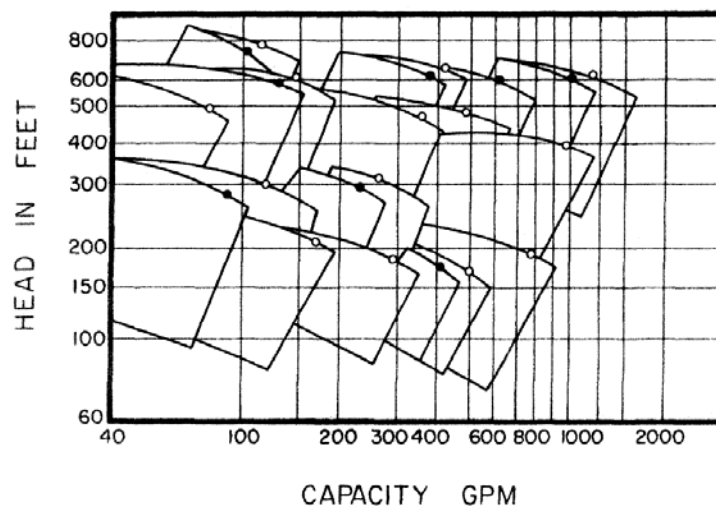


Figure 2-6 poorly planned performance chart [3]

Many old pump lines have poorly planned range charts, resulting in similar pump overlaps and uncovered gaps between pump sizes, such as in the chart shown in Figure 2-66. Black dots show pumps that could be eliminated, permitting a substantial reduction in inventory without hurting overall hydraulic performance. This type of chart is not recommended. A suggested, properly laid out performance range chart is shown in Figure 2-77. Steps to develop this chart will now be described [3].

1. Establish BEP of lowest capacity and lowest head pump required. In this example, this is 86 GPM, 150-ft head. Which is achieved by a 1-in. Pump, and a 7-in. Diameter impeller.

2. Extend BEP capacity coverage at a constant 150-ft head by multiplied of 1.75 Thus,  
 second pump BEP = 86 GPM \* 1.75 = 150 GPM.  
 Third pump BEP = 150 GPM \* 1.75 = 260 GPM, etc.

In this manner, the base line BEP is established.

3. Establish next size pump by multiplying each base line BEP by
  - GPM \* 1.75
  - Head \* 1.45
4. For all additional pump BEPs, multiplying preceding pump flow by 1.75 and head by 1.45.

The constants 1.75 and 1.45 are recommended for a well-planned performance chart following a number of constant specific speed lines. There are no gaps between pumps. each performance block can be covered by normal impeller trim, and there are no overlaps. The chart is also helpful to the designer. In this example, only six small pumps have to be designed and test checked [3].

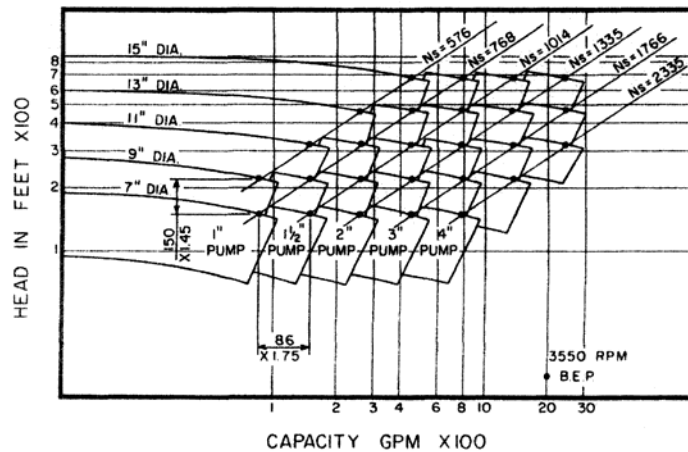


Figure 2-7 recommended performance chart [3]

The other sizes that follow specific speed lines can be factored up and their performance accurately predicted. Designed and tested checked. After the hydraulic performance chart is

complete, the designer should check the mechanical requirements as outlined by the applicable industrial specifications [3].

If a complete line is being designed, the following mechanical features should be checked:

- Shaft size
- Bearing arrangements
- Stuffing box design
- Bolting for maximum pressures
- Suction pressure
- Pump axial and radial balance
- Bed plates, motor support, etc.
- Gasketing
- Lubrication

The standardization and the use of existing parts should be considered at this time; however, hydraulic performances should never be sacrificed for mechanical or cost reasons. If sacrifice becomes necessary, adjust pump hydraulics accordingly [3].

## 2.3 Energy efficiency optimization in water distribution systems

### 2.3.1 Introduction

The operation of Water Distribution Systems generally requires high amounts of energy, which vary in relation to the characteristics of the served area, but also in design and management choices. The assessment of energy efficiency in water distribution systems is strongly influenced by the nature site-dependent of the water-energy nexus in pressurized networks. Understanding this link requires a systematic energy analysis to evaluate separately the influence of pumping stations, network, and water loss. Such an analysis can allow to highlight inconsistencies in the design and management that are reflecting on both the resources, water and energy [29].

### 2.3.2 Energy Efficiency Indicator for water networks

The growing attention brought to the so-called water-energy nexus is certainly driven by the non-negligible amount of energy required for operating water distribution systems. That is, energy-related aspects arise in water network, when one or more electromechanical devices (pumps) are present. Needless to say, the interest towards energy involves environmental, but especially cost issues. This should be kept in mind, while trying to find the most appropriate way for assessing (or improving) the energy efficiency of a given water system, because on the one hand there is the actual energy consumed, on the other hand there is the way that energy is properly or improperly spent. Finally, both aspects always need to be considered in conjunction with the level of service provided [29].

The Unavoidable Minimum Energy required (UME) is computed at each device and involves the definition of a reference hydraulic head ( $H_{ref}$ ) [29].

$H_{ref}$  is the minimum head to be granted at the downstream section of each pump, in order to satisfy the given level of service (namely, a minimum pressure value) throughout the network, during the whole day, considering that no leakages occur [29]. Therefore:

$$UME = \gamma \cdot W \cdot (H_{ref} - H_{ups})/3600000$$

*Equation 2-1 [29]*

where UME is the unavoidable minimum energy required at the pump (kWh);  $\gamma$  is the specific gravity of water ( $N/m^3$ );  $W$  is the total volume lifted by the pump ( $m^3$ ) over the considered period;  $H_{ref}$  is the above defined reference head (m) at the downstream section of the pump;  $H_{ups}$  is the average hydraulic head at the upstream section of the pump (m) [29].

The ratio between UME and the energy actually consumed  $H_{cons}$ , gives birth to the Energy Efficiency Indicator (EEI):

$$EEI = \frac{UME}{E_{cons}}$$

*Equation 2-2 [29]*

The  $H_{ref}$  calculation has required the following steps: pump closed; downstream end of the pump replaced by a “virtual” reservoir; all the emitters’ coefficients set to zero; pipe leading to the tank closed. The  $H_{ref}$  value for the assigned network is found by decreasing the hydraulic head of the virtual reservoir iteratively, until the minimum pressure at the nodes is met [29].

The  $E_{cons}$  value is assessed on a daily basis:

$$E_{cons} = E_{PC} - \Delta E_T = E_{PC} - \frac{\gamma \cdot A \cdot (H_{fin} - H_{ini})}{\eta \cdot 3600000}$$

Equation 2-3 [29]

where  $E_{PC}$  is the energy consumed by the pump, considering its electro-mechanical efficiency (kWh);  $A$  is the cross sectional area of the tank (m<sup>2</sup>);  $H_{fin}$  and  $H_{ini}$  are the hydraulic heads in the tank (m), respectively at time 0:00 and 24:00;  $H_P$  and  $\eta$  are respectively the average pump head and the average efficiency of the pump [29].





## 3 Micro-Hydro Generators using Pump as Turbine

### 3.1 Introduction to Micro-Hydro Generators

The basic principle of hydropower is that if water can be piped from a certain level to a lower level, then the resulting water pressure can be used to do work. If the water pressure is allowed to move a mechanical component, then that movement involves the conversion of the potential energy of the water into mechanical energy. Hydro turbines convert water pressure into mechanical shaft power, which can be used to drive an electricity generator, a grinding mill or some other useful device [197].

Hydropower is a very clean source of energy. It does not consume but only uses the water, after use it is available for other purposes (although on a lower horizontal level). The conversion of the potential energy of water into mechanical energy is a technology with a high efficiency (in most cases double that of conventional thermal power stations) [197].

The use of hydropower can make a contribution to savings on exhaustible energy sources. Each 600 kWh of electricity generated with a hydro plant is equivalent to 1 barrel of oil (assuming an efficiency of 38 % for the conversion of oil into electricity) [197].

The main advantages of hydropower are:

- power is usually continuously available on demand,
- given a reasonable head, it is a concentrated energy source,
- the energy available is predictable,
- no fuel and limited maintenance are required, so running costs are low (compared with diesel power) and in many cases imports are displaced to the benefit of the local economy,
- it is a long-lasting and robust technology; systems can last for 50 years or more without major new investments.

Against these, the main shortcomings are:

- it is a site-specific technology for sites that are well suited to the harnessing of water power and are also close to a location where the power can be economically exploited, which is not very common,
- there is always a maximum useful power output available from a given hydropower site, which limits the level of expansion of activities which make use of the power,
- river flows often vary considerably with the seasons, especially where there are monsoon-type climates and this can limit the firm power output to quite a small fraction of the possible peak output,
- lack of familiarity with the technology and how to apply it inhibits the exploitation of hydro resources in some areas.

To know the power potential of water in a river it is necessary to know the flow in the river and the available head. The flow of the river is the amount of water (in  $m^3$  or liters) which passes in a certain amount of time a cross section of the river. Flows are normally given in cubic meters per second ( $m^3/s$ ) or in liters per second (l/s). Head is the vertical difference in level (in meters) the water falls down [198].

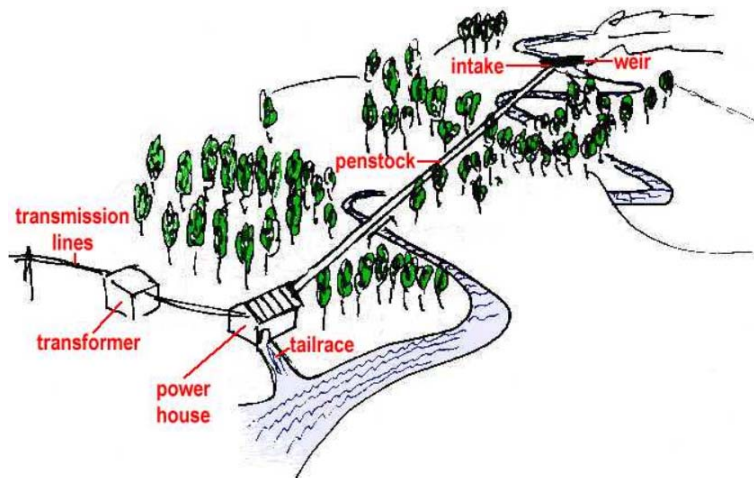


Figure 3-1 [198]

The theoretical power (P) available from a given head of water is in exact proportion to the head H and the flow Q [197].

$$P=Q \times H \times c \quad c = \text{constant}$$

Equation 3-1 The theoretical power

The constant  $c$  is the product of the density of water and the acceleration due to gravity ( $g$ ). If  $P$  is measured in Watts,  $Q$  in  $m^3/s$  and  $H$  in meters, the gross power of the flow of water is:

$$P=1000 \times 9.8 \times Q \times H$$

*Equation 3-2 the gross power of the flow of water [197]*

This available power will be converted by the hydro turbine in mechanical power. As a turbine has an efficiency lower than 1, the generated power will be a fraction of the available gross power [197].

Hydropower installations can be classified as follows (Table 3-1):

*Table 3-1 Hydropower installations [197]*

Name	Description
Large	All installations with an installed capacity of more than 1000 kW (according to some definitions more than 10,000 kW).
Small	General term for installations smaller than 1000 kW (or < 10,000 kW). Also used for installations in the range between 500 and 1000 kW.
Mini	Capacity between 100 and 500 kW.
Micro	Hydropower installations with a power output less than 100 kW (or less than 1000 kW).

Definitions of small, mini, and micro hydro plants found in literature (Table 3-2):

*Table 3-2 Source: Moreire, J.R. & Poole, A.D. (1993) Hydropower and its constraints. In: Johansson T.B. et al, (1993) Renewable energy: sources for fuels and electricity (ISBN 1-85383-155-7)*

Country	Micro (kilowatts)	Mini (kilowatts)	Small (megawatts)
United States	< 100	100 – 100	1 - 30
China	-	< 500	0.5 – 25
Russia	< 100	-	0.1 – 30
France	5-5000	-	-
India	< 100	101 – 1000	1 – 15
Brazil	< 100	100 – 1000	1 – 30
Norway	< 100	100 – 1000	1 – 10

various	< 100	< 1000	<10
---------	-------	--------	-----

### 3.2 PATs (Pump as Turbine)

Running pumps as turbines is a well-known concept in the water supply industry. It is seen as an efficient method of generating power as well as recovering energy and contributing to savings. The concept of running a centrifugal pump in reverse rotation mode has been recognized by pump manufacturers for many years and within the water supply industry this concept has been exploited to a limited degree as a means of generating power in locations where it is considered too expensive to purchase a hydro turbine. It has not gone unnoticed by water suppliers, operators of small hydropower plants and pump manufacturers that running pumps as turbines (PATs) is an efficient method of generating energy as well as recovering energy and contributing to energy savings. In the current economic climate, where reducing energy costs is becoming a high priority, it is not surprising that PATs are starting to create significant interest [199].

Using pump as turbine is an attractive and significant alternative. Pumps are relatively simple machines with no special designing and are readily available in most developing countries. Besides, their installation, commissioning and maintenance are easy and cheap. From the economical point of view, it is often stated that the capital payback period of PATs in the range of 5–500 kW is two years or less [199].

### 3.3 PATs working principle

In recent years, small and micro hydro power plants have become a possible new application area for PAT, which are aimed at replacing the more expensive conventional turbines. One way of overcoming the high-cost capital price of Micro/Pico hydropower stations is to use simple machines instead of more complex conventional turbines. Industrial pumps can be effectively operated as turbines. From the economic point of view, it is often stated that pumps working as turbines, in the range of 1–500 kW, allow capital payback periods of two years or less, a considerably shorter time than that of a conventional turbine [4].

Several researchers have become interested in pumps operating as turbines for many types of small applications. Pump manufacturers do not normally provide turbine mode performance for their products. Therefore, in recent years, many prediction techniques have been developed e.g. Sharma [5], Williams [6], Alatorre-Frenk [7], and more recently Ramos and Borga [8], [9], Valadas and Ramos [10], Singh [11], [12], Yang et al. [13], and Derakhshan and Nourbakhsh [14].

Due to the huge number of pumps on the market all possible sizes, appropriate machines, cheap and reliable, are readily available. Regarding maintenance, there are many advantages compared with custom-made turbines.

As a result of the fixed geometric conditions within the casing and impeller, pumps as turbines have a low part-load performance. This characteristic address one of the most important challenges for a Micro-Hydro system based on a PAT. A pump operating as a turbine is very sensitive towards changing boundary parameters, namely head and discharge. Hence, a wrong pump selection or rotational speed will result in a shift of the operating point, delivering a non-desired output, and ultimately even causing a possible failure of the project [2].

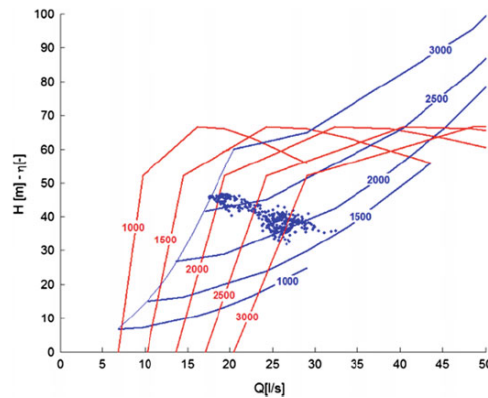


Figure 3-2 Typical performance curves for PAT for various rotational speeds [2]

Centrifugal pumps can be easily rotated as turbines in heads ranging from 15 to 100 m and with flow rates ranging from 5 to 50 l/s (Figure 3-2). Figure 3-4 shows the application of different pumps working as turbines. Cross flow turbines can be replaced by centrifugal, mixed flow and double suction PATs. The ranges for mixed flow PATs are 5–15 m and 50–150 l/s for head and flow rates, respectively. For heads ranging from 15 to 100 m and flow rates ranging from 50 to 1000 l/s, double suction pumps or multi centrifugal pumps in a parallel arrangement are suitable.

Pump manufacturers usually produce centrifugal and mixed flow pumps on a large scale, so these pumps are readily available on the market at a low price [4].



Figure 3-3 A centrifugal PAT-based pico hydropower station, installed in the West of Iran [4]

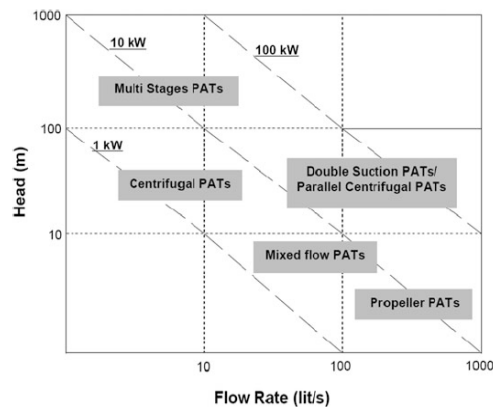


Figure 3-4 Application of various pumps as turbines [4]



Figure 3-5 An axial PAT based micro hydropower station, installed in the North of Iran [2]

When a pump runs as a turbine, the high-pressure fluid enters the machine and then leaves after the conversion of the energy has occurred within the impeller. Since the flow direction and the

rotational speed are reverse, the velocity triangles of both modes change. Although only the shaft rotation and flow direction are opposite in pump and turbine modes, their velocity triangles are different [2].

Considerations show that the inlet flow angle to the impeller in a PAT is not exactly the same as the outlet flow angle of the impeller in the pump mode. This angle ( $\alpha_v$ ) is approximately equal to the volute angle. In fact, the volute operates as a guide channel in turbine mode. Assuming the outlet flow angle from the impeller in reverse operation is equal to the impeller inlet flow angle in direct operation (i.e. with no whirl at the impeller exit), the same Euler heads for both modes can be considered [2].

### 3.4 PAT Applications

Nowadays, applications of PAT have been developed in villages, farms, irrigation systems, as pressure dropping valves and as small pump storage power stations. Since 1930, the main challenge in PAT usage was the selection of a proper PAT for a small hydro-site. Several case studies of applications of PAT will be reviewed in CHAPTER 4 and CHAPTER 5.

### 3.5 Components of PATs

Depending on the PAT type, the components of each machine are different. However, in general, PAT components are classified in two groups: rotary and stationary. The rotary group consists of the impeller and shaft. The stationary group includes the inlet parts (i.e., the inlet pipe and volute), outlet parts (i.e., the suction pipe and draft tube), and the casing and mechanical parts (i.e., rings, mechanical seals and bearings). However, the main hydraulic parts of a PAT are the impeller, volute and draft tube (Figure 3-6) [15].



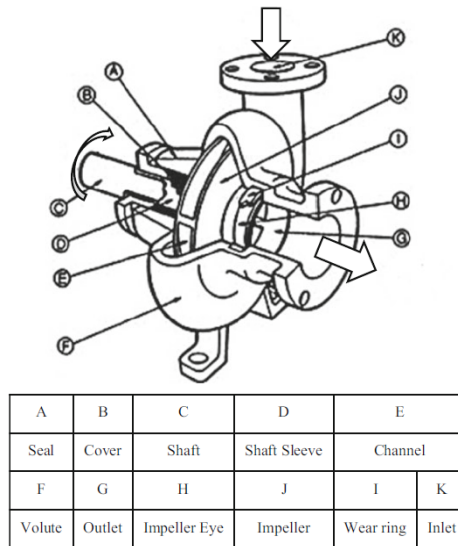


Figure 3-6 PAT components ([www.processindustryforum.com](http://www.processindustryforum.com))

### 3.5.1 The Volute

Although the volute of a PAT is designed to collect the water from the impeller of a pump, the design method for a pump is quite similar to a Francis turbine volute (i.e. a constant velocity method). Therefore, when the flow is reverse, the volute of a PAT will work properly as a distributor of the flow surrounding the impeller. However, the most important role of a volute is the balancing of radial pressure and forces. Figure 3-6 shows a typical volute of a PAT [200]. (Figure 3-7)

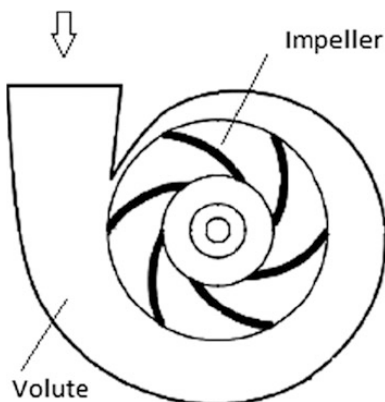


Figure 3-7 Plan view of PAT [15]

### 3.5.2 The Impeller

The impeller, the main component of a PAT, converts the hydraulic energy of the inlet flow to the mechanical shaft. Although the impeller has been designed to pressurize the liquid using the centrifugal force, it can also absorb the flow energy with a reasonable efficiency. The impeller usually has 5–8 blades, with a hydrofoil shape type [200]. An impeller and the details of a blade are presented in Figure 3-8.

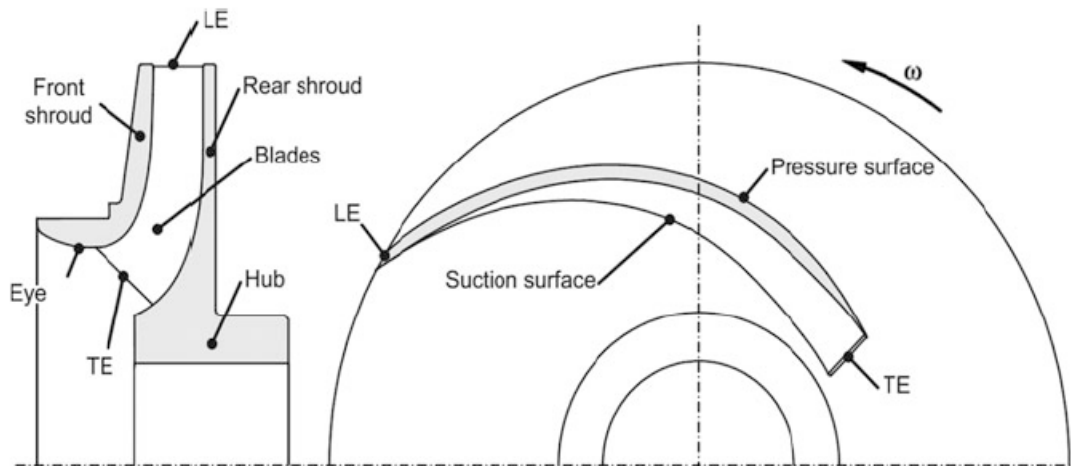


Figure 3-8 Impeller and details of a blade [15]

### 3.5.3 The Draft Tube

A small kinetic energy is required at the PAT outflow to minimize energy losses. Using a draft tube, the kinetic energy can be converted into potential energy. Therefore, a draft tube is designed based on the maximum conversion of velocity to pressure (according to the Bernoulli equation). Figure 3-9 shows a typical draft tube of a PAT [200].

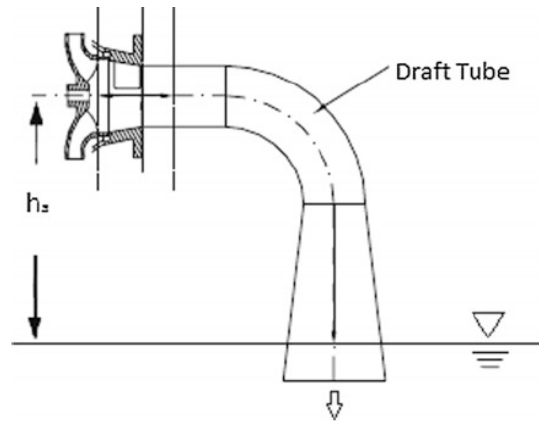


Figure 3-9 Draft tube of a PAT [15]

### 3.6 A state-of-the-art review on PAT

Hydropower is a renewable energy source based on the natural water cycle, and actually the most mature, reliable and cost-effective renewable power generation technology available [86]. It contributes to around 16% of the World electricity supply generated from about 20,053 TW h of installed capacity [87]. In many countries it is the main source of power generation e.g. Norway – 99%, Brazil – 86%, Switzerland – 76% and Sweden – 50% [88].

While large hydropower plants feed the national grid, typical off grid micro hydropower plant (MHP) is the most popular solution for electrification among rural communities, supplying the power in the range of 5–100 kW, usually using a run-of-the-river to divert some of the water from the river before dropping into a pressurized penstock [89].

However, in accordance with individual countries' administrative purposes [90],[91], hydropower plants have been classified in terms of head or installed capacity, with different upper and lower limits for each category. Table 3-3 shows one of the used classifications as found in the literature.

Hydro scheme	Capacity	Capacity
Large	More than 100 MW	More than 100 MW
Small	Up to 25 MW	1–10 MW
Mini	Below 1 MW	100 kW to 1 MW
Micro	6–100 kW	5–100 kW
Pico	Up to 5 kW	Up to 5 kW

Table 3-3 Hydropower scheme classification. [85]

The mostly met problem in micro turbines is their higher price compared to full scale ones with respect to the whole project budget, owing to their expensive manufacturing price. For instance, it's very difficult, time-consuming, and costly to develop such site-specific turbines in accordance with the local ecology [91].

The cost of electro-mechanical components in large hydro-power plants is around 20% but in MHPs it is relatively high and varies from 35% to 40% of the total project cost which may rise even up to 60% or 70% of the total project cost in some typical cases [92] Figure 3-10.

Renewable and Sustainable Energy Reviews 79 (2017) 148–179

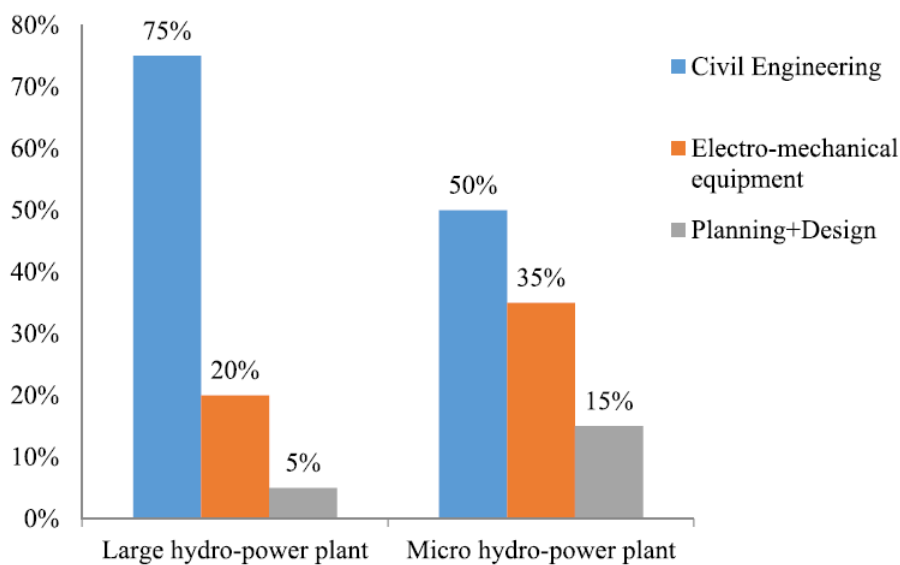


Figure 3-10 Cost distribution for large and micro hydropower plants.[92]

the first pump turbine had been set at a remote farm in the Yorkshire Dales of the North England in 1930. This scheme has been working for a five-year testing time, after which its reliability was confirmed before being transferred to other countries [93]. From then on, pump turbine has become a hot topic amongst researchers and field engineers, where indeed, it has been used at so many sites, mainly for electricity provision in remote hilly regions away from central grid reach (Table 3-4).

Location	Capacity of plant	Year of installation
Sainyabuli Province, Laos	2 kW	2008
Thima Kenya	2.2 kW	2001
Mae Wei village, Thailand	3 kW	2008
West Java, Indonesia	4.5 kW	1992
Kinko village, Tanzania	10 kW	2006
Fazenda Boa Esperanca, Brazil	45 kW	2007
Ambotia Micro-hydro project, India	50 kW	2004
British Columbia, Canada	200 kW	–
Vysni Lhoty, Czech Republic	332 kW	2008

Table 3-4 PAT installations [85]

Different researchers; Williams [93], Orchard and Sander [94], Ramos and Borga [95], Derakhshan and Ahmad [21], and Arriaga [96] among others, have provided information about the applications and advantages of a pump working as a turbine, mainly basing their arguments on its two most important features: “cost-effectiveness” and “simplicity”. Adding on the third one, “smallness”, which is also true in a way; However, owing to the philosophy behind the pump's functioning difference between conventional and reverse modes, pump turbines flow dynamics and operational characteristics have not been fully understood, thus requiring more research efforts in the same. As a matter of fact, many researchers have tried different PAT efficiency prediction methods but in vain, as the predicted results never got validated through experimentation, with errors of the order of  $\pm 20\%$  [97], and couldn't cover a wide range of pump operating conditions in reverse mode. PAT's simple structural design would reflect its easily understandable operations.

### 3.6.1 Pump-turbine selection

Typical micro hydropower plants convert the falling water-contained energy to mechanical energy by turning the pump turbine, which converts the water pressure into mechanical shaft power to

drive an electric generator. The power available is proportional to the product of head and volume flow rate as the general formula for hydropower systems shows [98]:

$$P = \eta\rho gQH$$

Equation 3-3

where P is power output,  $\eta$  hydraulic efficiency,  $\rho$  fluid density, g gravitational acceleration, Q volumetric flowrate and H water head. As shown in Equation 3-3, the turbine selection process for a MHP of interest, should be based on the head and flowrate available at the site. The power output may also be related to the head to express the turbine specific speed.

$$N_s = \frac{nP^{1/2}}{H^{5/4}}$$

Equation 3-4

where  $N_s$  is the turbine specific speed and n is the real rotation speed of turbine. This parameter characterizes the turbine runner, spiral casing, blade shape and other geometric design features, thus doesn't depend on the size but the shape of the machine of concern [91]. For instance, two machines of similar shape and different size may have same specific speed.

Different researchers; Orchard and Sander [94], Franc et al. [99], Chapallaz et al. [100], Fraenkel et al. [101] and Paish [98] among others, have so far provided head-flow charts depicting the range of application for different PATs (Figure 3-11).

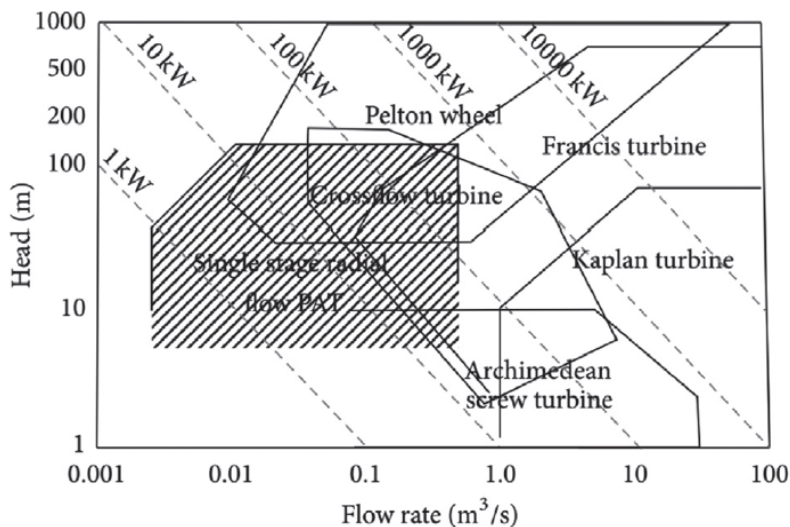


Figure 3-11 Head-flowrate selection chart [104]

PAT selection can also be carried out through a head-specific speed chart. Avellan [103] has presented a head-specific speed chart for Francis-type reversible pump turbines, where the PAT geometric design plays the key role in the classification process. PATs with narrow impeller channels at the runner inlet are characterized by high heads-low specific speeds, while PATs with wider impeller channels at the runner inlet are characterized by low heads-high specific speeds (Figure 3-12).

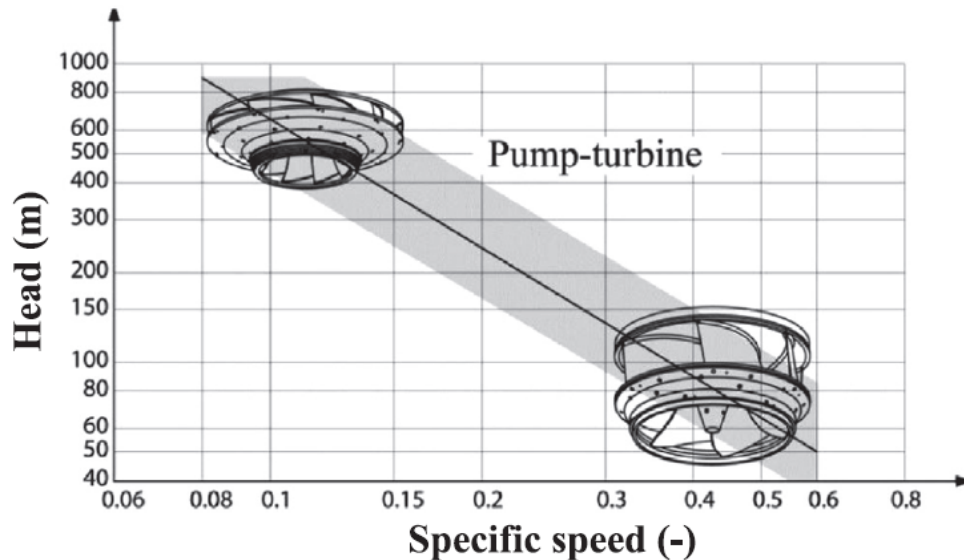


Figure 3-12 Head-Specific speed selection chart [104]

Kaunda et al. [90] has presented the systematic process of selecting the optimum turbine according to the site conditions, where both the importance of head-volumetric flowrate chart and the turbine specific speed were recognized (Figure 3-13), and different factors which can assist in pump selection decision making, viz. investment cost of the turbine, turbine design complexity, unit power generation cost, and the turbine performance, were discussed as well.

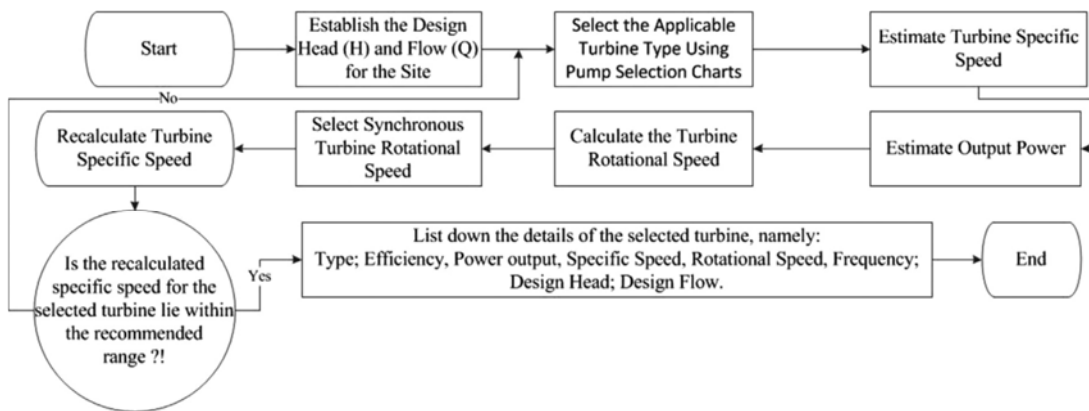


Figure 3-13 Turbine selection flow chart for micro hydropower schemes [90]

### 3.6.2 Pump-turbine performance prediction

due to the fact that the pump manufacturers do not offer performance curves of their pumps in turbine mode; the selection of a suitable pump turbine to run under site-specific operation conditions has become a big challenge [91]. A large number of theoretical and experimental studies have been done for performance prediction of reverse running centrifugal pumps [105].

Many researchers, e.g., Stepanoff [106], Childs [107], Sharma [5], among others, have developed PAT performance prediction relations based on pump best efficiency point (BEP) whereas others such as Gopalakrishnan [108], Diederich [109], and Grover [110] have developed their relations basing on the pump specific speed. However, theoretical prediction methods have not provided a completely reliable solution to the problem as their results were way erroneous as compared to field test results. Therefore, they may only be used to get a rough picture of the required PAT characteristics, which need validation adjustment by experimental methods. Selected PAT performance studies and their respective findings have been chronologically presented by Jain et al. [91] as shown in Table 3-5.

Year	Name of investigator	Criteria	Head correction ( $h$ )	Discharge correction factor ( $q$ )	Remarks
1957	Stepanoff	BEP	$\frac{1}{\eta_p}$	$\frac{1}{\sqrt{\eta_p}}$	Accurate for Ns: 40–60
1962	Childs	BEP	$\frac{1}{\eta_p}$	$\frac{1}{\eta_p}$	–
1963	Hancock	BEP	$\frac{1}{\eta_p}$	$\frac{1}{\eta_p}$	–
1980	Grover	Specific speed	$2.693 - 0.0229N_{st}$	$2.379 - 0.0264N_{st}$	Applied for Ns: 10–50
1982	Lewinsky-Kesslitz	Specific speed	$1.3 - \frac{6}{N_{st}-3}$	$1.3 - \frac{1.6}{N_{st}-5}$	–
1985	Sharma	BEP	$\frac{1}{\eta_p^{1.2}}$	$\frac{1}{\eta_p^{0.8}}$	Accurate for Ns: 40–60
1988	Schmiedl	BEP	$-1.4 + \frac{2.5}{\eta_{pp}}$	$-1.5 + \frac{2.4}{\eta_{pp}^2}$	–
1994	Alatorre-Frenk	BEP	$\frac{1}{0.85\eta_p^5 + 0.385}$	$\frac{0.85\eta_p^5 + 0.385}{2\eta_p^{9.5} + 0.205}$	–
1998	Sharma	BEP	$\left[\frac{N_g}{N_m}\right]^2 \times \frac{1.1}{\eta_p^{1.2}}$	$\frac{N_g}{N_m} \times \frac{1.1}{\eta_p^{0.8}}$	$N_g = 240 \times \frac{L}{P} - N$

Table 3-5 Performance prediction methods for pump-turbines. [85]

Barbarelli et al. [23], after discussing weaknesses as found in many published PAT performance predictions methods [20],[111],[112],[113], came to a conclusion that the PAT performance prediction model universality can only be achieved if, through direct PAT geometry identification without disassembly, the PAT performance curves could be developed.



More intensive theoretical, experimental and computational studies have so far been carried out on the PAT performance prediction, which eventually resulted in a big literature about PAT performance prediction, as described in the following sections.

### 3.6.2.1 Theoretical studies

Nourbakhsh and Derakhshan [114] carried out an investigation on PAT performance in small hydrous by theoretical and experimental methods. Different existing empirical PAT performance prediction methods were compared, to finally come out with a favorable choice which can be used in general cases. From experimental results as performed on a complete laboratory model of a mini hydropower plant built in Tehran University, it was found that, the discharge, head and efficiency were higher in turbine than pump mode. the turbine power output was higher than pump input power, and finally, the slight impeller modification could result in a considerable efficiency increase, where the pump with higher specific speed was surely expected to exhibit higher turbine mode efficiency. However, no universally reliable PAT performance prediction formula or theoretical method was found. [112]

Hossain et al. [115] carried out a comparative study between two mostly used theoretical PAT performance prediction methods (Chapallaz et al. [100] and Sharma [5] methods) to get an idea which is better than the others. The study, through a comparative scheme, concluded that Sharma method could only predict the PAT BEP and power whereas Chapallaz et al. method gave a wide range of operating points from minimum to maximum deviation, thus providing the access to the information about PAT operation at and away from BEP.

Yang et al. [112] carried out a PAT performance prediction study in which three methods, viz. theoretical, numerical, and experimental methods, were used. The theoretical and CFD methods were more accurate than the other two methods (Sharma [5] and Stepanoff [106] methods), as shown in Figure 3-14 and Table 3-6.

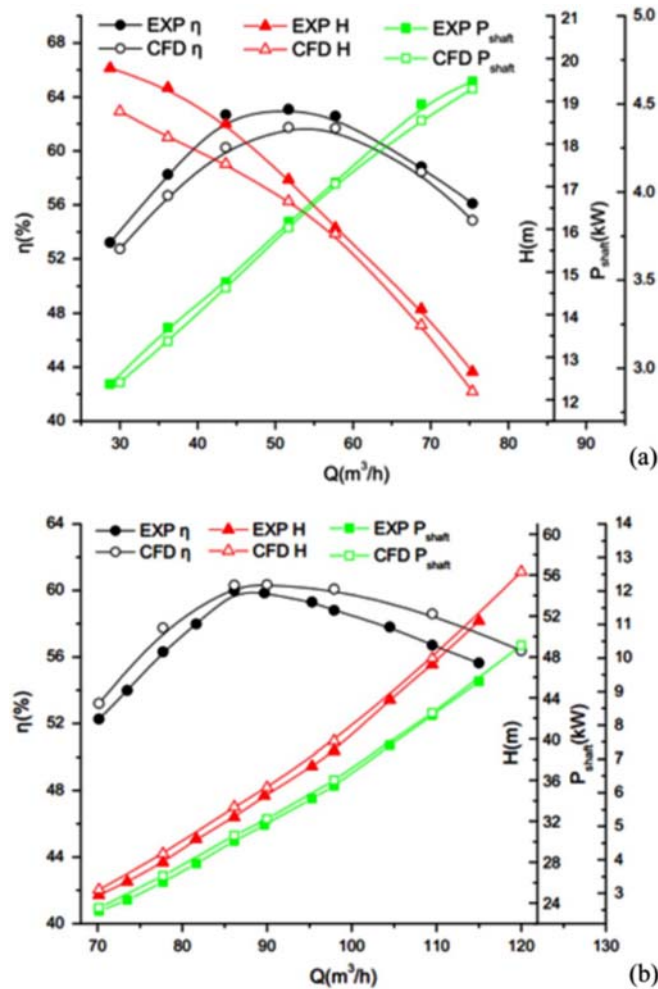


Figure 3-14 Comparison between Pump (a) and PAT (b) experimental and numerical results. [85]

	Experimental	Numerical	Theoretical	Sharma	Stepanoff
$h$	1.89	2.00	1.99	1.74	1.58
$q$	1.66	1.70	1.55	1.45	1.26
Error $h$ (%)	–	+5.3	+5.3	–7.9	–16.4
Error $q$ (%)	–	–2.4	–6.6	–12.7	–24.1

Table 3-6 BEP predictions by various methods.[85]

Williams [116] carried out a comparative study of eight different prediction methods on 35 pumps with specific speeds ranging from 12.7 to 183.3, where the main research focus was the impact of performance prediction methods errors (deviation between predicted and actual BEP values) on PAT operations.

Fernandez et al. [117] has, by applying experiments-derived pump hydraulic characteristics in both modes, modified the Euler's head equation to finally come up with a newly developed PAT performance prediction equation. It had been noticed that all PAT performance prediction methods were either, based on pump BEP characteristics similarity between both modes, or algebraic relations as a function of efficiency; where most importantly, the rotational speed was considered equal in both modes; which in fact was opposed in this study by considering different rotational speeds in both modes.

Carravetta et al. [118] proposed the turbomachinery affinity laws modification scheme to eliminate the big discrepancy between PAT performance theoretical and experimental prediction methods. In order to obtain the PAT BEP characteristics at a speed  $N^H$  ( $N^H \neq N_{MAX}$ ), the usual turbomachinery affinity laws were transformed to functions of the ratio ( $N^H/N_{MAX}$ ), as follows:

$$\begin{aligned}q &= \frac{Q^H}{Q_B^{MAX}} = f_1\left(\frac{N^H}{N_{MAX}}\right) \\h &= \frac{H_B^H}{H_B^{MAX}} = f_2\left(\frac{N^H}{N_{MAX}}\right) \\p &= \frac{P_B^H}{P_B^{MAX}} = f_3\left(\frac{N^H}{N_{MAX}}\right) \\\varepsilon &= \frac{\eta_B^H}{\eta_B^{MAX}} = f_4\left(\frac{N^H}{N_{MAX}}\right)\end{aligned}$$

*Equation 3-5*

Functions  $f_1$ ,  $f_2$ ,  $f_3$  and  $f_4$  were obtained from experimental results on several submersible pumps operated at different speeds. Using Suter parameters in conjunction with the obtained modified affinity laws, the decrease of scatter between the calculated and measured values was achieved.

Ramos and Borga [95] carried out a Suter parameters-based steady and transient flow regimes study aiming at proving the pump physical, economic and technical reliability not only in industrial processes but also in power generation sector. It was confirmed that using PATs is a good alternative to dissipation of excess flow energy that, normally would be lost.

Singh et al. [119] carried out a PAT performance prediction study at a 10 kW MHP site in Kinko, Tanzania; where the theoretically found results were compared to field performance characteristics. Deviation between the two methods outputs were noticed, where on-site characteristics at full load were slightly scattered from predicted ones with 4%, 2%, and 3% deviations for discharge, head, and electric power output respectively.

### 3.6.2.2 Experimental studies

Raman et al. [120] carried out an experimental study aiming at a better understanding of PAT characteristics. A centrifugal pump with 15.36, 22 m, and 8.31 l/s as specific speed, head, and flow rate respectively, was tested in a test rig as installed in the Mechanical Engineering Laboratory of the Universiti Tenaga Nasional. The pump selection process was performed following a reconnaissance technic as presented by Raman and Hussein [121];

Prasad et al. [92] carried out an experimental research to assess the PAT performance and cavitation characteristics. Two Kirloskar Brothers Limited (KBL) mixed flow pumps, namely pump A and B, having different specific speeds, were tested on a Maulana Azad National Institute of Technology-based test rig, at different rotational speeds, flow rates and heads. The experimental results were then compared to Chapallaz et al. [100] theoretical method ones, where different conclusions were drawn. It was found that, as usual, the heads and flows for turbine mode are always higher than in direct mode. However, the efficiency could be less or more irrespective of the pump specific speed.

Daniela et al. [122] studied the PAT characteristics to get an idea of the PAT benefits as compared to normal turbines. The experimental data were collected from a medium size river-based plant which recently got upgraded from normal turbine to PAT-based site. The measured PAT parameters were then used, through basic turbomachines calculations, to get the complete PAT performance curves. It was found that PAT worked at higher flow rates and heads, whereas the

efficiencies were almost the same for both operating modes. PAT was found to work in turbine mode without any mechanical complications.

Suarda et al. [123] presented an experimentally comparative research between two small pumps in their turbine operational modes, one of volute, another of diffuser type. Experimental findings showed the volute type performance more attractive than the diffuser type.

Singh et al. [124] studied the effect of casing eye ribs on the pump turbine hydraulics and performance characteristics. Two pump models, casing rib absent (CRA) and casing rib present (CRP), were both numerically and experimentally studied; where commercially available software, CFX, for which the K- $\epsilon$  turbulence model was selected, was used for simulations. The PAT flow experimental and numerical analysis was comparatively carried out for two operating modes, CRA and CRP, at six operating points, namely, A (51%  $Q_{BEP}$ ), B (70%  $Q_{BEP}$ ), C (88%  $Q_{BEP}$ ), D (100%  $Q_{BEP}$ ), and E (116%  $Q_{BEP}$ ), constituting the part, full, and over loads. The study results from both methods showed that CRA had higher efficiency and greater performance for the part load and overload operations as compared to CRP. A satisfactory similitude was noticed between experimental and numerical results, where the PAT exhibited good performance with 82% as the highest attained efficiency.

Nautiyal et al. [105] carried out an experimental study on PAT performance characteristics in the hope to come out with a more accurate prediction method. The test results on a pump of 18 (m, m<sup>3</sup>/s) as specific speed, running at 1500 rpm, confirmed that, as it had been demonstrated by many other researchers, the centrifugal pump can surely be used as turbine under various operating conditions, where the turbine operating mode is always characterized by higher flow rates and heads but with comparatively lower efficiencies.

Derakhshan and Nourbakhsh [20], based on experimental results as performed on a mini-hydropower test rig at the University of Tehran, has developed new correlation equations for PAT BEP prediction. Four centrifugal pumps in specific speeds range from 14.6 to 55.6 (m, m<sup>3</sup>/s) were

tested, where centrifugal pumps were again found to fit the turbine operating conditions with comparatively higher heads and flows and approximately equal efficiencies.

Singh and Franz [125] developed a new consolidated model from experimental results on many pumps of different shapes (20–80 rpm), mainly targeting its parsimony on PAT performance prediction, selection, and evaluation, which are its three main segments; in order to find a lasting solution for PATs modelling and establish a new basis of evaluating uncertainties, based on fundamental theory of turbomachines. The prediction segment required the pump shape and size to come out with complete PAT performance characteristics. The selection segment required only the site head and flow data to determine the suitable pumps for specific sites. And finally, the evaluation segment compared the selected pumps and their characteristics to decide the most suitable PAT for specific operating conditions.

Yang et al. [126] studied the influence of rotational speed to the PAT performance. In this paper, a rotational speed-based theoretical PAT performance prediction method was first developed where new correlation equations for flow rate, head, and shaft power; were developed as shown:

$$\begin{aligned}\frac{Q_1}{Q_2} &= \frac{n_1}{n_2} \\ \frac{H_1}{H_2} &= \left(\frac{n_1}{n_2}\right)^2 \\ \frac{P_1}{P_2} &= \left(\frac{n_1}{n_2}\right)^3\end{aligned}$$

*Equation 3-6*

where the subscripts 1 and 2 stand for first and next operating conditions in terms of speed. Experiments were carried out on a Jiangsu University based-test rig at different rotational speeds, viz. 1000 rpm, 1200 rpm, 1500 rpm, and 1800 rpm. And finally, the PAT model was numerically analyzed. The numerical study was performed by a CFD commercial code Ansys CFX, where the k-ε turbulence model was adopted, and static pressure inlet and mass flow rate outlet were selected as inlet and outlet boundary conditions respectively. Test, numerical, and theoretical results were in a quite acceptable agreement. However numerically predicted efficiency, head, shaft power

values tended to be slightly higher than test ones by 4.85%, 2.31%, 5.39% respectively. Nevertheless, theoretical results were higher than the two first, where wider deviation was found in Shaft power predictions. The developed theoretical method was found reliable but needing some perfections to get even better results.

### 3.6.2.3 Numerical studies

Many researchers have shown that CFD analysis is a reliable tool to predict the behavior of a pump machine operating as a turbine and to estimate the performance curves of the turbomachinery [127]. With CFD, complex fluid flow behaviors inside the PAT can be virtually previewed, which can substantially reduce both the design time and cost. A big number of studies have been carried out aiming at PAT flow characteristics understanding and performance prediction.

Ismail et al. [128] tested an end suction centrifugal pump by means of CFD simulations to determine its performance characteristics in both direct and reverse modes. The CFD modelling and simulations were performed by Ansys CFX14.0, where the K- $\epsilon$  was selected for flow turbulence modelling in a pump of 70 units (Euroflo EU50-20) as specific speed and working at a rotational speed of 1450 rpm. The computational domain was divided into three parts, viz. volute, impeller and draft tube; where inlet and outlet boundary conditions were set to mass flow rate inlet and static pressure out respectively. However, the reverse mode simulations had to be run at 1550 rpm in accordance with the used induction generator's speed. The flow simulations were then run at flows varying from 0.7 to 1.3 QBEP. After comparing both modes CFD predicted results to pump manufacture-provided ones, it was observed that BEP was attained at higher flows and heads in turbine than pump mode. However, efficiency was found higher in pump mode (72.63% against 71.62%). Numerical simulation method was confirmed viable for PAT performance prediction.

Fernandez et al. [129] presented a 3D flow simulation study on a pump as turbine aiming at validating the experimental results as previously presented in [117], using the sliding mesh technique to capture the interactions between the impeller and the volute tongue. The PAT flow numerical simulation was performed through a CFD commercial code Fluent at a rotational speed

of 1750 rpm under five different flow regimes viz 50, 65, 80, 100, and 120 m<sup>3</sup>/h. The pressure velocity coupling was achieved by SIMPLE algorithm and Standard k- $\epsilon$  model was selected for turbulence modelling. Numerical simulation and experimental results showed a neat agreement, especially for head and Power predictions (Figure 3-15).

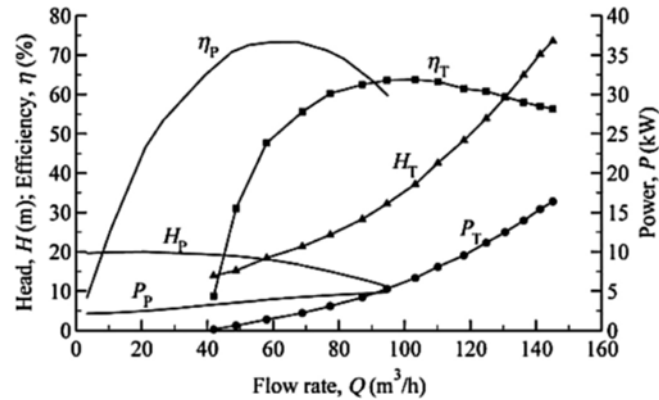


Figure 3-15 Performance characteristics for pump and reverse modes [111]

Páscoa et al. [130] carried out a numerical study on a centrifugal pump to check the validity of three randomly selected theoretical correlation methods, viz. Stepanoff, Sharma, and Viana methods. In this study, through a CFD commercial code Ansys Fluent, the flow in a NNJ125-250 pump was modelled, where Reynolds Averaged Navier Stokes (RANS) equations were solved through Spalart-Allmaras turbulence model. PISO algorithm was used for pressure-velocity coupling and stagnation pressure in and static pressure out were chosen for inlet and outlet boundary conditions respectively. Theoretical results were compared to computational ones, where an acceptable agreement was finally noticed between both. A new approach for PAT power plant design was also developed; where at each constant head, it was now possible and easy to know the most efficient PAT rotational speed. All computational results in this paper were achieved through a frozen rotor approach.

Peter and Varchola [130] carried out a numerical study on two mixed flow pumps, one with mixed-flow diffuser, and the other with an axial-flow diffuser, in both direct and reverse modes; aiming at examining the optimal operational parameters in both modes through a comparative scheme. A good agreement was noticed between Computational and experimental results.



Nautiyal et al. [132] presented a review of some already published works on PAT performance prediction through CFD. It was shown that CFD usage in the area of turbomachines has seen extensive growth in recent decades. Generally, manufacturers don't provide performance and flow characteristics of their pumps in turbine mode; so CFD has been a recent attempt for PAT performance prediction. It was mentioned that CFD made it possible to identify losses in different parts of PAT. However, there have been discrepancies between numerical and experimental predictions mainly from geometry simplification in computational studies, as reported in this paper. Nevertheless, it was pointed out that, numerical predictions accuracy would also depend on grid quality and numerical methods and used turbulence models. CFD was generally acknowledged as an effective design tool for PAT performance prediction.

Rawal and Kshirsagar [133] carried out a study through both numerical and experimental methods on a mixed flow pump with the objective of analyzing the accuracy of computational tools for PAT studies. The PAT flow was first numerically studied at five different flows, viz. 60%, 80%, 100%, 120%, and 140% of the BEP flow at a rotational speed of 1450 rpm. The k- $\epsilon$  turbulence model was adopted, where the chosen inlet and outlet boundary conditions were total pressure in and flow rate out, respectively. The experimental part was run at a test facility based at a major University in Karlsruhe, German (Figure 3-16). The single stage mixed flow pump with four mixed flow vanes was tested at three different speeds, viz. 800 rpm, 900 rpm, and 1000 rpm, under flows ranging from no load to maximum load. The agreement between computational and test results has been satisfactory. The numerical approach served in the identification of losses in PAT's different parts, and it was suggested that the use of finer mesh, better numerical methods and turbulence models, could improve on the numerical results accuracy.

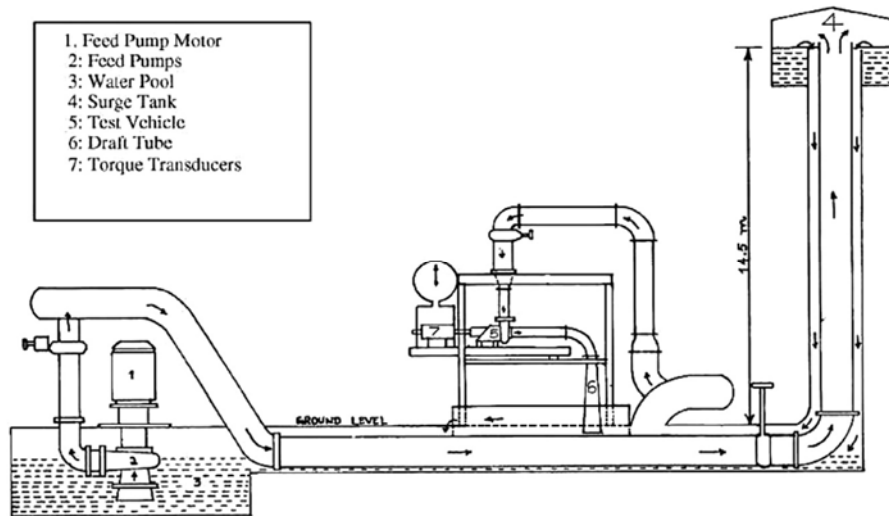


Figure 3-16 Karlsruhe University-based testing facility [96].

Baburaj et al. [134] presented a literature about the usage of computational methods for PAT flow studies, performance prediction playing a core role. As an example, a computational study was carried out on a single stage centrifugal pump at 2880 rpm. The CFD commercial code Ansys CFX was used where total pressure and mass flow rate were chosen for in and outlet boundary conditions, with the mass flow rate continually varied to come up with a complete PAT performance curve. The CFD usage for PAT flow studies was confirmed reliable.

Jovanović et al. [135] presented a comparative study between numerical and experimental results on a centrifugal pump running in both reverse and direct modes. In this paper, different PAT usages and performance prediction methods were discussed. From its different advantages over other mostly used methods, namely theoretical and experimental methods, CFD method was confirmed very effective for PAT flow studies. An example computational case-study was run through Ansys CFX commercial code, together with K- $\epsilon$  turbulence model for both modes, where extracted results were compared to collected experimental ones. Different frequently met problems in computational method usage were pointed out as well as their respective way outs. There was a good agreement between test and numerical results with comparatively small errors (less than 4%).

Milan et al. [136] simulated the flow in the middle stage of a radial flow multistage PAT to get the flow pattern information for efficiency improvement through geometrical modifications if by any means needed. CFD commercial code Ansys CFX was used to solve the fully unsteady three-dimensional RANS equations together with the shear stress transport (SST) turbulence model. The studied flow domain consisted of a six blades impeller with two different diameters (full and reduced) and an eight channels stator, where the selected boundary conditions were the flow rate and average static pressure for inlet and outlet boundary conditions respectively, for the turbine operational mode. Six interfaces, three rotor-stator and three stator-rotor interfaces, were used between rotor and stator, and the analysis was carried out at different rotational speeds and flow rates. The numerical results were in good agreement with experimental ones with an error of about 13% from the neglected loss estimations in the numerical study. Full diameter impeller version showed a comparatively better performance, and it was found that the multistage pump doesn't need any modification to become more efficient as it could get sufficiently higher efficiencies, unmodified.

### 3.6.3 Pump-turbines stability aspects

The general system stability aspect was defined by Greitzer [137] as the ability of the system to recover its initial state after a certain perturbation, where the system can either exhibit static or dynamic stability. The criterion for stability of the pump turbine is called dynamic when the shaft is disconnected from the generator and the speed of rotation varies with the unbalanced torque; On the other hand, when the pump turbine is connected to the generator with a frequency proportional to the electric grid frequency a static stability criterion applies [138]. In their everyday operations, pump turbines go through frequent switching between pump and turbine modes, thus sometimes working under off-design conditions. The fact that these machines can rotate and deliver the flow in two opposite directions, confer them the so called “four quadrants” operational characteristics at specific guide vane openings, allowing them to operate under five defined regimes, viz. turbine, turbine brake, pump, pump brake, and reverse pump (see Figure 3-17). Each regime characteristics and working conditions were presented by Amblard et al. [139].

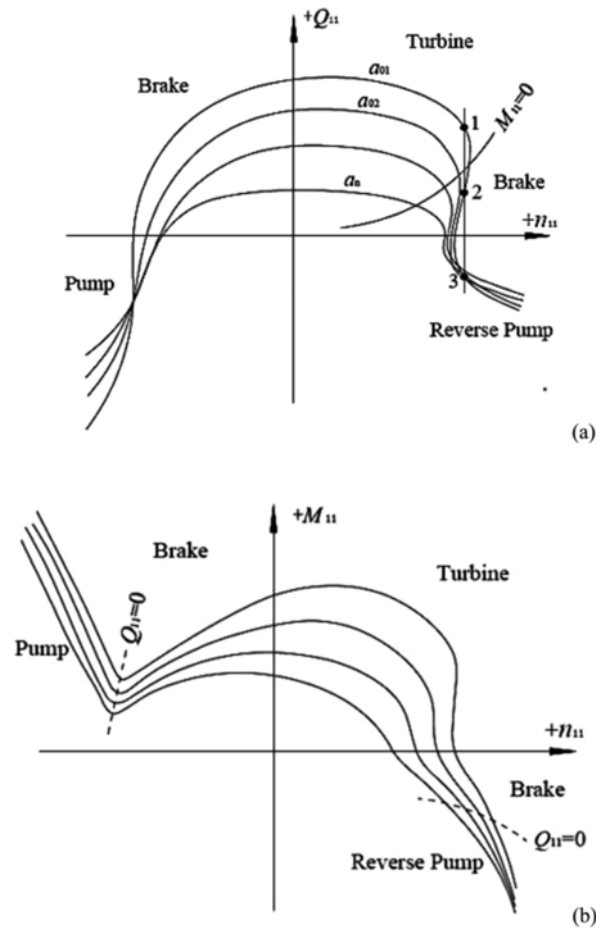


Figure 3-17 Four quadrant characteristics of a reversible pump turbine a) Flow-speed curve [139]

A pump turbine is basically a compromise between the pump and turbine but the geometry is more like the pump. Pump turbines are generally known to have steeper speed-flow characteristics than Francis turbines of same specific speeds, which under certain operating conditions, may be the source of stability problems within the machine. The pump turbine stability aspect can thus be assessed through the slope of its characteristics curves for both pumping and turbine modes through head-flow and flow-speed curves [85].

Because the pump mode of operation is known to be very sensible to decelerated flow field, which results in flow separation and related hydraulic losses as well as possible self-excited vibrations; the design of pump turbines has to be carried out with a big emphasis on the pump operating mode characteristics. [85].

Pérez-Díaz et al. [140] have classified the pump turbines instability features into two types; the first occurring at low load off-design operating conditions closer to the runaway (zero torque) in

turbine mode, otherwise called the “s-shaped” characteristics (Figure 3-18), and the second occurring at part-load in pumping mode, generally called the “saddle-type” characteristics or hump characteristics.

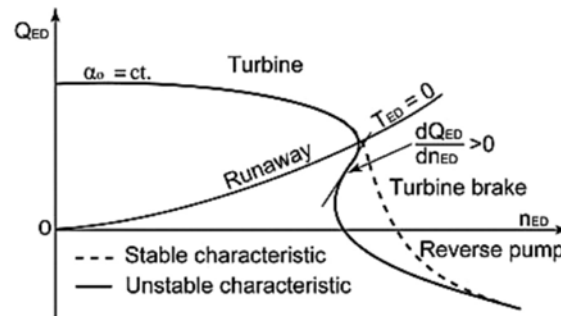


Figure 3-18 S-shape characteristics of a pump turbine [140].

According to Gentner et al. [141], the flow instability occurs in turbine mode when the head-flow and speed-flow curves have negative and positive slopes respectively ( $dQ/dH < 0$  and  $dQ_{ED}/dn_{ED} > 0$ ), whereas for pump mode instability, the head-flow curve presents a positive slope ( $dQ/dH > 0$ ) (see Figure 3-19).

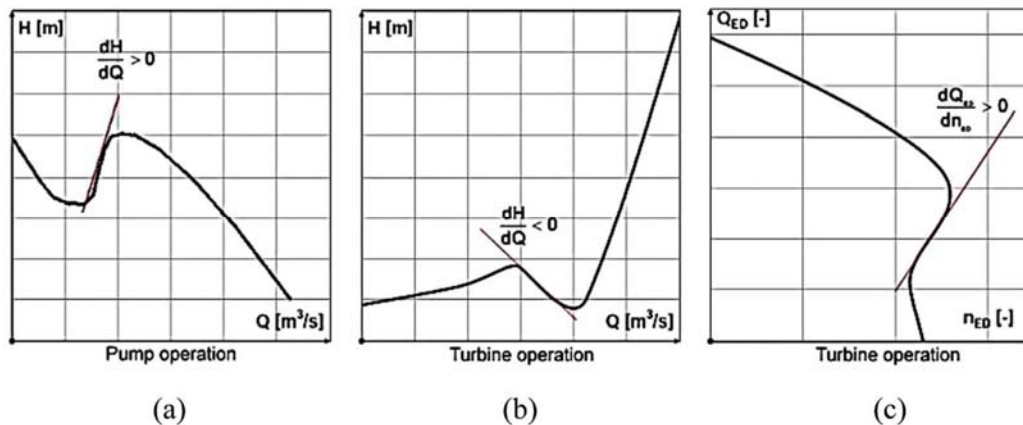


Figure 3-19 turbine instability conditions for both reverse (b, c) and conventional (a) modes [141].

Another necessary but not sufficient instability criterion for pump-turbine generating mode was derived by Martin [142], and state that the slope of Torque-Speed characteristic ( $T_{ED} - n_{ED}$ ) must be positive. However, with this slope being slightly positive, the system can still present stable characteristics depending on the fluid or the slope of flow-speed characteristics ( $Q_{ED} - n_{ED}$ ). The discharge, speed and Torque factors ( $Q_{ED}$ ,  $n_{ED}$  and  $T_{ED}$ ) are expressed as:

$$\begin{aligned}Q_{ED} &= Q/D^2\sqrt{gH} \\n_{ED} &= nD/\sqrt{gH} \\T_{ED} &= T/\rho gHD^3\end{aligned}$$

Equation 3-7

### 3.6.3.1 S-shaped characteristics

The S-shape induced instabilities are associated with fluctuations in flow rate, torque, speed, and head that have negative effects on the pump turbine start up, synchronization with the grid, and load rejection processes. For pump-turbines operating in the S-shaped operating characteristics region, some speeds correspond to three different flow conditions with a positive slope along the operating line which results in both positive and negative torques which can easily damage the pump-turbine components [143],[144]. At the start up, the machine works at no-load conditions where the acquired hydraulic energy is totally dissipated in form of energy losses. The developed flow instability at these areas is characterized by torque fluctuations and can, at a certain point, affect the machine operating mode as well as inflicting significant fluctuations of head and flow with possible self-excited vibrations and noise [102]. For runners, it has been generally found that, in terms of operational damage, one start-up operation is equivalent to years of operation under normal operating conditions [145],[146].

Many researchers such as: Seidel et al. [147], Hasmatuchi et al. [148], Gentner et al. [141], Houdeline et al. [149], Wang et al. [150], Sun et al. [151], Sun et al. [144], Li et al. [152], Cavazzini et al. [153], Yin et al. [154], Guggenberger et al. [155], Zhang et al. [156] Casartelli et al. [157], Billdal and Wedmark [158], Chen et al. [159], Edinger et al. [160], Gong et al. [161], Stens and Stefan [162], Liu et al. [163], have tried to explain the S-shape instabilities occurrence reasons and related flow dynamics, and the progress so far is of a substantial value. It was generally found that the S-shape induced instabilities are due to the head increase at part load, which is, in turn, associated to the blockage of some impeller channels by a developed rotating stall.

### 3.6.3.2 Saddle-type or Hump characteristics

The saddle-type pump instability is undoubtedly the most challenging problem to face in order to significantly increase the operating range of pump-turbines in pumping mode, even in case of variable speed pump-turbine. The operation stability for a pump turbine operating in pumping mode is only attained when the difference of head between steady state characteristics of the water conduit and the pump, increases with increasing flow [164]. Any slight deviation from the system stability characteristics will result in system flow unsteadiness- induced abnormalities.

Hump characteristics are a main feature of unstable behavior in pump turbines, which happen in pump mode under small discharge operation conditions [141], where strong noise can be heard during the starting period and the start time is prolonged [165]. Many more studies such as: Ješe et al. [166], Yao et al. [167], Li et al. [168], Liu et al. [169], Li et al. [170], Braun et al. [171], Liu et al. [172], have been carried out aiming at investigating, and by the way understanding the pump turbine instability under pump mode operating conditions.

Many other objectives that can be found in literature all has been considered by many researchers, where the highlights can be listed as follow:

Flow instability-related hydraulic phenomena

- a) Rotating stall
- b) Cavitation
- c) Rotor-stator interactions (RSI)

Pump-turbine stability improvement attempts

- a) Misaligned guide vanes (MGV)
- b) Inlet valve throttling
- c) Case-sensitive attempts





## 4 Selection of PATs

### 4.1 Methodology

Various researchers have theoretically and practically presented relations to select a proper PAT for known hydraulic data. [Figure 4-1](#) and [Figure 4-2](#) show some data reported for the centrifugal PAT head ratio ( $h$ ) and discharge ratio ( $q$ ) based on the pump head and discharge respectively [\[21\]](#) [\[22\]](#):

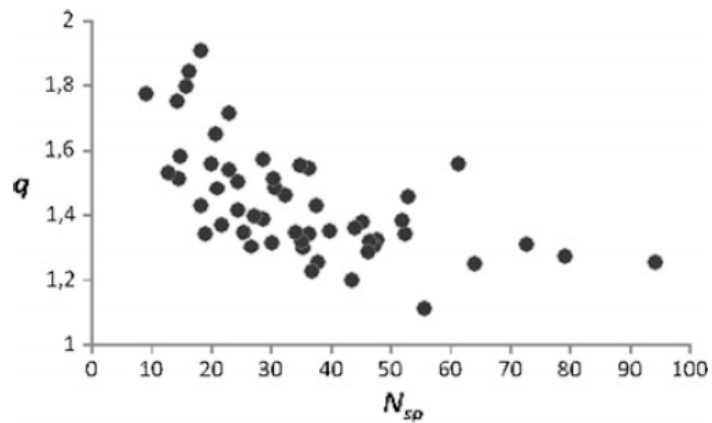


Figure 4-1 Head ratios of the tested PATs with various pump specific speeds [20]

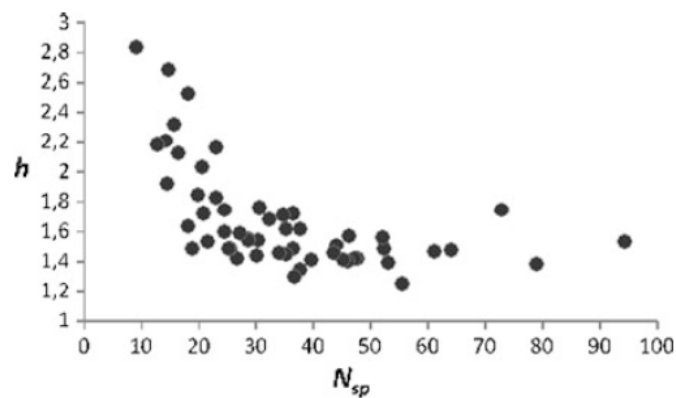


Figure 4-2 Discharge ratios of the tested PATs with various pump specific speeds [21]

The equations correspondent to the both [Figure 4-1](#) and [Figure 4-2](#) are:

$$h = \frac{H_T}{H_p}, q = \frac{Q_T}{Q_p}$$

Equation 4-1

In these figures, the  $h$  and  $q$  of the PATs are shown in relation to the pump specific speed and maximum efficiency. The definition of the specific speed of the pump is:

$$N_{sp} = N_P \frac{Q_p^{0.5}}{H_p^{0.75}}$$

Equation 4-2

It can be observed that two pumps with the same specific speeds could have a different  $h$  and  $q$ .

For  $N_{sp} < 50$ , a higher specific speed leads to a higher efficiency for the fixed head drop. However, for  $N_{sp} > 50$ , it is the reverse. From [Figure 4-1](#) and [Figure 4-2](#), it is clear that the lowest  $h$  and  $q$  are related to  $N_{sp} > 50$ .

A recent study developed by Novara et al. [25, 26] shows a set of PATs where the HBEP and QBEP have been plotted on the logarithmic H-Q space as in [Figure 4-3](#), highlighting with different colors the maximum efficiency of each machine for the radial PAT range presented by Chapallaz [27].

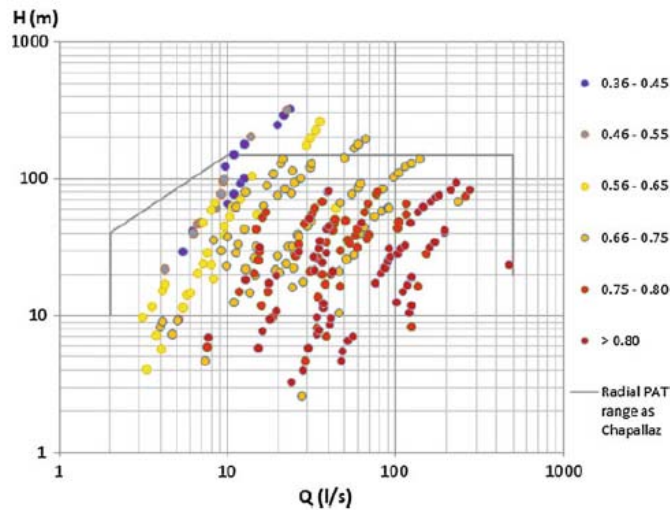


Figure 4-3 PAT maximum efficiency ranges against the H-Q space [25,26]

References [25] , [26] have developed analyses based on several PATs and proposed a three-dimensional representation of PAT efficiency (where  $N_s$  corresponds to  $N_{sp}$ ).

These selected machine PAT plus generator units are shown in Figure 4-4, while a two-dimensional contour chart similar to the one proposed for pumps by [27] is presented in Figure 4-5.

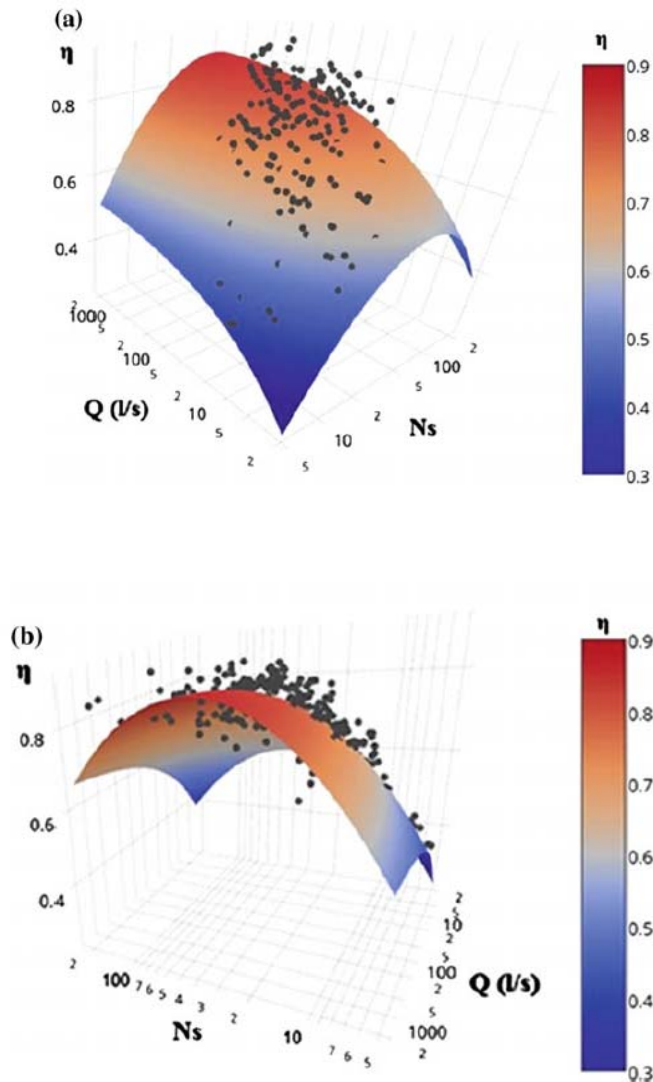


Figure 4-4 Proposed 3D representation for PAT efficiency estimation against the real efficiency of selected machines [28]

According to Figure 4-5, PATs with higher capacity and medium specific speeds of 50 have a better efficiency: to obtain the maximum efficiency in a pump working in reverse mode, devices

with lower rotational speeds and higher capacities are recommended for specific speeds less than 50.

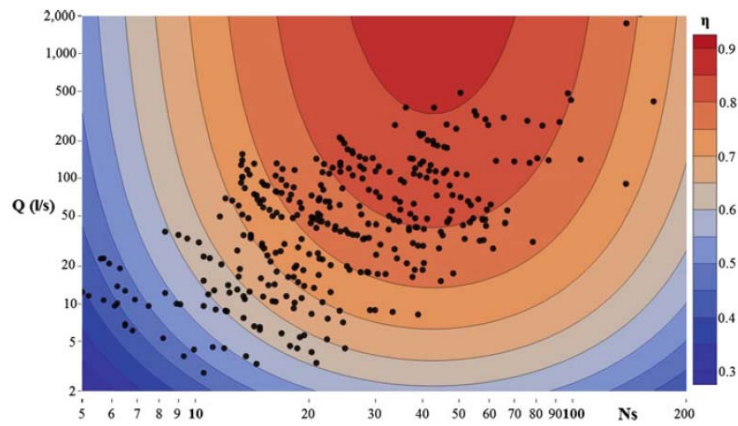


Figure 4-5 2D contours of the proposed function for PAT efficiency plotted against the nominal flow rate and specific speed of selected machines [28]

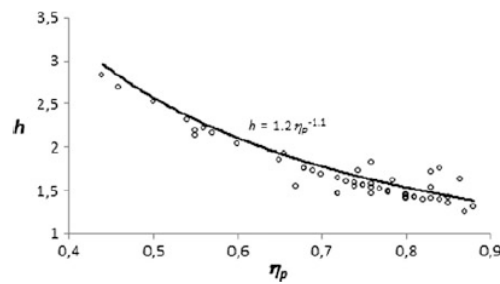


Figure 4-6 Head ratios of tested PATs with various pump maximum efficiencies [20]

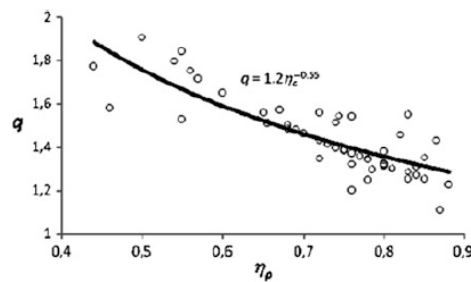


Figure 4-7 Discharge ratios of tested PATs with various pump maximum efficiencies [20]

Based on PAT theory [20], pumps with a higher efficiency work in lower  $h$  and  $q$  in turbine modes. From Figure 4-6 and Figure 4-7, the following relations can be found:

$$h = \frac{1.2}{\eta_p^{1.1}}$$

Equation 4-3

$$q = \frac{1.2}{\eta_p^{0.55}}$$

Equation 4-4

From Figure 4-8, the pump specific speed can be selected using the turbine specific speed with the following estimated relation:

$$N_{sp} = 1.125 N_{st} + 1.73$$

Equation 4-5

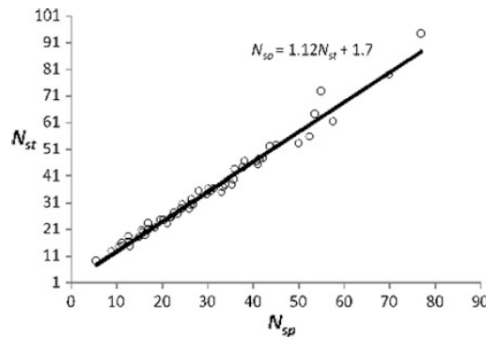


Figure 4-8 Turbine specific speed versus pump specific speed [20]

where:

$$N_{st} = N_t \frac{Q_t^{0.5}}{H_t^{0.75}}$$

Equation 4-6

It is useful to mention that a pump in inverse mode operates at its BEP always with a flow rate and head drop larger than in direct mode. Therefore, energy dissipations connected with the flux of water in the machinery are also greater in reverse mode.

There are various methods available in literature to select  $h$  and  $q$ , based on theoretical and practical issues presented by certain researchers. However, none of the methods presented can

predict the PAT behavior perfectly. The most commonly used methods to obtain values of h and q are summarized in Table 4-1.

In Figure 4-9 and Figure 4-10, the results of the design methods of Equation 4-3 and Equation 4-4 are compared with the results of the methods presented by Stepanoff and Sharma.

Method	h	q
Stepanoff	$\frac{1}{\eta_{p,BEP} \eta_{p,BEP}}$	$\frac{1}{\eta_{p,BEP}}$
Gopalakrishnan	$\frac{1}{(\eta_{p,BEP})^2}$	$\frac{1}{\eta_{p,BEP}}$
Childs	$\frac{1}{(\eta_{p,BEP})^2}$	$\frac{1}{(\eta_{p,BEP})^2}$
Sharma	$\frac{1}{(\eta_{p,BEP})^{1.2}}$	$\frac{1}{(\eta_{p,BEP})^{0.8}}$
Alatorre-Frenk	$\frac{1}{0.85\eta_{p,BEP}^5 + 0.385}$	$\frac{0.85\eta_{p,BEP}^5 + 0.385}{2\eta_{p,BEP}^{9.5} + 0.205}$
Nautiyal [41]	$41.667 \frac{\eta_{p,BEP}^{-0.212}}{\ln(N_{s,q,pump})} - 5.042$	$30.303 \frac{\eta_{p,BEP}^{-0.212}}{\ln(N_{s,q,pump})} - 3.424$
Grover	$2.693 - 0.229N_{s,q,turbine}$	$2.379 - 0.0264N_{s,q,turbine}$

Table 4-1 Review of methods to determine non-dimensional head and flow parameters (adapted from [30])

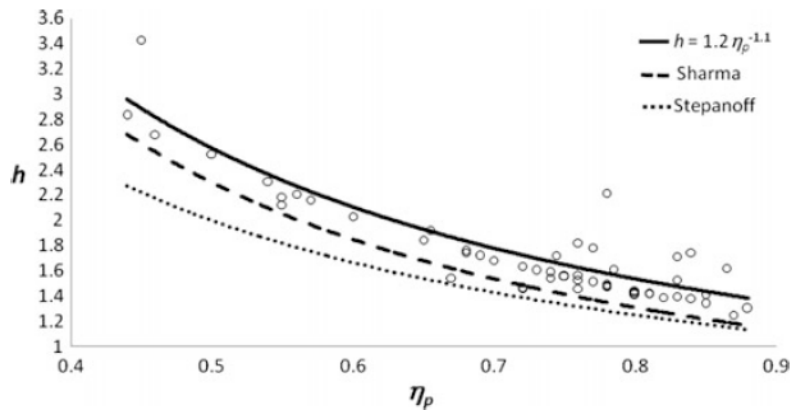


Figure 4-9 h of the tested PATs with various pump maximum efficiencies [20]

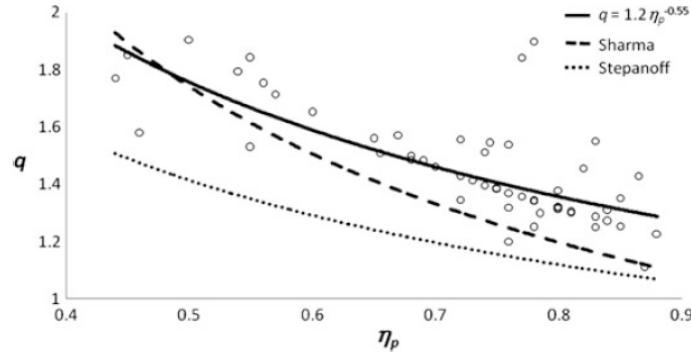


Figure 4-10  $q$  of the tested PATs with various pump maximum efficiencies [20]

## 4.2 Estimation of Characteristic Curves

Although a PAT may work at off-design conditions, most prediction methods have only predicted the BEP of the PAT. Therefore, estimating the complete characteristic curve of a PAT based on its BEP would be very expedient. Experimental data have shown that the dimensionless characteristic curves of centrifugal PATs based on their BEP are approximately the same. The above-mentioned dimensionless head and power curves of a PAT can be estimated as below, using second and third order polynomials, respectively [31] and [32]:

$$\frac{H_t}{H_{tb}} = 1.0283 \left( \frac{Q_t}{Q_{tbep}} \right)^2 - 0.5468 \left( \frac{Q_t}{Q_{tbep}} \right) + 0.5314$$

Equation 4-7

$$\frac{P_t}{P_{tb}} = -0.3092 \left( \frac{Q_t}{Q_{tbep}} \right)^3 + 2.1474 \left( \frac{Q_t}{Q_{tbep}} \right)^2 - 0.8865 \left( \frac{Q_t}{Q_{tbep}} \right) + 0.0452$$

Equation 4-8

To predict the operation of a PAT outside the BEP, other experimental reports are obtained from tests carried out on seven types of pumps, supplied by Caprari, with  $N_s$  between 14 and 16 ( $m, m^3 / s$ ) (Artina, Bragalli, Liserra, Marchi, & Naldi, 2010) The efficiency curve can be obtained for each point by:

$$\frac{H_t}{H_{tbep}} = 1.1154 \left( \frac{Q_t}{Q_{tbep}} \right)^2 - 0.7481 \left( \frac{Q_t}{Q_{tbep}} \right) + 0.6239$$

Equation 4-9

$$\frac{P_t}{P_{tbep}} = -0.3351 \left( \frac{Q_t}{Q_{tbep}} \right)^3 + 2.4269 \left( \frac{Q_t}{Q_{tbep}} \right)^2 - 1.3673 \left( \frac{Q_t}{Q_{tbep}} \right) + 0.2581$$

Equation 4-10

$$\eta_t = \frac{P_t}{(\rho \cdot g \cdot Q_t \cdot H_t)}$$

Equation 4-11

However, it must be noted that this method can only provide an approximate view of the characteristic curves of a PAT.

In a recent study [33] a large data set relative to the behavior of 17 different pumps operating as turbines has been analyzed, as shown in Table 4-2. The following considerations were possible by means of the comparison of the classic affinity law with experimental data:

- the agreement between the experimental and the calculated curves is worse when the difference between the rotational speed of the prototype and that of the simulated machine increases;
- the entity of the discrepancies is not dependent on the machine type;
- when the characteristic curves are calculated by means of the affinity law and Suter parameters with a 20% difference in rotational speed compared to the prototype, the error in the evaluation of the head drop is lower than 3%;
- out of the above-mentioned range of differences in rotational speed compared to the prototype, the error in the evaluation of the head drop could be as large as 12%, and the mean error in the whole range of rotational speed is 4.8%;



- the error in the evaluation of  $\eta$  is less than 15%, if the difference in rotational velocity with the prototype ranges between  $-40\%$  and  $+50\%$ ;
- out of the above-mentioned range of differences in rotational speed compared to the prototype, the error in the evaluation of  $\eta$  could be even larger than 40%, and the mean error in the whole range of rotational speed is 7.1%.

Table 4-2 Machine data set

PAT	Pump type	No. of stages	Speed range (rpm)
a	HCM	2	1550–3050
b	HCM	2	1550–3050
c	HCS	1	1550–3050
d	HCS	1	1550–3050
e	HCS	1	1550–3050
f	SSS	1	780–1550
g	SSS	1	1050–1550
h	SSS	1	780–1550
i	SSS	1	780–1860
j	SSS	1	780–1860
k	SSS	1	780–1550
l	SSS	1	780–1550
m	SSS	1	750–1550
n	HCM	3	1550–3050
o	HCM	4	1550–3050

(HCM Horizontal Centrifugal Multi-stage, HCS Horizontal Centrifugal Single-stage, SSS Submersible Semiaxial Single-stage)

To overcome these problems, a new model (Relaxation of the Affinity Equations—RAE) for the estimation of the performance of semi-axial PATs has recently been proposed, based on the following experimental evidence:

- the efficiency at the BEP attains its maximum value  $\eta_B^{MAX}$  for a specific rotational speed  $N_{max}$ , and  $N_{max}$  depends on some geometrical parameters of the machine;

- the position of the BEP at a certain value of speed ( $N$ ) depends on the ratio ( $N/N_{MAX}$ );
- generalized dimensionless performance curves  $h = h(q)$ ,  $p = p(q)$  and  $e = e(q)$  can be defined for a given pump type, based on experimental results (instead of Suter parameters), where:

$$q = \frac{Q}{Q_B} \quad h = \frac{H}{H_B} \quad P = \frac{P}{P_B} \quad e = \frac{\eta}{\eta_B}$$

Equation 4-12

In [Figure 4-11](#) the geometrical parameters of a semi-axial PAT useful for the identification of  $N_{MAX}$  are shown:  $D$  is the diameter of the runner,  $u$  the diameter of the PAT body and  $F$  the length of the PAT stage. The following relation was found to be representative of the experimental results:

$$N_{max} = \alpha D^\beta \varphi^\gamma F^\delta$$

Equation 4-13

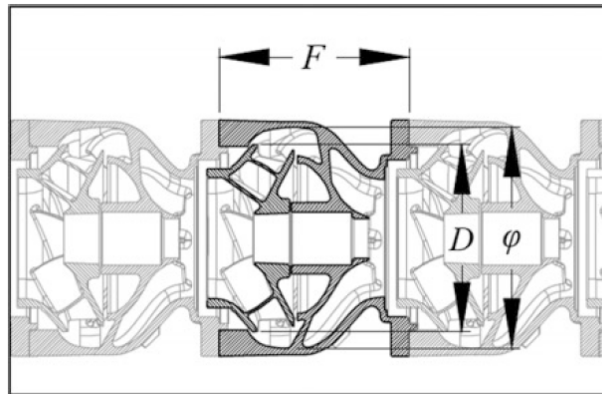


Figure 4-11 Geometrical parameters of a semi-axial PAT [34].

The new generalized characteristic and efficiency curves determined by a calibration with the experimental data set of the Submersible Semi-axial Single-stage pumps of [Table 4-2](#) Machine data set are plotted in [Figure 4-11](#). By the use of RAE, the error in the evaluation of the head drop has been reduced to 3.9%, and the error in the evaluation of  $\eta$  has been reduced to 2.5%, compared with a 4.8 and 7.1% error, respectively, relating to the classic affinity law ([Figure 4-12](#)).

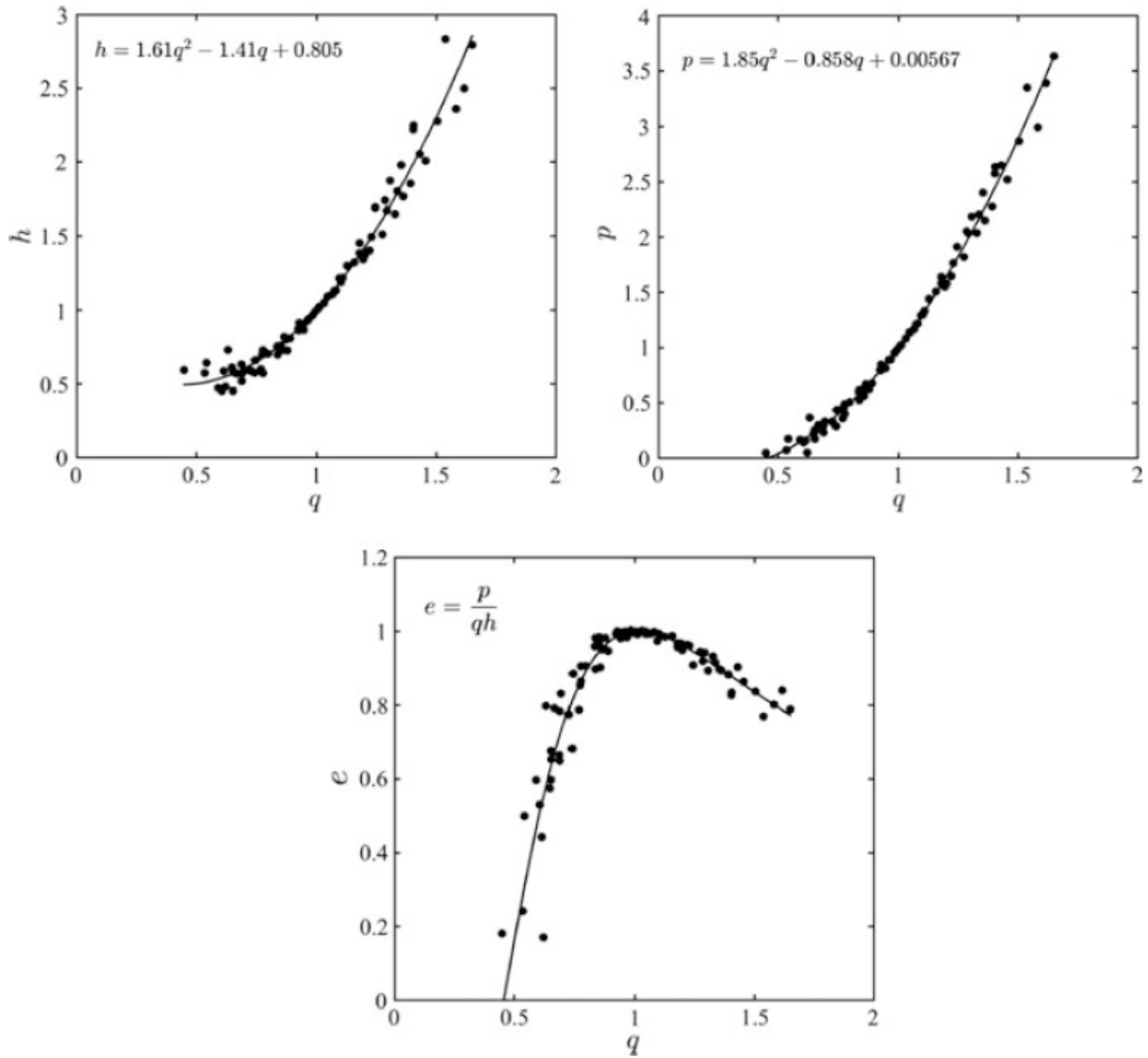


Figure 4-12 Generalized characteristic and efficiency curves by RAE [34]

Even if no such an in-depth analysis has been performed for other pump types, some recommendation can be derived in the use of the affinity law for all pump types and in the design of mini and micro hydro power plants using industrial PATs. The potential discrepancies in terms of pressure drop and efficiency between the real PAT behavior and the theoretical prediction are small for small differences in rotational speed compared to the test conditions ( $\pm 20\%$ ). Even in the presence of large differences in the rotational speed the error in terms of pressure drop is contained, but the difference in terms of efficiency could become huge. As a consequence, in the absence of any experimental data coming from industrial tests, the main problem in power plant design could be an overestimation of the PAT production.

## 4.3 Performance, Stability and suitable Machinery

### 4.3.1 Introduction

The main challenge related to PAT field application is that pump manufacturers do not usually provide the performance curves of pumps running in reverse mode. The designer therefore lacks data, which negatively affects the choice of the most suitable machine. Therefore, establishing a correlation that enables the transformation from pump performance curves to turbine performance curves is crucial. Many researchers have presented some theoretical and empirical relationships for predicting the Best Efficiency Point (BEP) of a PAT.

Derakhshan and Nourbakhsh tested several centrifugal pumps while running as turbines and derived some relationships to predict the respective best efficiency points based on pump hydraulic characteristics. Two equations were also presented to estimate the complete characteristic curves based on their best efficiency point [20].

The same authors predicted the best efficiency point of an industrial centrifugal pump running as a turbine by using a theoretical analysis and also simulated the pump in direct and reverse modes by using a three-dimensional computational fluid dynamic model [21]. More recently, Derakhshan and Kasaeian have further investigated the use of computational fluid dynamic tools to optimize the geometry of the blades of an axial pump used as a propeller turbine, to achieve maximum hydraulic efficiency [22].

Barbarelli et al. [23] presented a one-dimensional numerical code, with the aim of identifying the geometry and performance of a generic PAT based on passage sections and losses in each section of the machine. Starting from catalogue information and using design techniques, the one-dimensional numerical code computes a virtual geometry and then calculates fluid dynamic losses to estimate the geometrical parameters involved in the simulation. The method was validated by using laboratory test data for six PATs.

Barbarelli et al. [24] also presented the results of an experimental and theoretical activity regarding PATs. The experimental activity dealt with twelve pumps measured both on a test rig and during normal operation. A statistical method involving polynomials was implemented, thus allowing the determination of performance curves.

#### 4.3.2 Model Description

The knowledge of the geometrical parameters of a generic PAT is fundamental both for calculating the hydraulic losses and the characteristic curves. The proposed idea consists of the reconstruction of a geometric model or prototype to refer to the application of hydraulic correlations of habitual use. This prototype has to be similar to the machine studied but simpler.

Figure 4-13 shows the geometrical shape taken as a reference. The geometric model presents a straight conical suction and a volute with a rectangular section with linearly variable height. The final diffuser has a truncated pyramid shape.

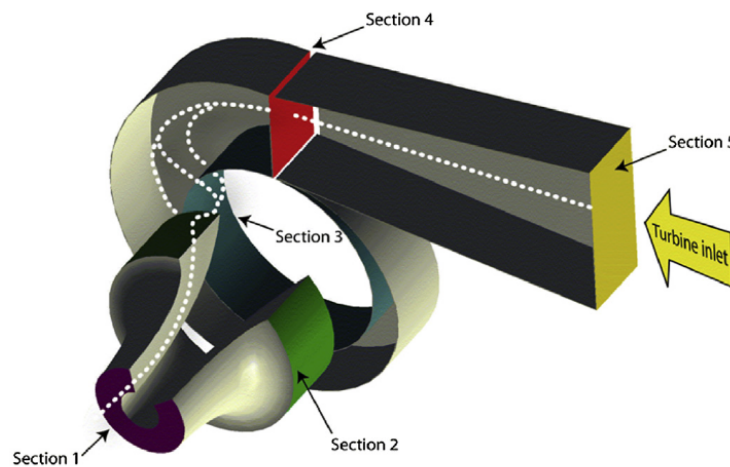


Fig. 1. Reference geometry.

*Figure 4-13 Reference geometry. [23]*

All useful geometrical parameters are computed as Lobanoff [3] suggests. The sizing procedure of the reference prototype needs the knowledge of 6 parameters available in the manufacturers catalogues: head ( $H_e$ ) and flow rates ( $Q_e$ ) at BEP of the pump, maximum power  $QP_e$ , head ( $H_{mo}$ )

at the shut off, impeller diameter ( $D_2$ ) and size of the pump ( $Y_p$ ). It also makes use of other secondary parameters like surface roughness, blade thickness, clearances, materials employed and so on, which do not change significantly from pump to pump. They are estimated by experience and directly implemented in the model.

In [Figure 4-14](#) a flow chart, which summarizes the fundamental steps related to the geometry calculus, is illustrated. All the above-described inputs are highlighted in the orange boxes (in the web version) while the outputs are set in the blue boxes (in the web version).

The main input visible in [Figure 4-14](#) is the specific speed  $n_s$  of the PAT defined as:

$$n_s = n \frac{\sqrt{Q_e}}{H_e^{0.75}}$$

*Equation 4-14*

This parameter is the input of the 4 blocks (design charts) stacked on the left of the figure:

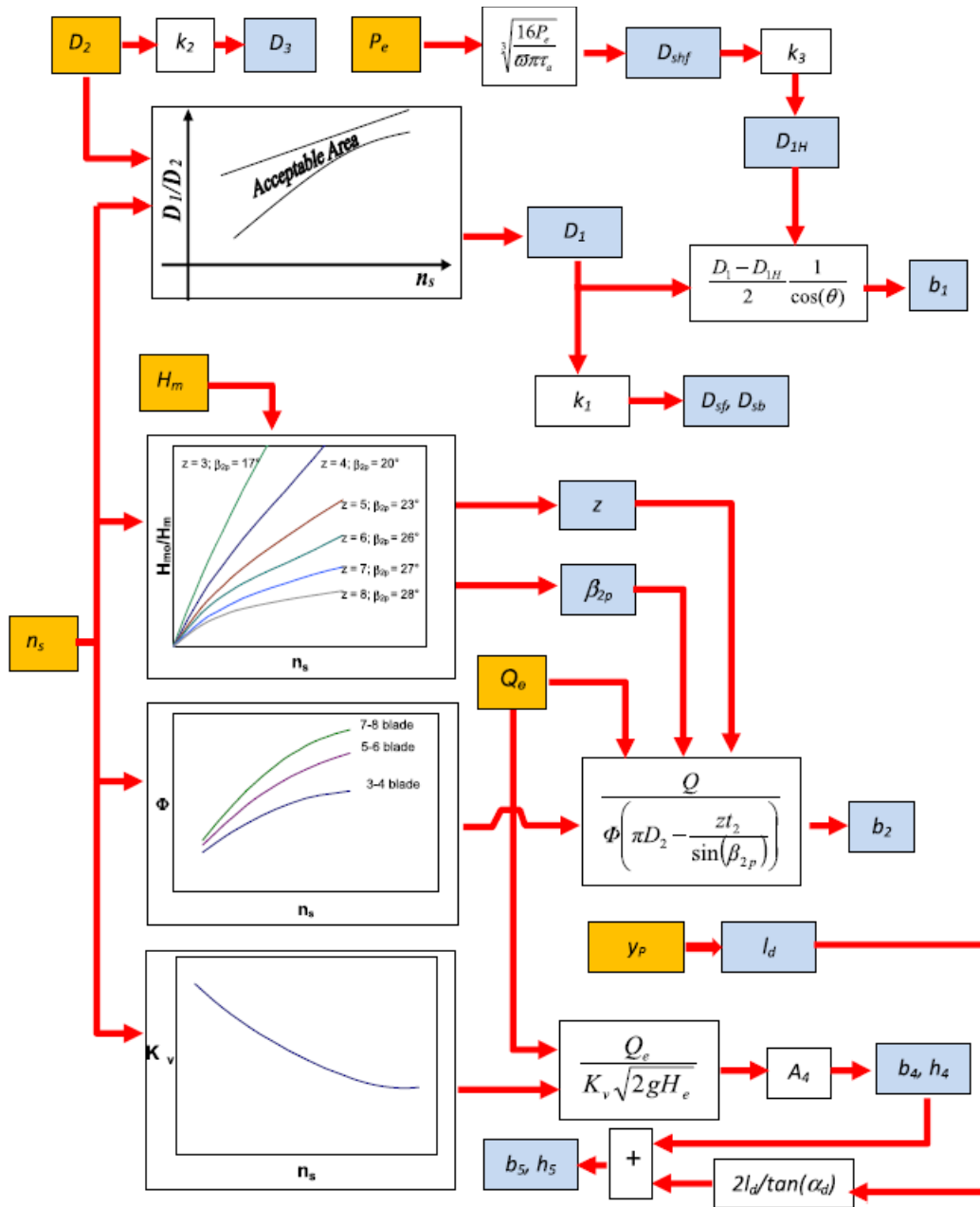


Figure 4-14 Flow chart of the geometry modelling. [23]

From the first block ( $D_1/D_2$  vs  $n_s$ ) it is possible to get the impeller eye diameter ( $D_1$ ); this parameter allows calculating the impeller width ( $b_1$ ) at section 1 as:

$$b_1 = \frac{D_1 - D_{1H}}{2} \frac{1}{\cos(\theta)}$$

Equation 4-15

The  $\theta$  angle represents the inclination of the blade with respect to the radial direction. For all the pumps measured at the hydraulic laboratory of the DIMEG this parameter is about  $40^\circ$ . The hub diameter  $D_{1H}$  present in Equation 4-15 is calculated once the shaft diameter  $D_{shf}$  is defined by means of the maximum power  $P_e$  of the pump as:

$$D_{shf} = \sqrt[3]{(16P_e) / \pi \tau_a}$$

Equation 4-16

The formula is applied by referring to iron usually employed for these applications with a torsional stress  $\tau_a$  of 7.5 MPa on average [35]. The hub diameter  $D_{1H}$  is then calculated as:

$$D_{1H} = k_3 D_{shf}$$

Equation 4-17

From measurements taken on the sample pumps it results that the coefficient  $k_3$  is about 1.5.

From the second block ( $H_{m0}/H_m$  vs  $n_s$ ) the number of blades  $z$  and the vane angle ( $\beta_{2b}$ ) can be obtained.

From the third block ( $\Phi$  vs  $n_s$ ) the impeller width ( $b_2$ ) at section 2 can be determined as follows:

$$b_2 = \frac{Q_e}{\Phi \left( \pi D_2 - \frac{z \tau_2}{\sin(\beta_{2p})} \right)}$$

Equation 4-18

The thickness  $t_2$  to which the model refers is set to 0.002 m. From the fourth block ( $K_v$  vs  $n_s$ ) the exit volute Area  $A_4$  can be determined as:

$$A_4 = \frac{Q_e}{K_v \sqrt{2gH_e}}$$

Equation 4-19



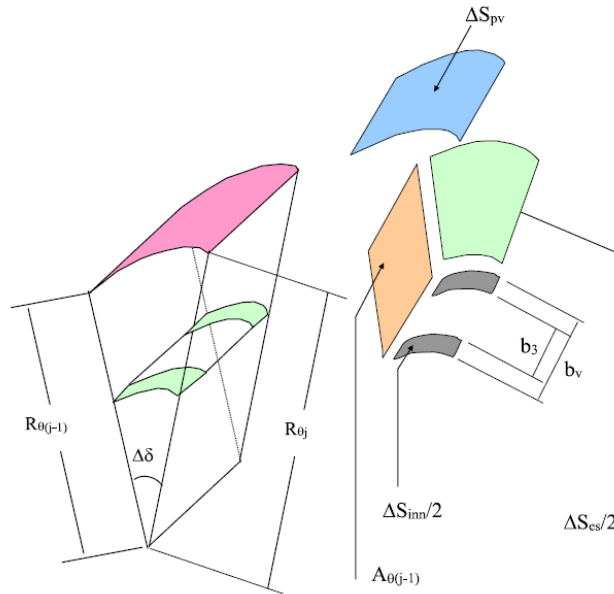


Figure 4-15 Geometry of the sector  $j$  [23].

Volute width ( $b_4$ ) is constant and equal to the maximum value between the square root of  $A_4$  and a recommended value related to the impeller width  $b_2$ . Volute height is, on the contrary, variable along the angular position, with linear law, from zero to  $h_4 = b_4$ . In the next sections, the two parameters  $h_4$ ,  $b_4$  are also identified as  $b_v$  and  $h_v$  (throat section of the volute).

Finally, the final diffuser length  $l_d$  is derived from the pump height  $y_p$ : this data available in the catalogue represents the distance between the center of the impeller and the diffuser exit. By considering that the diffuser is designed as a truncated pyramid with an inclination angle  $\alpha_d$ , the final size of this component, set as a square section, is obtained as:

$$h_5 = b_5 = b_4 + 2 \frac{l_d}{\cos \alpha_d}$$

Equation 4-20

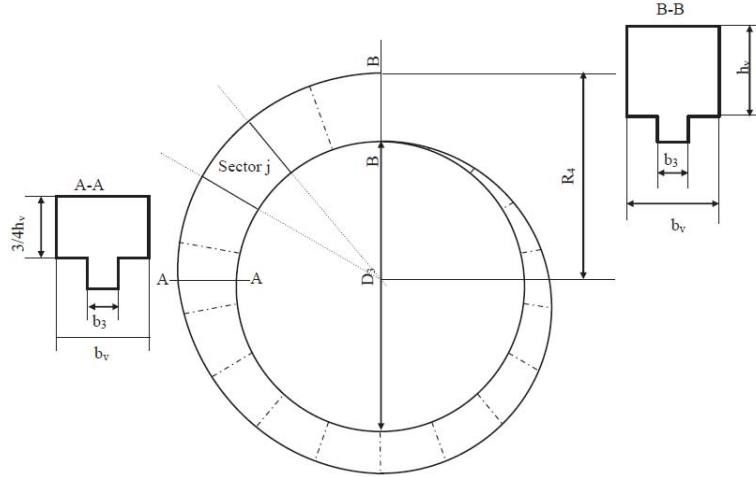


Figure 4-16 Outline of the volute geometry. [23]

The angle  $\alpha_d$  to which the model refers, is set to  $3.5^\circ$

Table 4-3 Hydraulic losses. [23]

	Friction losses	Dynamic losses
Inlet	$h_{fd} = \frac{\lambda}{8 \sin(\alpha_d)} \left[ 1 - \left( \frac{A_4}{A_5} \right)^2 \right] \frac{c_1^2}{2g}$	$h_{dd} = 0.5 \cdot \left[ 1 - \left( \frac{b_4}{b_5} \right)^2 \right] \frac{c_1^2}{2g}$
Volute	$h_{fv} = \sum_{j=1}^N \lambda \frac{c_1^2}{2g} \frac{(\Delta S_{vj} + \Delta S_{vn} + \Delta S_{vj})}{4A_{vj}} \frac{Q}{Q}$	
Vaneless diffuser	$h_{fc} = \frac{\lambda}{2g} \frac{1}{D_3} \frac{c_{m1}^2}{\sin(\alpha_d)} \frac{D_1}{D_2} \left( \frac{D_1 - D_2}{2} \right) h_{lowflow} = k (Q - Q_{BEP})^2$	$h_{inlet} = 0.5 \cdot \left( 1 - \frac{D_2 b_2}{D_1 b_1} \right) \frac{c_{m1}^2}{2g}$
Impeller	$h_{fi} = \lambda \frac{w_2^2}{2g} \left( \frac{L}{D_{hw}} \right)$	$h_{shock} = \frac{[w_2 \sin(\beta_{2f} - \beta_{2p})]^2}{2g}$
	$h_{dmg} = C_D \sigma \frac{w_2^2}{2g} \frac{1}{\sin \beta_w}$	$h_{sr} = (\xi_1 - 1) \frac{c_2^2}{2g}$
Discharge	$h_{dsc} = 0.25 \left( \frac{Q/\pi D_2^2}{4} \right)^2 \frac{1}{2g} + \frac{c_2^2}{2g}$	

### 4.3.3 Calculation of the losses model

The losses model is strictly referred to that exposed in [36] with in addition the evaluation of the losses in the diffusion region between the volute and the impeller due to vortex motions which happen mainly due to low flow rates [37].

The calculation model is applied to the various sections of the above-developed geometric prototype and shown in Figure 4-13. The losses evaluation is divided into: inlet (Section 5), volute (Section 4), diffusion region (Section 3), impeller (Section 2) and discharge (Section 1).

The velocity triangles are determined at Sections 1 and 2 of the impellers. In the diffusion region, between impeller and volute, velocities are determined assuming a free vortex motion ( $c_u \cdot r = \text{const}$ ). In order to obtain velocities along the volute, it was ideally divided into  $N$  sectors (see Figure 4-15 and Figure 4-16).

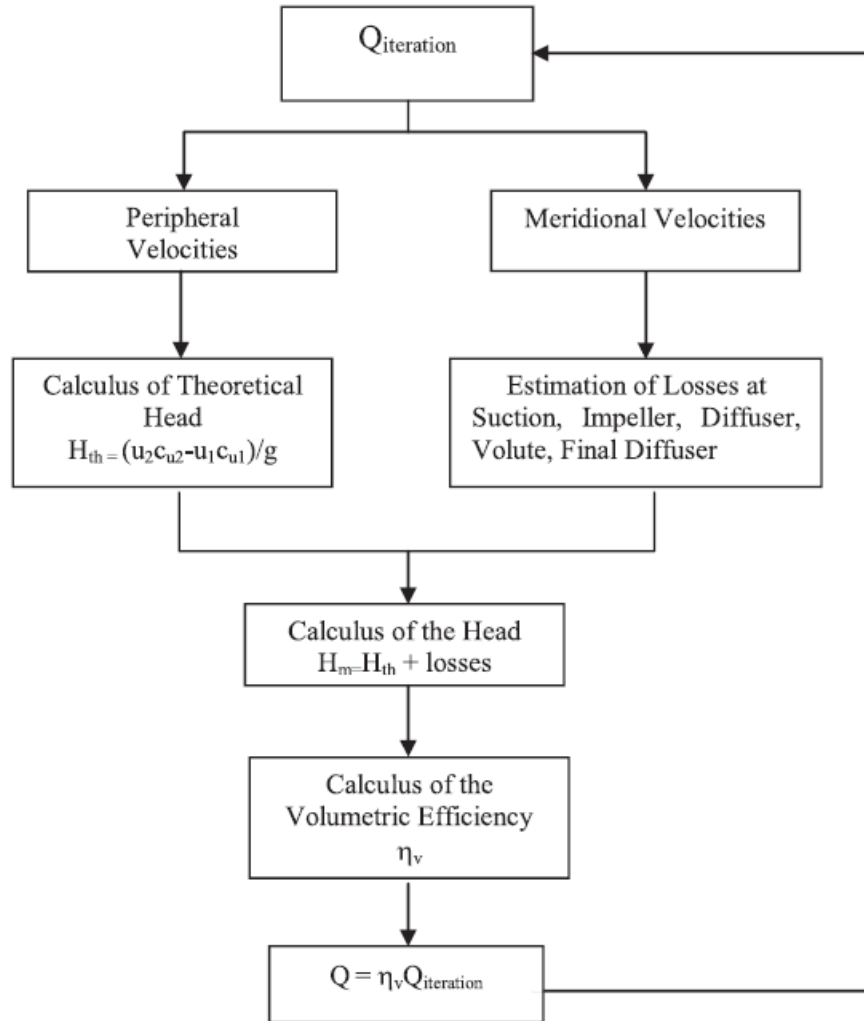


Figure 4-17 Head calculus flow chart. [23]

Velocities are expressed through the conservation of mass ( $Q = c A$ ) into the final diffuser. Two kinds of losses are distinguished: friction losses and dynamic losses, both determined by the velocities, according to following formulas:

$$h_f = \lambda \frac{c^2}{2g} \left( \frac{1}{D_h} \right)$$

$$h_d = \zeta \frac{c^2}{2g}$$

Equation 4-22

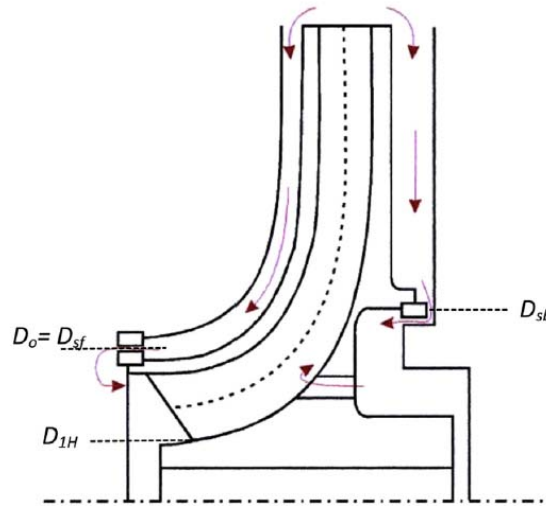


Figure 4-18 Leakage path. [23]

Now it is necessary to obtain the hydraulic diameters [38] and coefficients of both dynamic ( $z$ ) and friction ( $l$ ) losses. Generally, the  $l$  coefficient is obtained from Colebrook's formula but paying attention to the vanes camber (RB) when the calculus is referred to the impeller [39] and [40].

Regarding the losses evaluated in the diffusion region (Section 3 of Figure 4-13), a further loss is computed at low flow rate because of vortices in this region which reduce their dimension when the flow increases [37]. The loss is computed as:

$$h_{low\ flow} = k (Q - Q_{BEF})^2$$

Equation 4-23

The coefficient  $k$  is estimated by [24] by means of the following statistic correlation set up on the pumps sample tested at hydraulic test rig [35]:

$$k = \frac{1}{53.67 + 0.0077 \cdot n_s^{3.44}}$$

Equation 4-24

where  $n_s$  is the specific speed of the PAT.

Finally, the distributed losses into the impeller have been estimated by introducing an average diameter as Neumann suggests [38].

#### 4.3.4 Result

For validating the model, six centrifugal pumps measured at the DIMEG of the University of Calabria, at the CNPM in Milan and at the University of Trento, have been used. In the next table (Table 4-4).

Table 4-4 Main parameters of the six pumps. [23]

PAT	$n_s$	$Q_{BEP}$	$H_{BEP}$	$P_e$ [kW]	$H_{mo}$ [m]	$D_2$ [m]	$y_P$ [m]
40-335	9.08	49.30	99.52	5.60	41.00	0.33	0.25
40-250	12.80	38.33	43.66	2.65	22.60	0.26	0.225
50-160	28.70	52.50	12.50	1.50	10.90	0.174	0.18
80-220	30.31	123.00	20.00	5.45	16.50	0.219	0.25
80-200	34.11	120.00	17.60	3.90	13.50	0.198	0.25
100-160	64.07	157.07	7.82	4.00	10.20	0.185	0.28

the main inputs of the six Pumps, useful for applying the sizing procedure, are reported. All these pumps have specific speeds between 9 and 65 [ $\text{rpm m}^{3/4} \text{s}^{-1/2}$ ].

The model can be used in:

- “design mode”: the design step is performed and the unknown geometry is then reproduced.
- “geometry known mode”: the geometrical parameters are known.
- “mixed mode”: some geometrical parameters are known; the others are calculated by the model.

The following figures (from Figure 4-19 to Figure 4-30) show a comparison of the calculated curves with the experimental ones, for the six PATs when the model operates in “design mode” (from Figure 4-19 to Figure 4-24) and when it operates in “geometry known mode” (from Figure 4-25 to Figure 4-30).

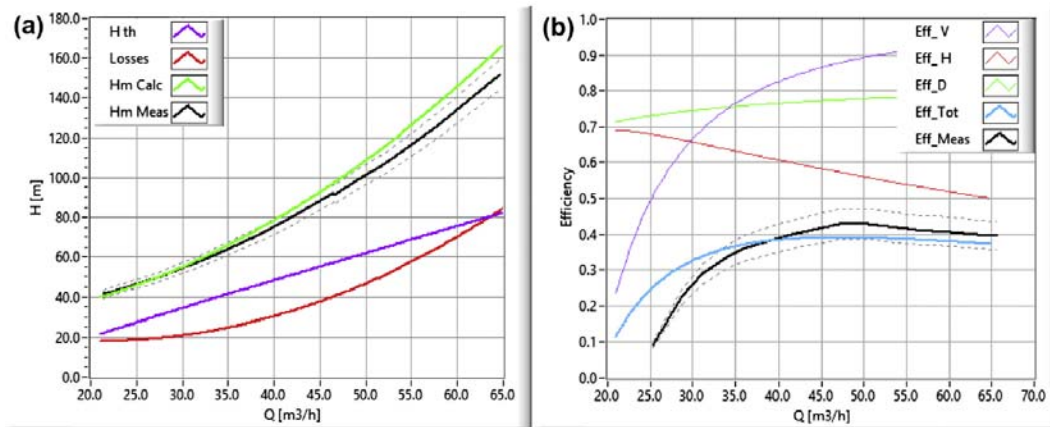


Figure 4-19 Head (a) and efficiency (b) for the PAT 40-335 ( $n_s = 9.1$ ) - design mode. [23]

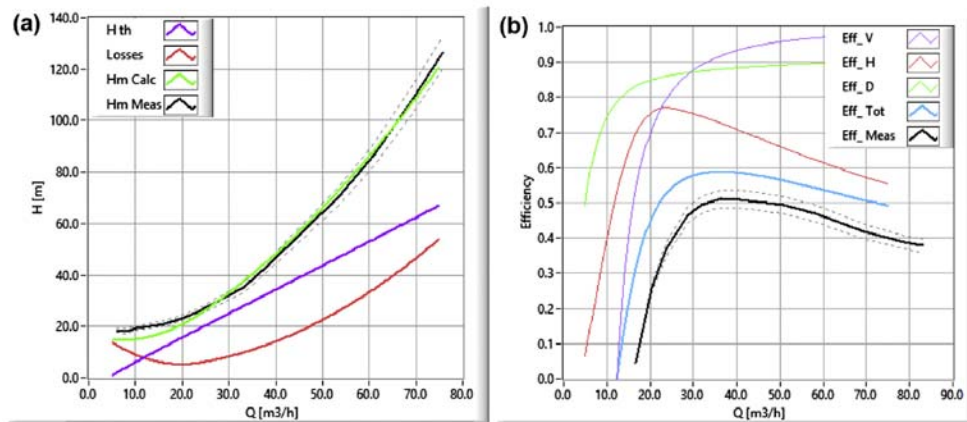


Figure 4-20 Head (a) and efficiency (b) for the PAT 40-250 ( $n_s = 12.5$ ) – design mode. [23]

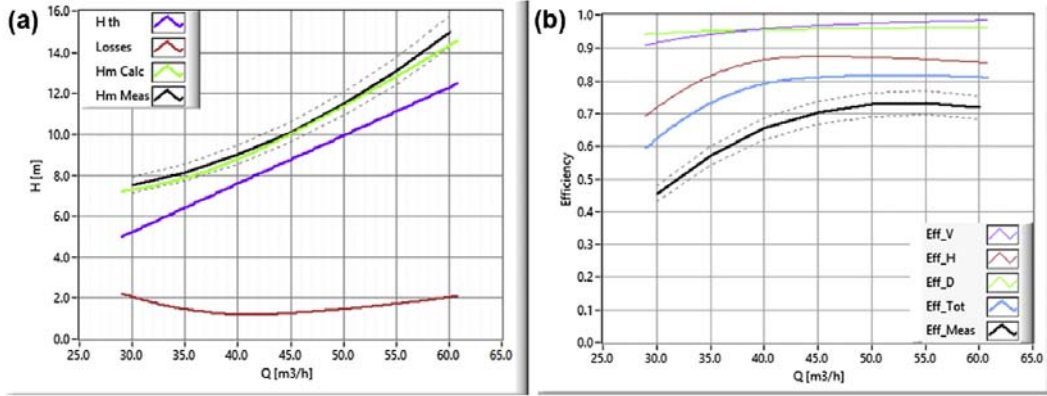


Figure 4-21 Head (a) and efficiency (b) for the PAT 50-160 ( $n_s = 28.7$ ) – design mode. [23]

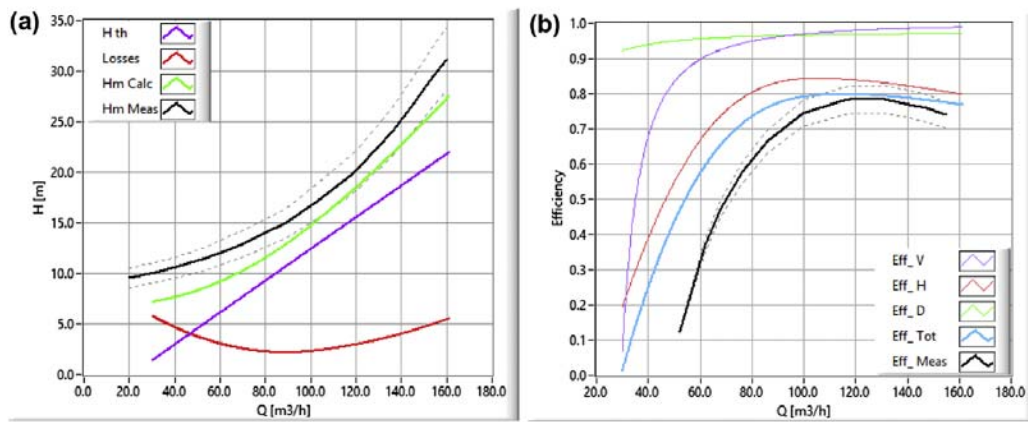


Figure 4-22 Head (a) and efficiency (b) for the PAT 80-220 ( $n_s = 30.3$ ) – design mode. [23]

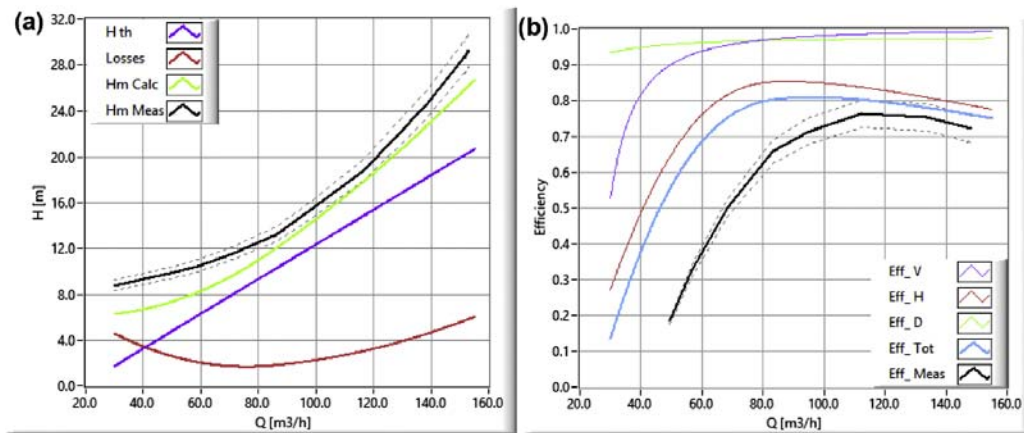


Figure 4-23 Head (a) and efficiency (b) for the PAT 80-200 ( $n_s = 34.1$ ) – design mode. [23]

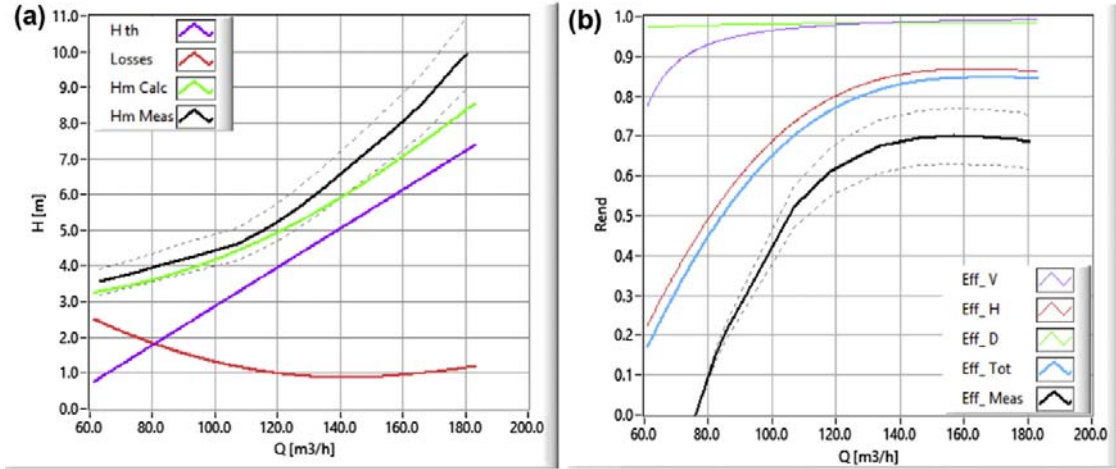


Figure 4-24 Head (a) and efficiency (b) for the PAT 100-160 ( $n_s = 64$ ) e design mode. [23]

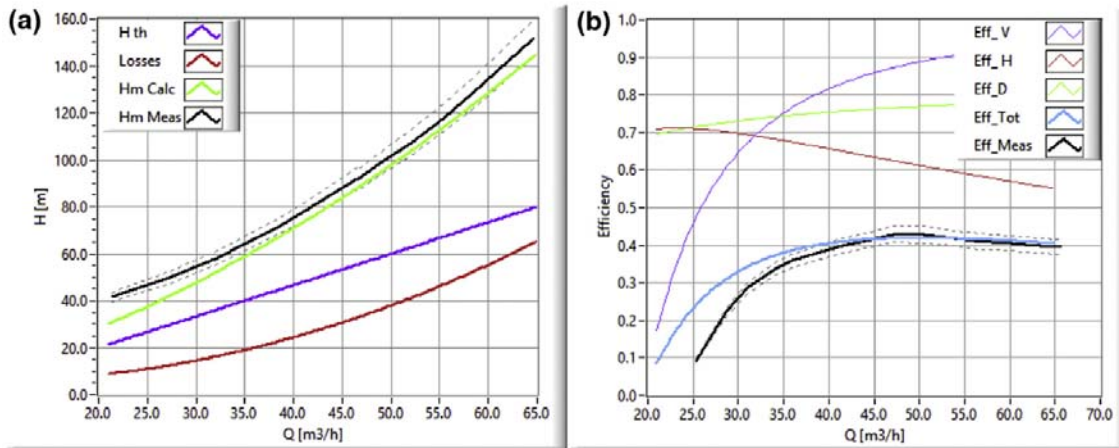


Figure 4-25 Head (a) and efficiency (b) for the PAT 40-335  $n_s = (9.1)$  e geometry known mode. [23]

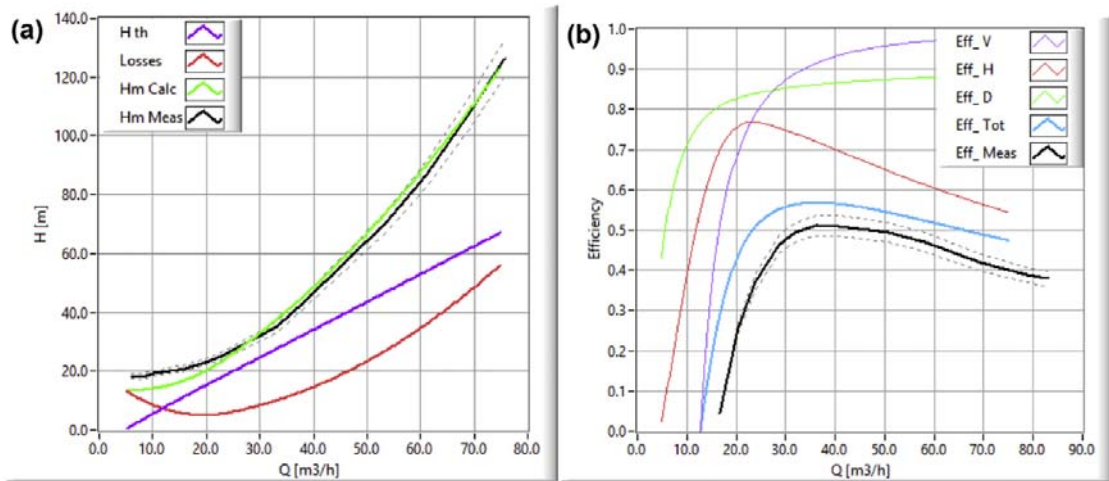


Figure 4-26 Head (a) and efficiency (b) for the PAT at 40-250 ( $n_s = 12.5$ ) e geometry known mode. [23]



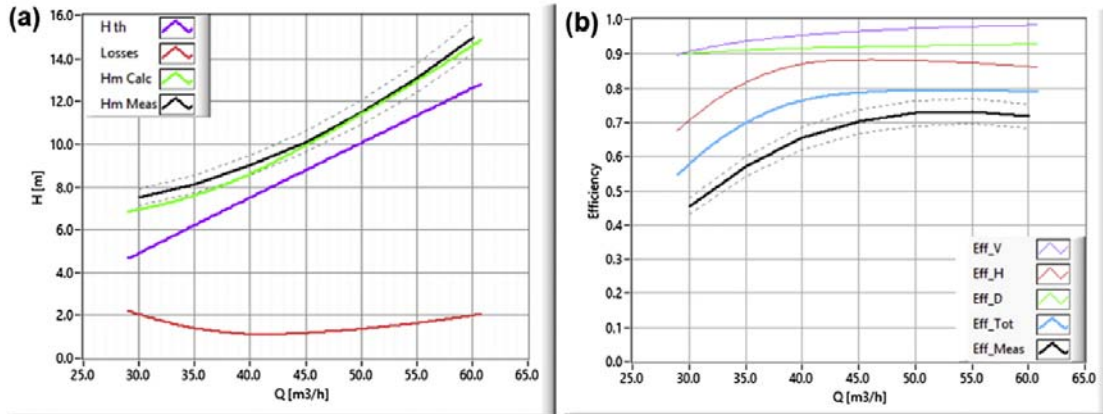


Figure 4-27 Head (a) and efficiency (b) for the PAT 50-160 ( $n_s = 28.7$ ) e geometry known mode. [23]

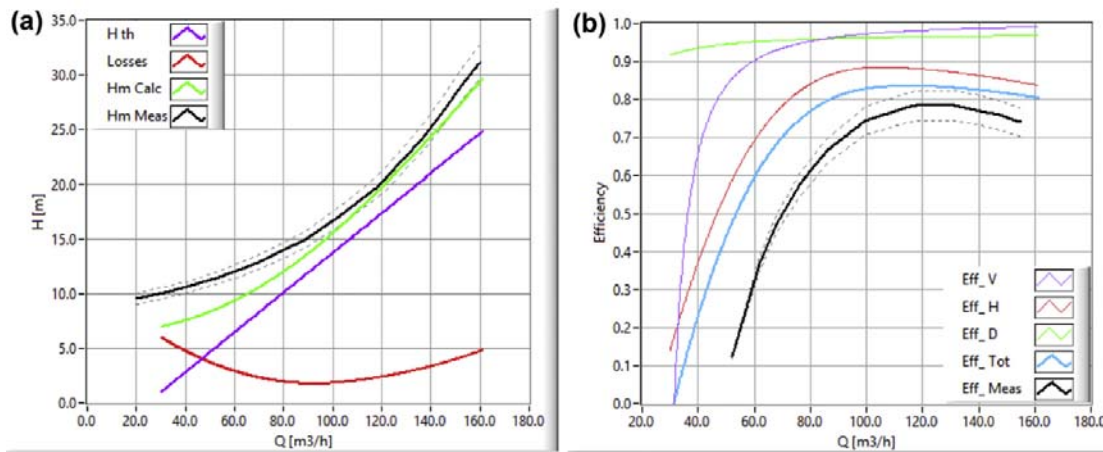


Figure 4-28 Head (a) and efficiency (b) for the PAT 80-220 ( $n_s = 30.3$ ) e geometry known mode. [23]

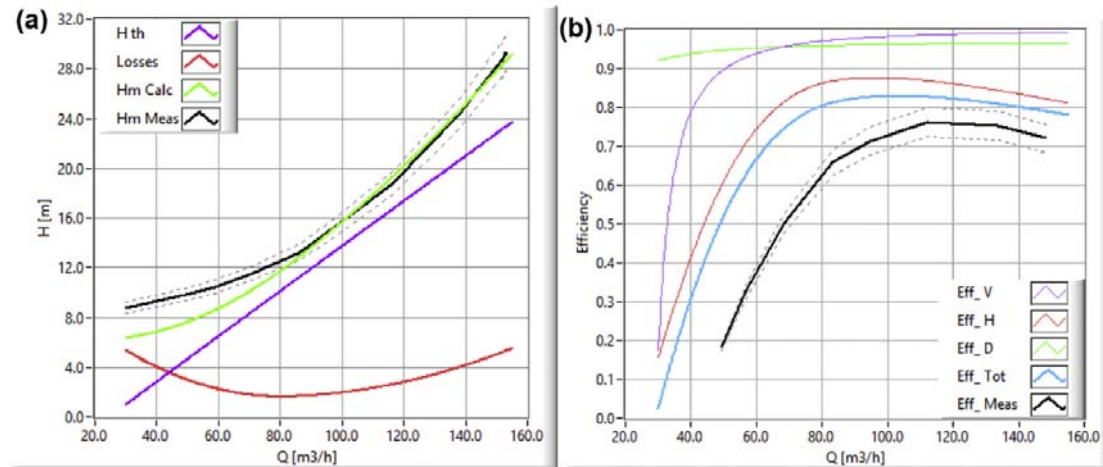


Figure 4-29 Head (a) and efficiency (b) for the PAT 80-200 ( $n_s = 34.1$ ) e geometry known mode. [23]

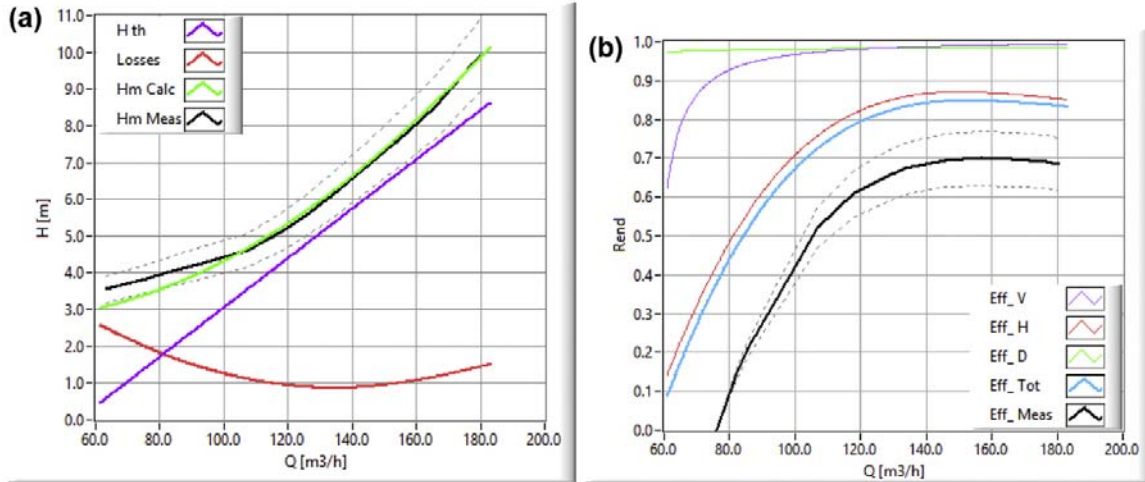


Figure 4-30 Head (a) and efficiency (b) for the PAT 100-160 ( $n_s = 64$ ) e geometry known mode. [23]

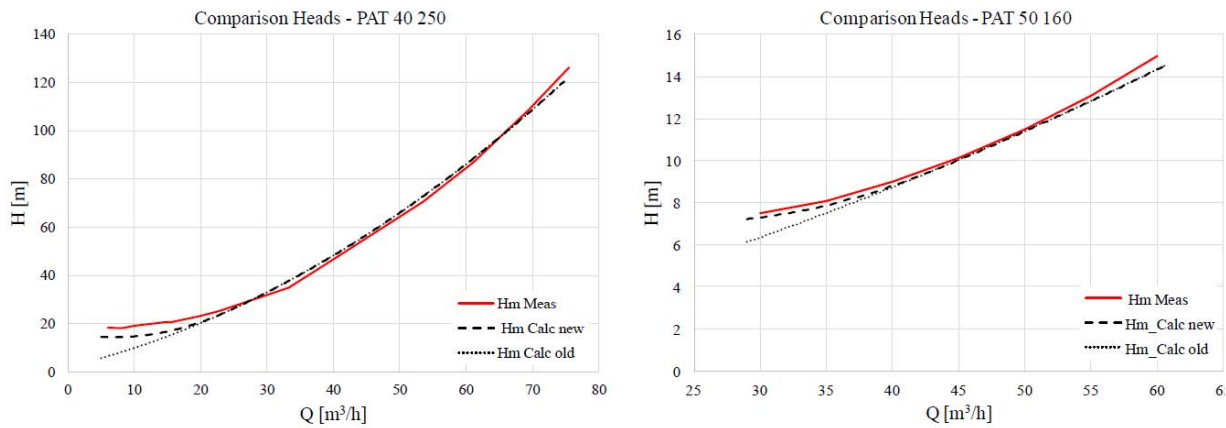


Figure 4-31 Comparison, for the PATs 40e250 (left side) and 50e160 (right side), between experimental data and numerical simulations (new model e dashed line e and old model [23])

Each figure shows the characteristic curves (a) and the efficiencies (b) for turbine behavior. The plots of both computed and measured data are shown. In all the figures a band of 5% is added to the measured head and to the measured efficiency. In some cases, for the PAT 100-160 operating both in design mode and in geometry known mode (Figure 4-19 and Figure 4-30) and for the PAT 80-220 operating in design mode (Figure 4-28) the band has the wide of 10%.

The from Figure 4-19 to Figure 4-30 show that the model is able to predict the performances of different PATs the geometry of which changes significantly, according to the specific speed. The results are obviously better if the model works in geometry known mode, i.e. the geometry is known, as Figure 4-25, Figure 4-30 illustrate. The worst prediction is made for the head of the

PAT 80-220 (Figure 4-28) and of the PAT 100-160 (Figure 4-24): it improves when the model is applied in geometry known mode.

At low flow rates, the model is often unable to predict the trend of the head giving errors up to 25%. As it is a one-dimensional model, it cannot take into account vortex or reverse flows that modify the velocity field significantly, particularly when the flow rate is low and, with the same cross-section areas, the patterns are less regular [37]. If the vortex distribution were known it would be possible to calculate the root-mean-square velocity which is greater than the mean velocity. Furthermore, the flow rate reduction could give an increase of friction loss coefficient, as in small machines the Reynolds number is in the transient region. For all these reasons at low flow rates the errors in losses calculation can increase.

Nevertheless, through the evaluation of the new loss  $h_{lowflow}$  the model improves its prediction with respect to that presented in Ref. [36]. Figure 4-31 shows a comparison between the heads evaluated without the loss  $h_{lowflow}$  [36] and the heads evaluated by considering what is shown for the PAT 40-250 and for the PAT 50-160. Figure 4-31 shows how the new loss introduced in this work compensates the difference between the calculated head and measured one in the field of the low flows, leaving them unchanged at increasing flows.

When the flow rates  $Q$  are close to the BEP (see Figure 4-19 - Figure 4-30), the predicted curve lies closer to the real one, within a range of  $\pm 5\%$ . The calculated curves related to the efficiency, although their trends agree with the real ones, are higher than the latter. From a comparison of the above-illustrated figures an overestimation of the efficiency in the range of 5 ÷ 15% results.

This aspect can indicate an underestimation of some loss, but at the moment the measurement strategies adopted do not allow the entity of the single losses and their weight to be distinguished in relation to the total efficiency. So, with respect to each single loss, it is impossible to assess between theoretical and experimental data and consequently it is impossible to understand what loss has been underestimated. In the next from 20 to 25, the loss distribution at BEP in percentages for the six PATs, ordered with  $n_s$  increasing when the model operates in “design mode”, is anyway reported.

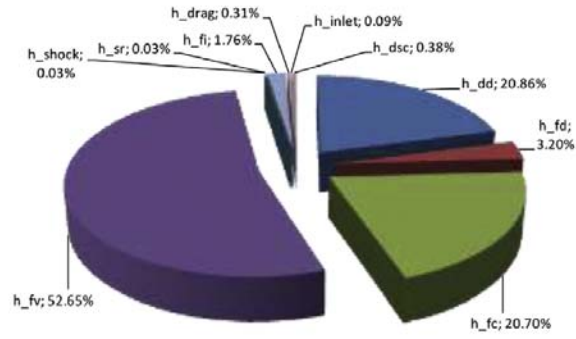


Figure 4-32 Losses distribution at BEP e PAT 40-335  $n_s = 9.08$ . [23]

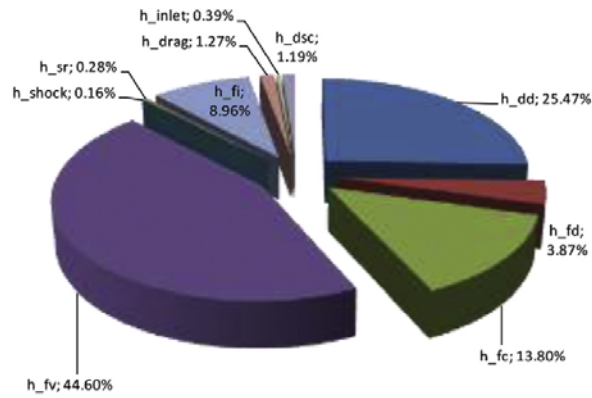


Figure 4-33 Losses distribution at BEP e PAT 40-250  $n_s = 12.80$ . [23]

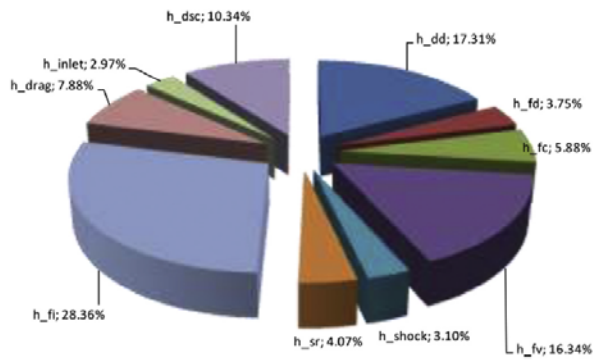


Figure 4-34 Losses distribution at BEP e PAT 50-160  $n_s = 28.70$ . [23]

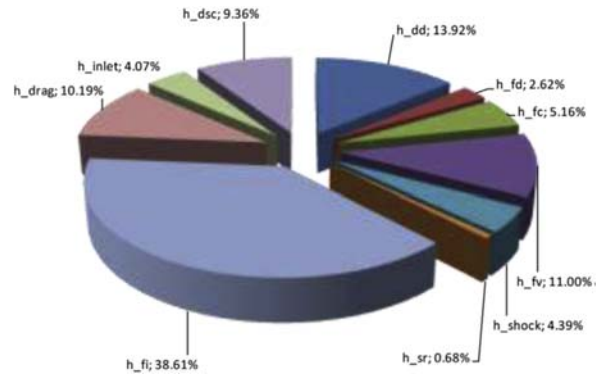


Figure 4-35 Losses distribution at BEP e PAT 80-220  $n_s = 30.31$ . [23]

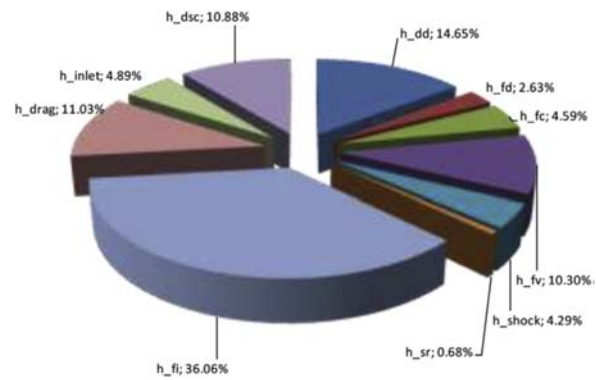


Figure 4-36 Losses distribution at BEP e PAT 80-200  $n_s = 34.11$ . [23]

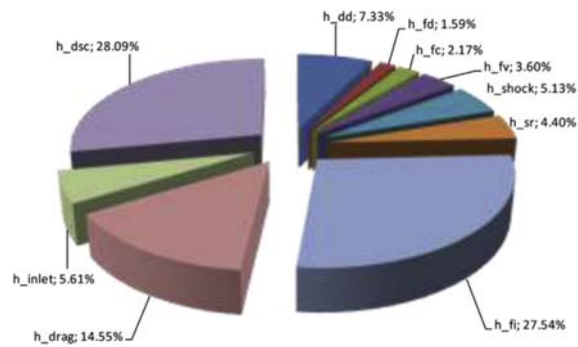


Figure 4-37 Losses distribution at BEP e PAT 100-160  $n_s = 64.07$ . [23]

The figures shown above demonstrate that generally the rotor losses increase while the stator losses decrease with  $n_s$ . This is anyway only an indicative trend, because of the peculiarity related to each single PAT and it points out the difficulty of predicting the BEP localization by the simple correlations based only on  $n_s$  [41] and [42].

On the other hand, this is an important result that gives indications on the experimental activities. In the next research steps [23] tried to measure the losses in the stator because it is easier to insert probes in the stator than in the rotor.

Differently from the simple correlations found in the literature [41] and [42], the BEP prediction of the proposed model is more satisfactory. In Table 4-5 and Table 4-6 head and capacity at BEP, carried out by the model both when it operates in design mode (Table 4-5) and in geometry known mode (Table 4-6), are reported. In these tables the calculated values ( $_{calc}$ ) and the measured values ( $_{meas}$ ) are reported, as well as their relative errors. The PATs 80-220 and 80-200 totalize the worst predictions in design mode: the errors on the Head are about 20%.

Table 4-5 Head and flow rate data at BEP: computed by model ( $_{calc}$ ) and experimental ( $_{meas}$ ) e model operating in “design mode”. The highest errors are highlighted with gray shade. [23]

PAT	$n_s$	$Q_{BEP\_calc}$	$Q_{BEP\_meas}$	$e\%_Q$	$H_{BEP\_calc}$	$H_{BEP\_meas}$	$e\%_H$	C
40-335	9.08	46.75	47.08	0.70%	98.19	93.28	-5.26%	0.31
40-250	12.8	36.25	38.33	5.43%	42.3	43.66	3.11%	0.18
50-160	28.7	52.5	55	4.55%	11.96	13.1	8.70%	0.30
80-220	30.31	115.75	131.46	11.95%	17.69	22.4	21.03%	0.71
80-200	34.11	96.25	112.4	14.37%	13.84	17.6	21.36%	0.69
100-160	64.07	168.25	157.07	-7.12%	7.58	7.82	3.07%	0.51

Table 4-6 Head and flow rate data at BEP: experimental ( $_{meas}$ ) and computed by model ( $_{calc}$ ) e model operating in “geometry known mode”. The highest errors are highlighted with gray shade. [23]

PAT	$n_s$	$Q_{BEP\_calc}$	$Q_{BEP\_meas}$	$e\%_Q$	$H_{BEP\_calc}$	$H_{BEP\_meas}$	$e\%_H$	C
40-335	9.08	50	47.08	-6.20%	97.83	93.28	-4.88%	0.20
40-250	12.8	36.25	38.33	5.43%	42.46	43.66	2.75%	0.19
50-160	28.7	52.5	55	4.55%	12.18	13.1	7.02%	0.23
80-220	30.31	115.5	131.46	12.14%	18.77	22.4	16.21%	0.51
80-200	34.11	103	112.4	8.36%	16.33	17.6	7.22%	0.27
100-160	64.07	152.5	157.07	2.91%	7.56	7.82	3.32%	0.11

In the last column of the two tables, the prediction indicator C, proposed by Williams [43], is also reported. This indicator, expressed by the following formula, has the meaning of a weighted “distance”, in a normalized H-Q plane, between the foreseen BEP and the real one.

$$C = \frac{5}{3} \sqrt{\left(\frac{Q_{BEP\_calc}}{Q_{BEP\_meas}} + \frac{H_{BEP\_calc}}{H_{BEP\_meas}} - 2\right)^2 + 9\left(\frac{H_{BEP\_calc}}{H_{BEP\_meas}} + \frac{Q_{BEP\_calc}}{Q_{BEP\_meas}}\right)^2}$$

Equation 4-25

In the plane H-Q, a curve defined by  $C = \text{const}$  is an ellipse. The prediction is acceptable if  $C < 1$ . When  $C = 1$ , the maximum allowed variations of H and Q with respect to BEP are 21% following the major axis of the ellipse and 7% following the minor axis. In the next from [Figure 4-37](#) to [Figure 4-41](#), the Williams Ellipses corresponding to values of C from 0.25 to 1.75 are reported. In these figures the forecasts of Childs [41], Hancock [44], Stepanoff [45], Sharma [46], Alatorre [47], Schmiel [48], Hergt [42], Grover [50], together with the prediction of the model when it operates in “design mode” and in “geometry known mode”, are also reported. In all the cases shown, the prediction of the model is inside the ellipse corresponding to  $C = 1$ .

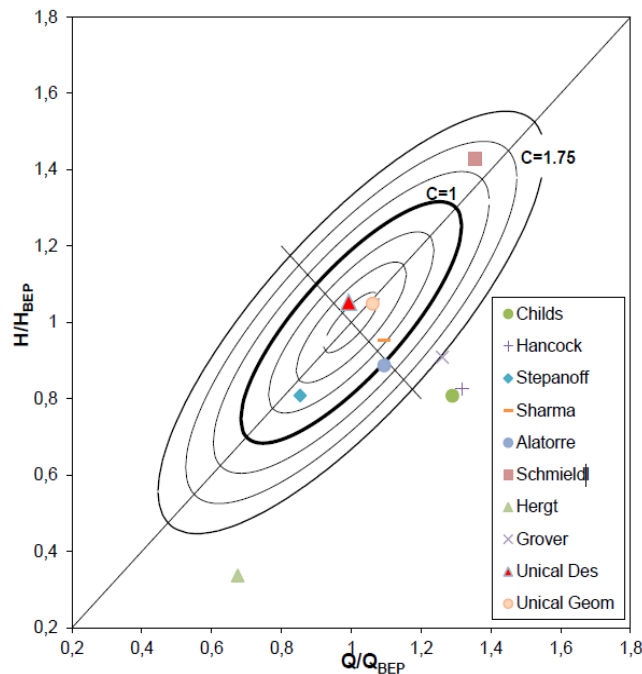


Figure 4-38 Predictions comparison in the Williams plane for the PAT 40-335. [23]

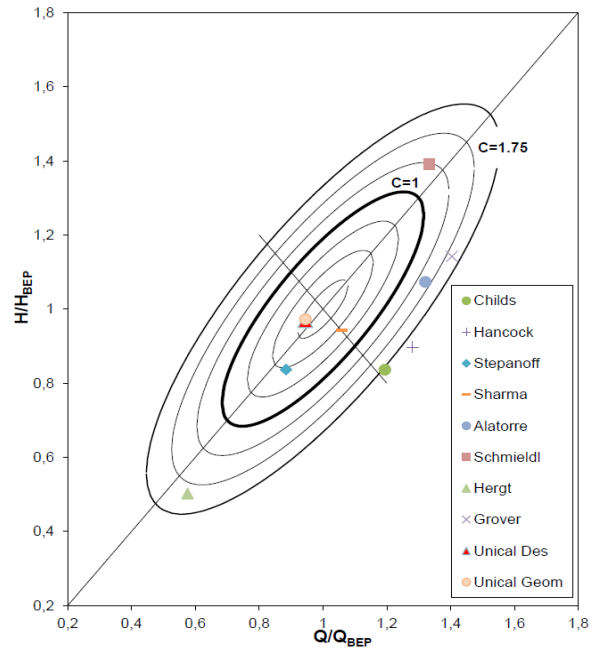


Figure 4-39 Predictions comparison in the Williams plane for the PAT 40-250. [23]

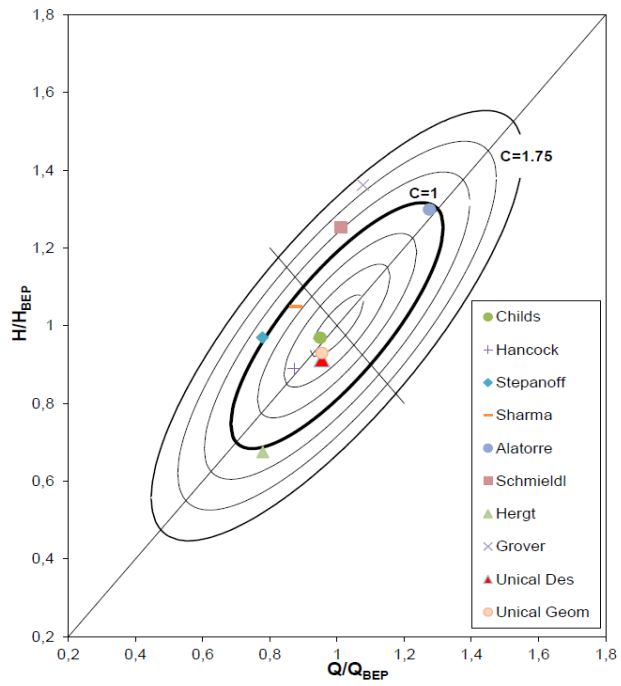


Figure 4-40 Predictions comparison in the Williams plane for the PAT 50-160. [23]



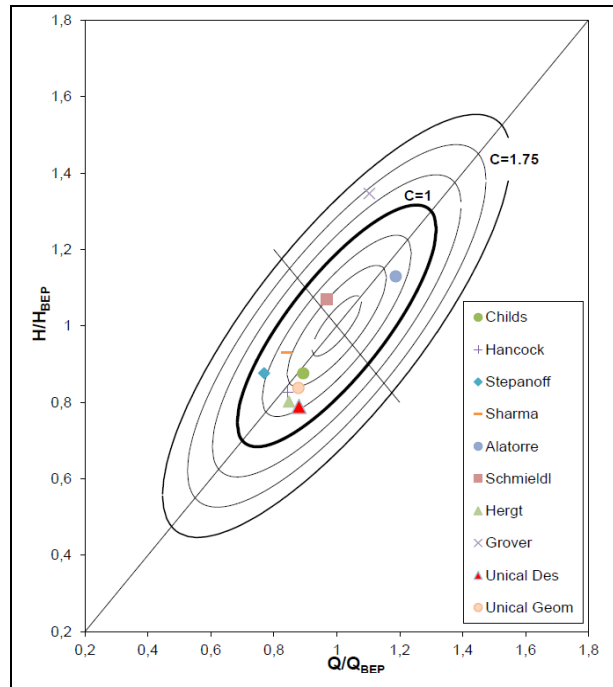


Figure 4-41 Predictions comparison in the Williams plane for the PAT 80-220. [23]

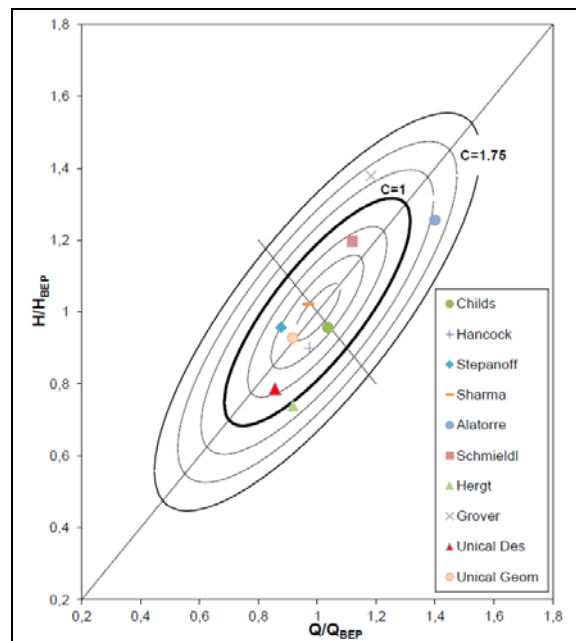


Figure 4-42 Predictions comparison in the Williams plane for the PAT 80-200. [23]

The prediction performed by the model operating in design mode (Unical Des) is quite good ( $C \approx 0.7$ ). Sharma's method, in second place according to William's criterion, has also  $C \approx 1$ , but for the 50-160 pump,  $C$  is near to 1. The model, by using geometry known mode (Unical Geom), obtains even better results but, of course, this change is not useful at PAT selection time.

Finally, in the next tables (Table 4-7 and Table 4-8) a comparison between the efficiency calculated at BEP by the model and the efficiency measured at BEP is shown both when the model operates in design mode and in geometry known mode.

Table 4-7 Efficiency at BEP: computed by model ( $\eta_{calc}$ ) and experimental ( $\eta_{meas}$ ) e model operating in “design mode”. The highest errors are highlighted with gray shade.

PAT	$n_s$	$\eta_{calc}$	$\eta_{meas}$	$e\%_{\eta}$
40-335	9.08	0.39	0.43	9.30%
40-250	12.8	0.59	0.52	-13.46%
50-160	28.7	0.82	0.73	-12.33%
80-220	30.31	0.80	0.78	-2.56%
80-200	34.11	0.81	0.76	-6.58%
100-160	64.07	0.85	0.70	-21.43%

Table 4-8 Efficiency at BEP: experimental ( $\eta_{meas}$ ) and computed by model ( $\eta_{calc}$ ) e model operating in “geometry known mode”. The highest errors are highlighted with gray shade.

PAT	$n_s$	$\eta_{calc}$	$\eta_{meas}$	$e\%_{\eta}$
40-335	9.08	0.42	0.43	2.33%
40-250	12.8	0.56	0.52	-7.69%
50-160	28.7	0.80	0.73	-9.59%
80-220	30.31	0.84	0.78	-7.69%
80-200	34.11	0.83	0.76	-9.21%
100-160	64.07	0.85	0.70	-21.43%

The model improves its prediction when it works in geometry known mode for the PATs 40-335, 40-250 and 50-160. While for the PATs 80-220 and 80-200, although the predictions of the efficiency at BEP are worse, the predicted trends are better if the model operates in geometry known mode. The PAT 100-160 exhibits the maximum errors of the order of 21% in both modi operandi.

Anyway, the data shown in the above tables indicate that the global efficiency predicted is always greater than the global efficiency measured except for the pump 40-315 with a mean overestimation of 6%. Nevertheless, the graphs shown in [Figure 4-19](#) to [Figure 4-30](#) indicate that the efficiency curves trend agrees with the experimental one.

#### 4.3.5 Conclusion

A numerical model, to foresee the performances of centrifugal pumps used as turbines, has been proposed. The main characteristic of the model is its capability to operate only with input coming from pumps' catalogues. It performs a standard design of the pump, in order to take into account geometrical parameters, without the burden of measuring them.

Using the experimental test on 6 centrifugal pumps with specific speed between 9 and 65 the model has been validated by comparing the head and efficiency foreseen with the measured ones. Differences noticed are in some cases wide but the BEP localization is instead satisfactory. The computed head-capacity curves show a trend similar to the measured ones with the highest relative error at BEP of 21.4% in Head prediction of KSB 80-200.

When actual detailed geometrical parameters are given, the error is reduced to 7.2%. As further expedient to validate the goodness of the model, the Williams's indicators of the model predictions are better than the ones carried out by correlation formulas proposed by 8 different authors.

The errors of the model are lower when the real geometrical data (the measured ones) are known: this means that the first part of the proposed model, which performs the pump sizing, has, obviously, influence on the final results and it can be improved.

Finally, the model gives a good trend of the performances curves which generally agree with the real ones although the predicted efficiency is slightly higher than the real one. The overestimation of the efficiency can be due to an underestimation of some loss, but at the moment it is impossible to establish what. To be certain of the real value of the losses as well as of other parameters involved in the model such as, fluid dynamic angles, friction coefficients, vortex distribution and so on, experimental strategies and separated measurements are necessary. However, any similar

comparison is a hard challenge because of the difficulties involved in inserting probes into the machines while they are working. The next step of this research is to find the best measurement strategies for improving the model estimations and its reliability despite the good level achieved so far. [23]

## 4.4 Market Obstacles (Interview)

### 4.4.1 Interview

Interviewee: Mr. Ing Holger Winter



KSB SE & Co. KGaA, Verkauf Installed Base  
Address: Vertriebshaus Hamburg Carl-Zeiss-Straße 4-6, 21465 Reinbek  
Mobil: +49 172 625 1353 Festnetz: +49 40 69447-229 Fax: +49 40 69447-255  
Mail: [holger.winter@ksb.com](mailto:holger.winter@ksb.com)  
Website: <https://ksb.com>

Regarding to an interview with Mr. Ing Holger Winter, a mechanical engineer as an advisor of the Hamburg region of KSB, one of the leading companies in centrifugal pumps industry. During his professional career, he was part of the main team of the PAT production line in the KSB. Author asked him about the certainty in the PAT market, he developed his answer as below:

Since in the northern part of Germany there are not many hills, obviously this contact with the PAT technology can be rare somehow. All over a year maybe 10 times being in touch with customers who are interested in PAT. By considering significant Advantages of PAT like almost maintenance free technology, very low emission rate, Simple technology... still the market of the PAT is very uncertain. One reason for that could be the topography of the region. Specially in Hamburg, Germany is a very flat area in compare of other part of the Europe. Another problem is that not so many people are aware of using this technology as a simple alternative for Hydro-generating. Another point to be consider is for big producing company such as KSB, the small demand for this

technology is another big issue. Where those companies try to produce hundreds of thousands pump per year, and in compare of a very small market demand such as 20 Pump as Turbine per year, is not a high number for them.

For few years KSB had a special department for PAT. also the company itself pushed the product into the market. advertising and promoting it worldwide. But for a few numbers of project potential customers showed interest. For example, between 20 interests we received 5 orders. That was not enough to establish this department for longer time. KSB can still deliver PAT in northern Germany but not proactively.

Since this technology is mainly base on physical properties of the project in areas with more topological properties, there are many smaller companies which can produce PAT with better focus rather than KSB.

But For instance, A customer in Hamburg area such as HamburgWasser. The project is not based on the geographical height differences. The customer has a water reservoir, which is filled out with pressurized water system during the night. And during the day when the customer needs to take out water from the system through the distribution network, the water supplier (Hamburg Wasser) with centrifugal pump will deliver the water to the network. But as it seems to be clear in the pressurize system, they are not using from that energy dissipating through network, so that is the point we are trying to convince the customer to use PAT when in the night 5000m<sup>3</sup> water going into the reservoir, with the pressure of 5 bar, by dissipating the energy during the vane. and by replacing PAT in the system it will be possible to reserve the energy during the night and use that energy during the day to pump the water inside the network.

It is also necessary to mention in many cases it happens that the reservoir system is already existed for many years and in order to imply the new application over the reservoir customer needs to make many changes such as pipeline, electrical control system, concrete chamber if it is needed, and so on and so forth, which basically means from the first place there will exist a big resistance against this even if it can bring some benefit for the customer.

Another problem will be the complication of the electrical control system, which are not very easy to calculate the generated energy from the system, so that many customers after being interested, still have big problem with realization of it. Except for having a reference in the region that you can refer to them, then is much easier to convince them.

Author followed the question with asking about the average range of electrical regeneration form this system in northern Germany:

the average for the northern Germany will be between 10 to 50 kW as a typical size. This technology is all benefit for customer who are user of centrifugal pumps. But I also would like to summarize it experimentally that when the regeneration of energy is about 15 kW or 2000 working hours per year approximately then we can say the cost-Benefit correlation will be positive for the customer.

To conclude the discussion, it is important to know, that this technology of PAT is not really new, and the system is somehow well-known, but not by the end users. Also, as it comes later there are an example of planning document for PAT from KSB which can help to have a closer look to the main frame.

#### 4.4.2 Application-Oriented Planning Documents for Pumps as Turbine by KSB [16]

##### 4.4.2.1 Generation of Planning Documents

For more than 35 years now, KSB has been receiving queries about and order for, revers-running pumps. According to a recent market study, policy decision like Kyoto Protocol, in combination with the increasing cost of energy, are generating increasing demands for alternative, renewable sources of energy in all market segments. In Germany alone, there is posited potential for pumps as turbines (PATs) on the order of 100 – 250 MW installed electric generating capacity. Most of that potential is still being wasted in water handling systems and industrial facilities equipped with throttling elements, even though it would be very easy and extremely economical to harness that potential with PATs

What makes PATs so worthwhile?

- Short payback period thanks to:
  - Series production and accordingly minimal initial investment costs.
  - Very good optimum point efficiency and, hence, revenues from the power yield.
- Low life cycle maintenance and repair costs
  - Very low maintenance and repair costs.

Obviously, a growing sense of ecological responsibility and the fact that this kind of power generation can be very profitable have helped enkindle a waxing general interest in renewable energy.

#### 4.4.2.2 Economic Efficiency

The following, very simplified equation is useful for estimating how much power (P in kW) can be captured with the aid of a PAT system:

$$P \approx 7 \cdot Q \cdot H$$

With: P[kW] power  
           Q [ $m^3/s$ ] flow rate  
           H [H] head

Process efficiency (approx. 70%), gravitational acceleration and density are already factored in.

The power yield can either be used to reduce the internal consumption of expensive grid electricity, hence distinctly reducing expenditures for purchased line power, or it can be fed into the local grid in return for feed-in compensation. To calculate the achievable annual revenues, the specific output merely has to be multiplied by the number of annual operating hours and the feed-in tariff:

$$\text{Annual revenues} = p \cdot \text{operating hours} \cdot \text{feed-in tariff}$$

With: annual revenues [€/a]  
           P [kW] power  
           Operating hours [h/a]  
           Feed-in tariff [€/kWh]

Owing to the low initial investment costs and high energy prices, it takes only few years for PAT system, to pay for itself.

#### 4.4.2.3 Planning a PAT System

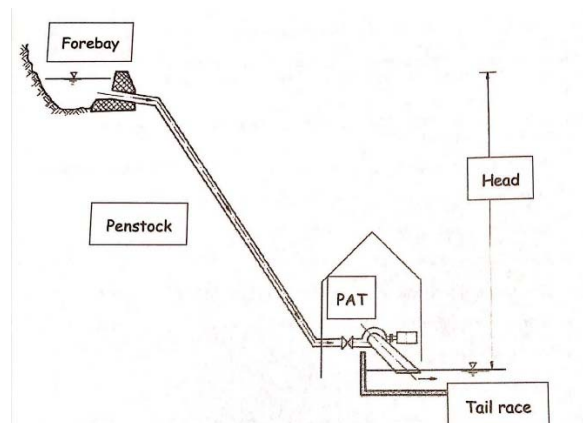


Figure 4-43 Conceptual sketch of PAT system

Before the planning for PAT system like that sketched out begins, both the temporal distribution of flow and the head should be known. With those data, the most effective, most economical size of PAT system can be found. The following pointers should be adhered to for PAT system planning:

- Layout of the PAT by your contract partner.
- Elaboration of plant concept (electric/electronic and mechanical system).
- Electronic and mechanical integration of the PAT into the plant concept.

#### 4.4.2.4 Products

Considering the nearly seamless spectrum of pumps to be found for practically all conceivable pumping situations and types of installation, an optimal type of set can also be found for turbine



service operation in most power generation applications. To help narrow down the choice, presents a pump-as-turbine range chart:

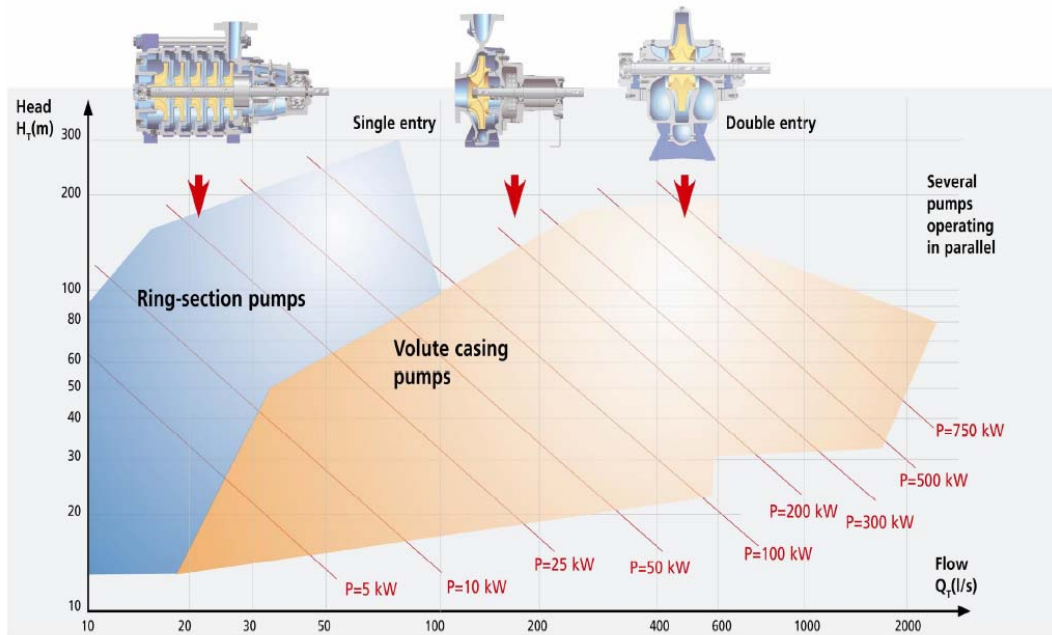


Figure 4-44 Pump-as-turbine range chart [16]

#### 4.4.2.5 Safety relevance

Care must be taken to ensure that the PAT system always remains safely within its reliable range of operation. To ensure this, the chosen pump must be certain to withstand the elevated turbine service stress levels, and all rotating parts must be reversible. In case of load rejection (e.g., power outage during mains operation), the "turbine" would accelerate to runaway speed. It is therefore important that appropriate safety measures be taken to ensure that such systems are not exposed to excessive loads. Other plant-specific factors such as resistance to pressure surge (water hammer) and susceptibility to cavitation also must be clarified in advance. A system pressure surge must always be anticipated, when the conditions of flow are altered, for instance by closure of a valve or when the impeller/rotor accelerates due to a power outage. We therefore recommend that the pressure surge susceptibility be calculated in advance. While cavitation rarely occurs in PAT systems, it is nevertheless important to investigate the system pressure conditions in order to

completely rule out any chance of cavitation. Such aspects as the chemical composition and temperature of the medium are important both in that connection and for the selection of a PAT.

#### 4.4.2.6 PAT System Control

With a view to making a PAT system as economical as possible for any and all combinations and fluctuations of flow rate and head, there are three ways to adjust the PAT to its duty point. First, however, it must be clear whether the PAT system will be operating on a mains mode or an island mode. In the mains mode, the generated power is fed into an existing power grid, while the electricity generated on the island mode must be directly available to consumers at a frequency of 50 or 60 Hz.

##### 4.4.2.6.1 Constant speed

If constant-speed operation is assumed, the PAT can only be designed for one particular volumetric flow rate and one particular head. All other conditions have to be accommodated by means of throttling elements and/or a bypass (Figure 4-45). This, of course, causes part of the energy potential to be lost.

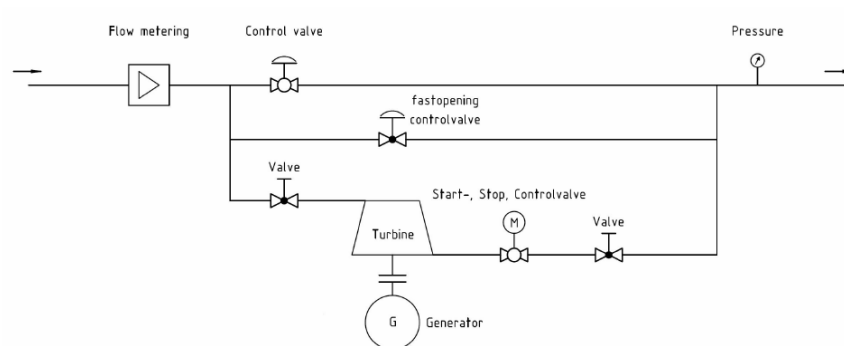


Figure 4-45 Hydraulic diagram of a PAT system [16]

Table 4-9 lists the components required for PAT system:

Flow measurement	Inductive flow meter Ultrasonic flow meter
Control valve	Annular piston valve, diaphragm valve
Quick-operating control valve	Annular piston valve, diaphragm valve
Shut-off valve	Annular piston valve, diaphragm valve
Start/stop valve	Butterfly valve, ball valve, gate valve
Pressure measurement	Pressure pickup

Table 4-9 Required PAT system component [16]

On the other hand, such systems are technically uncomplicated, easily controllable and, above all, very inexpensive. The speed is maintained by way of the existing power grid, so this option is unsuitable for island operation. Figure 4-45 shows the system's hydraulic arrangement, and Figure 4-46 illustrates its electrical layout - both for a postulated constant speed. It is also possible to use a synchronous generator in place of an asynchronous motor, depending on the outcome of a cost efficiency analysis. For island operation, the use of a synchronous generator is frequently more expedient.

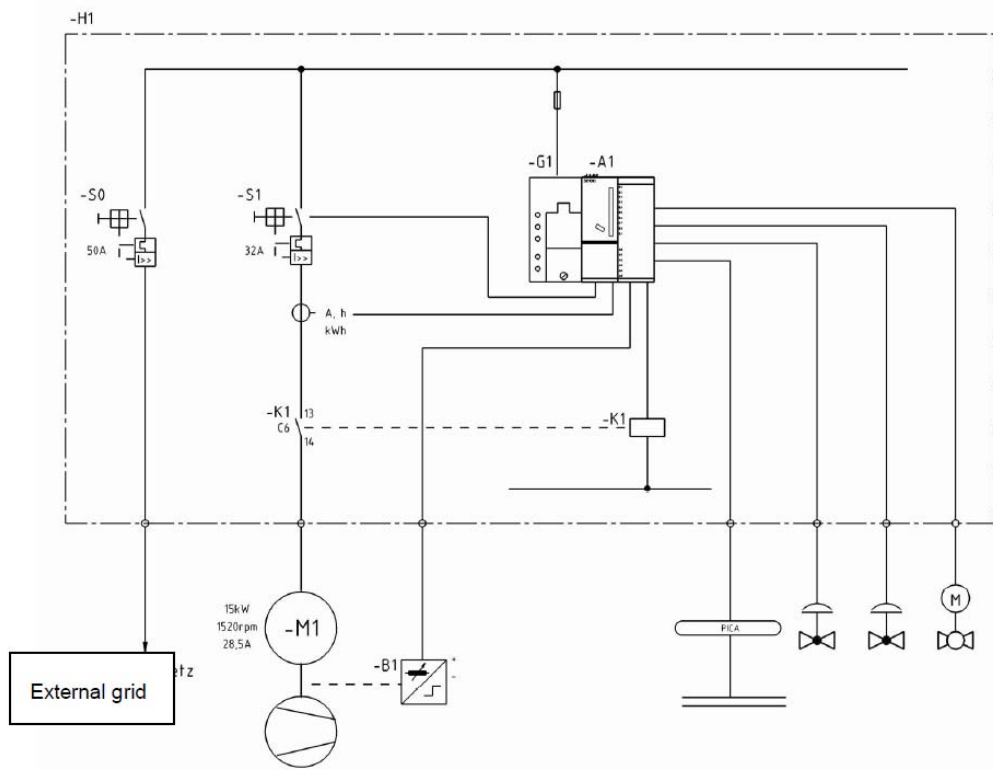


Figure 4-46 system diagram of a constant-speed PAT [16]

#### 4.4.2.6.2 Variable Speed

The basic idea behind the variable speed approach is to exploit, if possible, the entire available energy potential with no further throttling. The following options are available:

- **Negative- feedback frequency converter**

One possible is to install a negative-feedback frequency converter. In combination with standard three-phase motors, this cost-effective solution enables the user of other speed ranges for the PAT and the plant. It should be noted that frequency converter cannot be operated on an island mode.

- **Variable speed gear**

Speed adjustment can also be enabling by a variable speed gear – an option that calls for an advanced cost efficiency analysis.

#### *4.4.2.6.3 Control with several constant-speed PATs in parallel*

one good way to make optimal use of the energy potentials affected by pronouncedly fluctuating flow rates is to split the volumetric flow among several PATs. As in the cascade arrangement [Figure 4-47](#):



*Figure 4-47 Four of eight parallel PATs in service at the water utility authority (Zweckverband Landeswasserversorgung, Stuttgart, Germany) [16]*

#### *4.4.2.6.4 Direct coupling with a machine*

If the idea is to either drive a machine directly or disburden its prime mover, a PAT can be connected up to the machine by means of a continuous shaft or gearing. Finally, hybrid forms of the aforementioned configuration can be employed to achieve the targeted results ([Figure 4-48](#)).

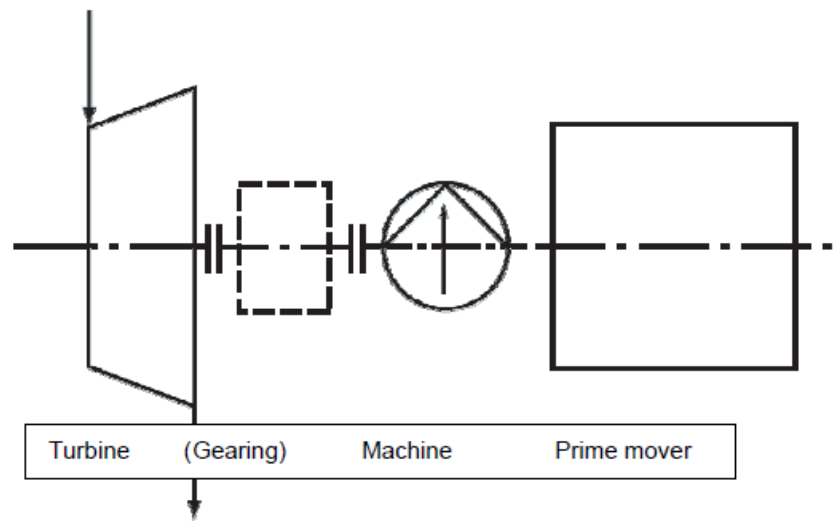


Figure 4-48 Direct coupling[16]

Finally, Hybrid forms of the aforementioned configuration can be employed to achieve the targeted result.

#### 4.4.2.7 Subsidies

##### 4.4.2.7.1 Germany

At the end of 2008 Germany’s Bundestag (Parliament) enacted the Renewable Energy Sources Act (EEG) 2009, which entered into force on 1 January 2009. According to that directive, new facilities commissioned from 2009 onwards are entitled to the guaranteed feed-in tariffs, in cent/kWh, shown in Table 4-10. The extent to which the potential yield satisfies the renewable energy criteria established in the EEG must be determined on a case-by-case basis.

Power share	EEG 2009 (Bundestag Resolution, 6 June 2008) [cent/kWh]
<500 kW	12.67
500 kW – 2MW	8.65
2 MW – 5 MW	7.65

Table 4-10 Feed-in tariffs for new facilities up to 5 MW [16]

A full comparison of EEG feed-in compensation instruments for 2009 (in German only) can be

found at:

[http://www.umweltministerium.de/files/pdfs/allgemein/application/pdf/eeg\\_verguetungsregelung\\_en.pdf](http://www.umweltministerium.de/files/pdfs/allgemein/application/pdf/eeg_verguetungsregelung_en.pdf)

For more information on the Renewable Energy Sources Act, please consult the website of the German Federal Ministry for the Environment, Nature Conservation and Nuclear Safety at:

<http://www.umweltministerium.d>

#### 4.4.2.7.2 Austria

In Austria, the feed-in tariff is determined by way of the 2009 Ökostromverordnung (~green electricity regulation) according to which, since 1 January 2009, new or revitalized facilities in which the average annual output has been increased by more than 50 % are eligible for the feed-in tariffs listed in [Table 4-11](#), below.

Tariff [cent/kWh]	
For the 1 <sup>st</sup> GWh	6.23
For the next 4 GWh	4.99
For the next 10 GWh	4.15
For the next 10 GWh	3.92
For any quantity of exceeding 25 GWh	3.76

Table 4-11 Feed-in tariffs acc. to the 2009 green electricity regulation 50%. [16]

For revitalized facilities in which the average annual output is increased by at least 15 %, the 2009 Ökostromverordnung describes the somewhat lower tariffs listed in [Table 4-12](#) below:

Tariff [cent/kWh]	
For the 1 <sup>st</sup> GWh	5.94
For the next 4 GWh	4.56
For the next 10 GWh	3.79
For the next 10 GWh	3.42
For any quantity of exceeding 25 GWh	3.29

Table 4-12 tariffs acc. to the 2009 green electricity regulation 15%. [16]

According to the Ökostromverordnung, these tariffs are subject to the condition that the facility be commissioned on or before 31 December 2009, and that the increase in average annual output be documented by the expert's opinion of a certified engineer.

For more information on the Austrian provisions, please go to:

<http://www.oem-ag.a>

#### 4.4.2.7.3 Switzerland

Switzerland's revised Energy Act includes a package of measures for promoting renewable energy sources and electric efficiency. The main pillar of that act is the break-even feed-in tariffs table for electricity generated from renewable energy sources. Constructed according to the Swiss Federal Council's energy regulation (EnV), the anticipated feed-in tariffs will basically consist of three elements. For information beyond that contained in the following brief overview, please consult the quoted sources.

Base rate: The applicable output for determining the feed-in tariff is the equivalent output, i.e., the quotient of the amount of electricity, in kWh, measured at the feed-in point in the course of the year in question, divided by the total number of hours of the year in question less the number of elapsed hours prior to the facility's commissioning and/or subsequent to its shutdown. The equivalent-output-dependent base rate is calculated proportionally for the power classes listed in

Table 4-13:

Power class [kW]	Hydraulic engineering bonus [Rp./kWh]
< 10	26.0
< 50	20.0
< 300	14.5
< 1 MW	11.0
< 10 MW	7.5

Table 4-13 se-rate feed-in tariff in Switzerland acc. to power class [16]



Pressure class bonus: The pressure class bonus is prorated according to the gross head of the system relative to the head categories shown in [Table 4-14](#) below:

Power class [kW]	Hydraulic engineering bonus [Rp. /kWh]
< 5	4.5
< 10	2.7
< 20	2.0
< 50	1.5
> 50	1.0

*Table 4-14 pressure class bonus in Switzerland acc. to head category [16]*

Hydraulic engineering bonus: If the implemented, state-of-the-art hydraulic engineering (incl. discharge lines) accounts for less than 20 % of the overall first cost of the project, no hydraulic engineering bonus is granted. For shares in excess of 50 %, the full bonus is granted. Shares ranging from 20 % to 50 % are linearly interpolated. The bonus is prorated according to the facility's equivalent output in line with the power classes listed in [Table 4-15](#). "Dotierwasserkraftwerke" ("remuneration" hydropower stations) are excluded from this bonus.

Power class [kW]	Hydraulic engineering bonus [Rp. /kWh]
< 10	5.5
< 50	4.0
< 300	3.0
> 300	2.5

*Table 4-15 Hydraulic engineering bonus in Switzerland acc. to power class*

The source of the above information and additional data can be found at:

Energy Act: [http://www.admin.ch/ch/d/sr/c730\\_0.html](http://www.admin.ch/ch/d/sr/c730_0.html)

Energy Regulation: [http://www.admin.ch/ch/d/sr/c730\\_01.html](http://www.admin.ch/ch/d/sr/c730_01.html)

General information: <http://www.admin.c>



## 5 Review of Two PAT Case Studies

### 5.1 Pumps as Turbines substituting pressure reducing valves

#### 5.1.1 Selection and location of Pumps as Turbines substituting pressure reducing valves

Rational use of natural resources is increasingly important, for both economic and environmental reasons. Water supply system efficiency is critical to sustainable development of a city, since suboptimal operations can elevate energy consumption in pump stations and increase leakage in the network. Climatic, social, and political factors influence consumption, and consequently the operations of water supply systems. In this context, the concept of smart water networks arises, which, through field measurements and mathematical modeling, allow decisions to be made quickly, ensuring optimized, high quality operations. [52].

Pressure control is one of the most important issues in optimizing the operation of networks. It is important to reduce leakage volume and avoid pipeline disruption. The topography and topology of the system define high- and low-pressure zones. Technical standards establish the maximum and minimum values accepted for operation.

In low pressure areas, boosters with frequency inverters can be installed to maintain proper pressure on the network. For high-pressure zones, it is common to use Pressure Reducing Valves (PRVs) to maintain sufficient pressure in the entrance sector, maintaining the desired minimum pressure in the critical node. Several studies explore optimized PRV operation and its location, minimizing leakage losses [53], [54].

However, from the energy viewpoint, PRV dissipates pressure energy, adding a localized head loss to the system. This energy loss opposes modern principles of rational use of resources. In our new paradigm, energy pressure could be used to actuate a turbine coupled to a generator, producing electricity and maintaining the pressure reduction commitment in the sector. Due to the low power found at such sites, use of conventional turbines is not feasible [55] [56], [57].

However, these turbines are not manufactured at large scale yet, making their immediate application difficult. An alternative is to use PATs, which have low cost and good efficiency [58]. show a similar behavior between PAT and PRV, indicating the viability of this solution.

However [59], [60] carry out simulations over an extensive period and observe that during periods of low consumption, PAT is not able to insert a sufficient head loss to reduce pressure to acceptable standards, [61] finds a similar response between PAT and PRV in a system in Iran, where demand change throughout the day is not very significant.

The method to be used for PAT selection and location in water supply network operations, is based on maximizing the benefit represented by the produced energy and the leakage volume reduced. As an operating constraint, the method requires that the PAT should be able to maintain the pressure on each node of the network within the established limits. The BEP of the machine and its location are set through an optimization process based on Particle Swarm Optimization (PSO).

From these values, the specific speed of the machine is obtained, selecting the nearest curve available. To accomplish this, a set of complete characteristic curves of pumps found in Ref. [62] and represented in the Suter plan is used. In the final stage, the network is simulated with the selected machine to calculate the energy produced and the node pressures. The method is applied to three fictitious networks, available in Refs. [63] , [64], and the results are compared with the PRV operation.

## 5.1.2 Pump as turbine modeling

### 5.1.2.1 “Pipe + PAT” boundary

Several methods can be used to perform a hydraulic simulation of water supply networks notably the gradient method, now widely used. In this study, the steady-state problem is solved through transient flow equations, using the Method of Characteristics (MOC), as proposed by Refs. [66][67]

Applying the continuity law to a generic node, as shown in [Figure 5-1](#), and using the MOC positive line to calculate flow at convergent pipes, and the negative line for divergent pipes, the node general equation is obtained ([Equation 5-1](#)).

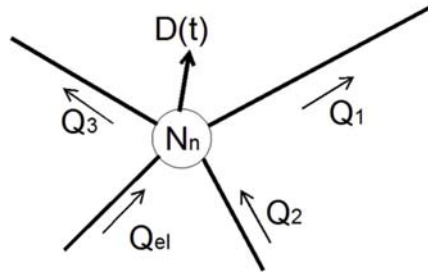


Figure 5-1 Connections in a generic node. [65]

$$\left[ \sum_{i=1}^{CP} \frac{CA(i)}{BB(j)} + \sum_{j=1}^{DP} \frac{CB(i)}{BB(j)} - D(t) \right] - \left[ \sum_{i=1}^{CP} \frac{1}{BA(i)} + \sum_{j=1}^{DP} \frac{1}{BB(j)} \right] \cdot HN - Q_{el} = EN - BN \cdot HN - Q_{el} = 0$$

Equation 5-1

where:

CA [m], BA [s/m<sup>2</sup>] - coefficients of positive line of MOC;

CB [m], BB [s/m<sup>2</sup>] - coefficients of negative line of MOC;

CP [dimensionless] - number of convergent pipes connected to the node;

DP [dimensionless] - number of divergent pipes connected to the node;

HN [m] - node head;

$Q_{el}$  [m<sup>3</sup>/s] - flow through a non-pipe element.

To obtain the best location for PAT installation, a non-tube element called “Pipe þ PAT” is created. This element considers the existence of a PAT immediately after the pipe upstream node. A fictitious node is created to connect PAT with pipe, as shown in [Figure 5-2](#). Thus, the optimization algorithm searches the pipe identification number with best conditions for PAT installation and replaces the pipe with this element. The algorithm also considers the possibility of inversion between downstream and upstream nodes. If the flow occurs in the opposite direction, the element is disconnected from the network, maintaining the original condition only with the pipe. This procedure simulates a bypass, which can be used in periods in which PAT operation is not feasible.

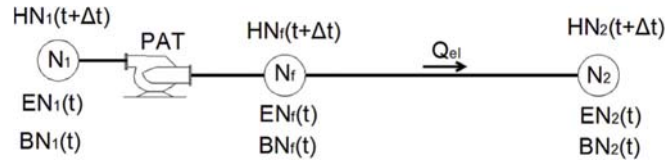


Figure 5-2 Non-pipe element "Pipe p PAT00. [65]

Using the nodes general equation for  $N_1$  and  $N_f$ , the general equation for non-pipe elements is obtained (Equation 5-2). With three variables to be determined ( $HN_1$ ,  $HN_f$ , and  $Q_{el}$ ), boundary conditions are necessary to solve this equation. In this case, pump characteristic curves of head and flow are used.

$$HN_1 - HN_f = \left( \frac{EN_1}{BN_1} - \frac{EN_f}{BN_f} \right) - \left( \frac{1}{BN_1} - \frac{1}{BN_f} \right) \cdot Q_{el}$$

Equation 5-2

### 5.1.2.2 Pump characteristic curves

Characterization of hydraulic machines is made through curves relating head, flow, torque, and speed. Alternation of the signs of these parameters defines eight distinct operational areas, which can be represented by the Suter plan [68].

Figure 5-3a show an example of the 14 curves available in Ref. [62]. The empty markers show the operating zone as a turbine. For each of the available curves, this operational area is identified, and considering nominal rotational speed, new curves relating the dimensionless coefficients of flow,  $q$ , and head,  $h$ , are obtained, as shown in Figure 5-3b. This new representation allows adjustment of a power curve (Equation 5-3). Therefore, with the BEP machine only, its characteristic curve in turbine mode can be obtained, using the available dimensionless curve with the nearest specific rotation.

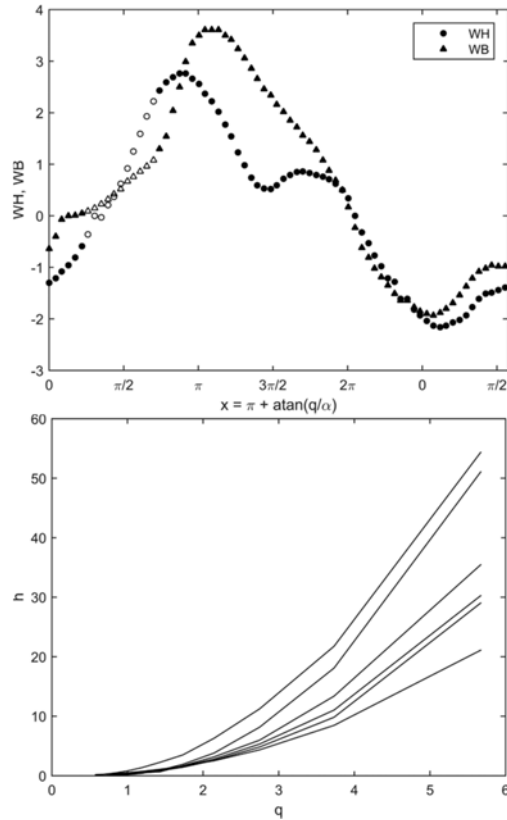


Figure 5-3 a) Head and torque curves in Suter plan; b) Dimensionless curves in turbine mode.[65]

$$h = a \cdot q^b$$

Equation 5-3

where:

a, b [dimensionless] - curve adjustment coefficients;

h [dimensionless] - head coefficient;

q [dimensionless] - flow coefficient.

### 5.1.3 PAT selection and location procedure

PAT selection and location are made simultaneously, based on maximizing the benefit, defined by the energy produced and leakage volume reduced. Thus, considering the energy and water tariffs, the objective function is written as follows:

$$FO = \sum_{i=1}^{24} \left[ t_e \frac{\gamma Q_i H_i \eta_i}{1000} + \sum_{j=1}^n t_a \cdot K \cdot (\sqrt{P_{j1}} - \sqrt{P_{j2}}) \cdot 3600 \right] + Pen$$

Equation 5-4

Where:

FO [\$] - objective function to be maximized;

$t_e$  [\$/kWh] - energy tariff;

$g$  [N/m<sup>3</sup>] - water specific weight;

$Q_i$  [m<sup>3</sup>/s] - PAT flow in time  $i$ ;

$H_i$  [m] - PAT head in time  $i$ ;

$\eta_i$  [dimensionless] - PAT efficiency in time  $i$ ;

$n$  [dimensionless] - nodes affected by PAT operation;

$t_a$  [\$/m<sup>3</sup>] - water tariff;

$K$  [1/s·m<sup>1/2</sup>] - leakage coefficient;

$P_{j1}$  [m] - node  $j$  pressure in time  $i$  before PAT installation;

$P_{j2}$  [m] - node  $j$  pressure in time  $i$  after PAT installation;

Pen [\$] - penalty function.

The penalty function is based on problem constraints. In this case, all nodes must maintain a minimum pressure through a 24-h period. Therefore, the penalty function can be calculated using [Equation 5-5](#). The penalty coefficient is very important to achieving accurate results with bio-inspired algorithms. According to [69], the penalty function can be neither too hard, so as to avoid a wide search across the space, nor too soft, leading to unfeasible solutions. Therefore, the value of 100,000 was adopted as the penalty coefficient.

$$Pen = \sum_{i=1}^{24} \sum_{j=1}^n \alpha \cdot |P_{min} - P_{j,i}|$$

Equation 5-5

where:

$\alpha$  [\$/m] - penalty coefficient (a value of 100,000 is adopted);

$P_{min}$  [m] - node  $j$  pressure in time  $i$ ;

$P_{j,i}$  [m] - minimum pressure established.



#### 5.1.4 Results and discussion

To evaluate the proposed method, three fictitious networks, presented by Refs. [63] ,[64], are studied. These networks are studied to achieve the best District Metering Area (DMA) configuration and PRV location, minimizing water losses, making them a good example for which to compare PAT location results.

According to [70], leakage modeling in pressurized pipes is similar to an orifice, and can be generalized by Equation 5-6. The exponent N depends on the leakage orifice area. In this work, leakage behavior is considered equal to an orifice, with N equal to 0.5. The K value is adjusted for each case study to maintain water loss to around 30%, a common value observed in Brazilian water supply networks [72]. Thus, in addition to demand, a leakage contribution is added in each node, calculated by Equation 5-6. This procedure allows comparison of PAT performance in leakage control with a PRV. In this case, the minimum pressure for the critical node is 10 m, as established by ABNT [71].

$$Q_1 = K \cdot P_n^N$$

*Equation 5-6*

where:

$Q_1$  [l/s] - leakage flow;

K [l/s.m<sup>1/2</sup>] - leakage coefficient;

N [dimensionless] - leakage exponent;

$P_n^N$  [m] - node pressure.

##### a) Example 1

The first network created by Ref. [63] has 12 pipes and 10 nodes, supplied by a reservoir, as shown in Figure 5-4. Defining PAT location is straightforward, since maximum power is obtained by installing the machine just after the reservoir, which also ensures the best pressure control, since all nodes are at the same elevation. Nevertheless, the proposed method is applied, identifying the first pipe as the ideal site for PAT installation, as shown in Figure 5-4.

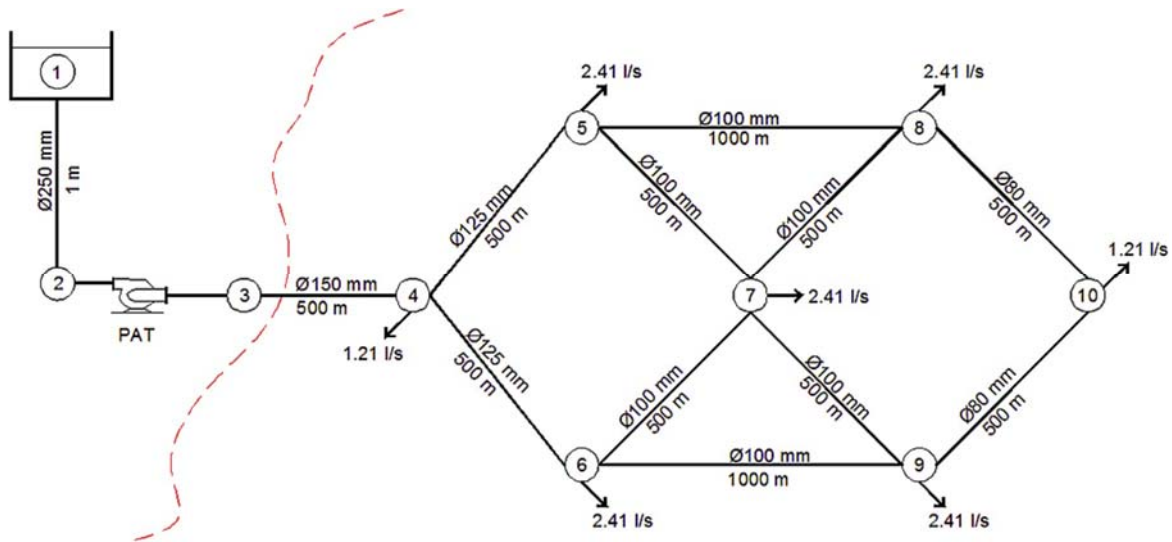


Figure 5-4 Layout of network 1 and PAT location. [65]

Using the same location found for PAT installation, a new simulation is made with a PRV with constant outlet pressure, adjusted for 33 m, which supplies critical node during the maximum consumption period. Table 5-1 shows the results obtained in each case. Note that PAT is selected to operate during higher consumption periods (7-24 h), when more energy is available.

Table 5-1 Results of PAT selection and location for Example 1 [65]

PAT	1	2
Number of objective function evaluations	3024	2768
Number of particles	16	16
$Q_{PAT}$ [l/s]	29.11	9.51
$H_{PAT}$ [m]	21.32	30.85
Energy produced in 24 h [kWh]	78	94
$K$ [l/s · m <sup>1/2</sup> ]	0.0002	
Leakage reduction - PAT [m <sup>3</sup> ]	62.5	86.2
PRV outlet pressure [m]	33	33
Leakage reduction - PRV [m <sup>3</sup> ]	156.4	156.4
Leakage difference between PAT and PRV [%]	39.94	55.06

During this period, PAT behavior is similar to a PRV, However, when consumption declines, there is no energy production and the pressure remains high. Thus, the PAT performance in leakage reduction represents only 39.94% of PRV results.

To improve PAT pressure control, a second machine is selected to operate in parallel during the period of 1-6 h. Although energy production and leakage control improve, PRV continues to show better pressure control.

Figure 5-5 compares critical node pressure for each case studied, where the problem described for low consumption periods can be observed in detail.

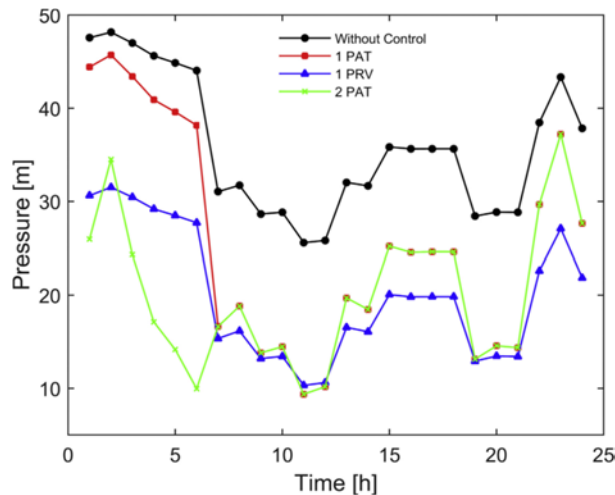


Figure 5-5 Critical node pressure for Example 1. [65]

#### b) Example 2

The second network presented by Ref. [64] is composed of 24 pipes and 17 nodes, with a reservoir as water source (Figure 5-6). At first, only one machine is selected to perform pressure control. The pipe just after the reservoir is selected for PAT installation, since this location allows pressure reduction in the whole network and uses maximum flow in energy production.

two sectors with slightly different pressures can be identified: the first with 17.2 m of mean pressure and the second with 21.6 m, indicating the possibility of the use of an additional machine. Therefore, a new selection is made considering the use of two machines, obtaining the configuration shown in Figure 5-6. In this scenario, the network is divided into two DMAs, since the flow through nodes 4 and 9 has little influence on the pressure of the second DMA. This configuration improves energy production and leakage reduction. It is also the same configuration proposed by Ref. [64], who also recommends the closure of pipe between nodes 4 and 9.

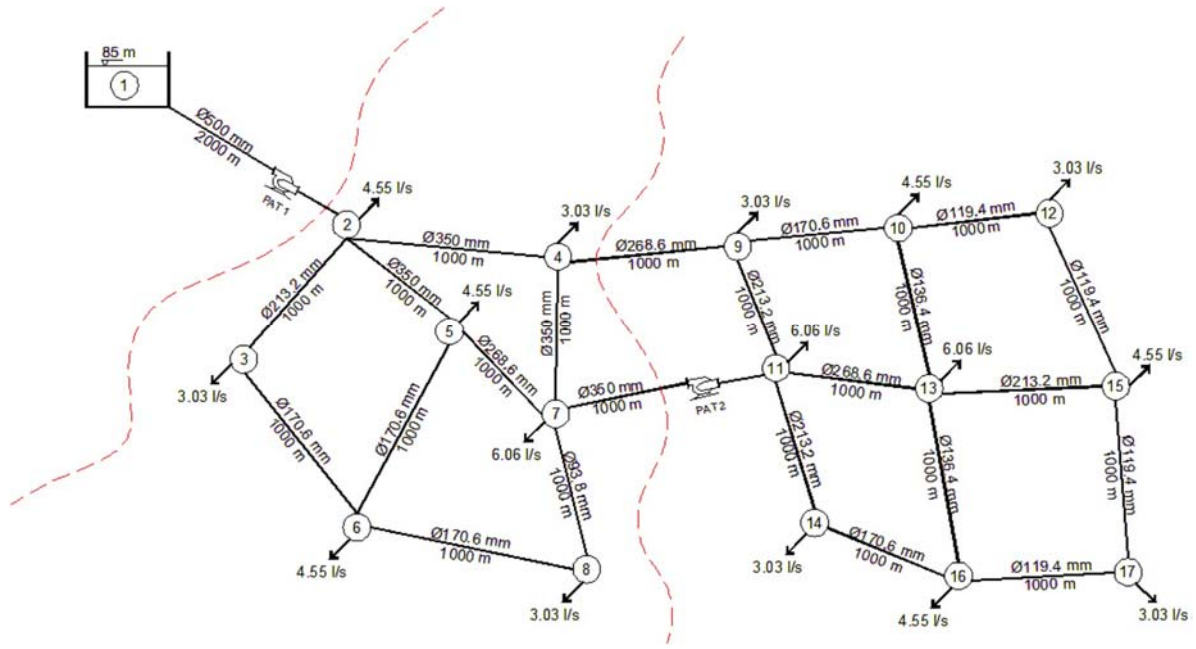


Figure 5-6 Layout of network 2 and PAT location. [65]

Table 5-2 shows the results for PAT selection and location, considering one and two PATs. Note that the leakage reduction improves more than the energy production. This fact can be explained due to the reduced head of PAT 1, which has the higher potential. PAT 2 uses only a part of total inflow, contributing less energy. As observed in Example 1, the operating point of the machines is selected considering the maximum consumption period, when energy production and leakage reduction are higher. Note the high number of particles in the PSO optimization algorithm to avoid premature convergence in local minimums.

Table 5-2 Results of PAT selection and location for Example 2.[65]

Case	1	2	
PAT	1-2	1-2	7-11
Number of objective function evaluations	14,240	22,400	
Number of particles	160	320	
$Q_{PAT}$ [l/s]	182.9	162.32	134.6
$H_{PAT}$ [m]	32.57	26.21	18.45
Energy produced in 24 h [kWh]	463.7	464.7	
$K$ [l/s·m <sup>1/2</sup> ]	0.0002		
Leakage reduction - PAT [m <sup>3</sup> ]	445.8	490.18	
PRV outlet pressure [m]	16	16	20
Leakage reduction - PRV [m <sup>3</sup> ]	854.2	982.8	
Leakage difference between PAT and PRV [%]	52.2	49.9	

Figure 5-7 shows that addition of a second machine results in a pressure reduction throughout the 24 h simulation only for the second sector, which contains node 17. For comparison, the two scenarios are simulated considering the use of PRV with 16 m and 20 m constant outlet pressure, respectively.

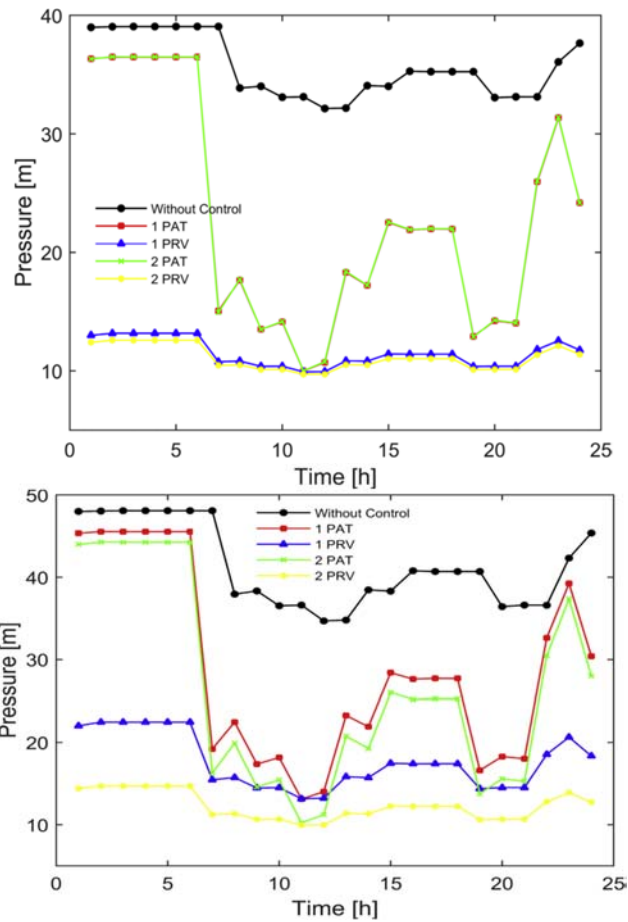


Figure 5-7 Critical nodes pressure for Example 2: a) Node 8; b) Node 17. [65]

For maximum consumption, PAT and PRV performance in pressure control are identical. However, with consumption variations over 24 h, the low consumption problem observed in Example 1 continues, and PRV performance remains better resulting in major leakage reduction.

### c) Example 3

The last network proposed by Ref. [63] is the biggest, with 83 pipes and 76 nodes, also supplied by one reservoir, as shown in Figure 5-8. Considering the use of just one PAT for pressure control, the pipe just after the reservoir is selected to install the machine, as observed in Examples 1 and 2.

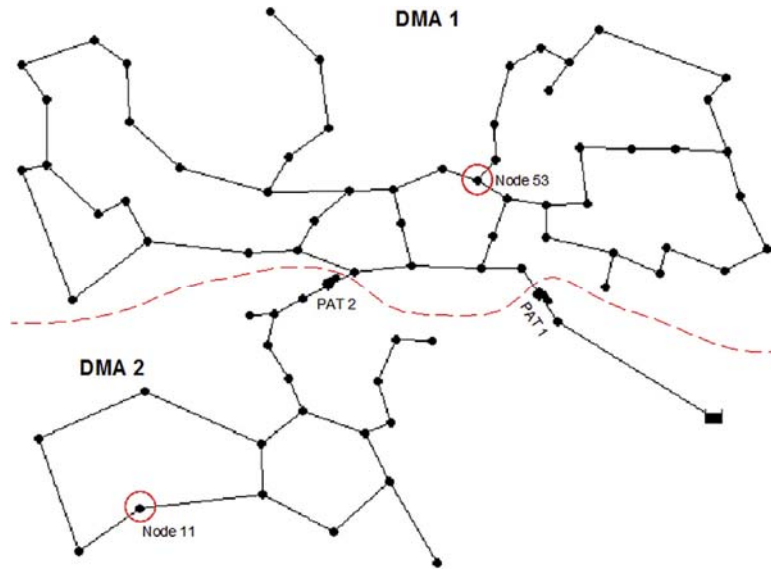


Figure 5-8 Layout of network 3 and PAT location. [65]

Evaluating pressure zones shown in Figure 5-9, a low-pressure zone can be observed in the right-most part of network. The other part has a similar pressure over the area, which indicates no need for a second machine. Nevertheless, a second machine is selected, creating two DMAs (Figure 5-8).

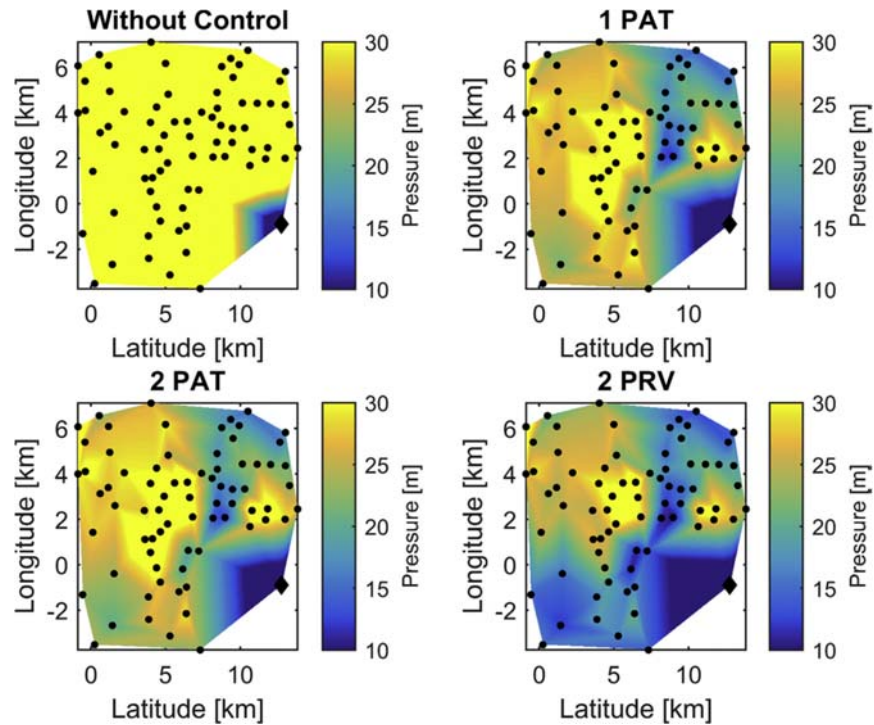


Figure 5-9 Pressure zones of network 3 for maximum consumption. [65]

As shown in [Table 5-3](#), in this scenario, the addition of a second machine reduces the benefits. This occurs because PAT 1 reduces energy production, since its head reduces to allow the insertion of a second machine.

*Table 5-3 Results of PAT selection and location for Example 3. [65]*

Case	1	2	
PAT	54–76	54–76	4–22
Number of objective function evaluations	20,160	46,400	
Number of particles	160	320	
$Q_{PAT}$ [l/s]	71.78	53.21	51.04
$H_{PAT}$ [m]	36.07	13.25	12.35
Energy produced in 24 h [kWh]	356.54	325.8	
$K$ [l/s · m <sup>1/2</sup> ]	0.0003		
Leakage reduction - PAT [m <sup>3</sup> ]	268.6	243.1	
PRV outlet pressure [m]	10	10	26
Leakage reduction - PRV [m <sup>3</sup> ]	424.0	473.9	
Leakage difference between PAT and PRV [%]	63.3	51.3	

Although the second sector shows a small pressure reduction, as shown in [Figure 5-9](#), DMA 1 is bigger and contributes more for total leakage volume. Observing specific nodes, as shown in [Figure 5-10a](#), the effects of an additional PAT are observed for each sector. [Figure 5-10b](#) shows a node inside sector 1, where the pressure using 1 PAT is slightly lower than using 2 PATs. In contrast, [Figure 5-9](#) shows a node of DMA 2, where the additional PAT slightly improves pressure control during high consumption periods. Using PRV with constant outlet pressure adjusted to 26 m and 10 m, respectively, a small improvement is observed, since the second sector shows a significant pressure reduction.



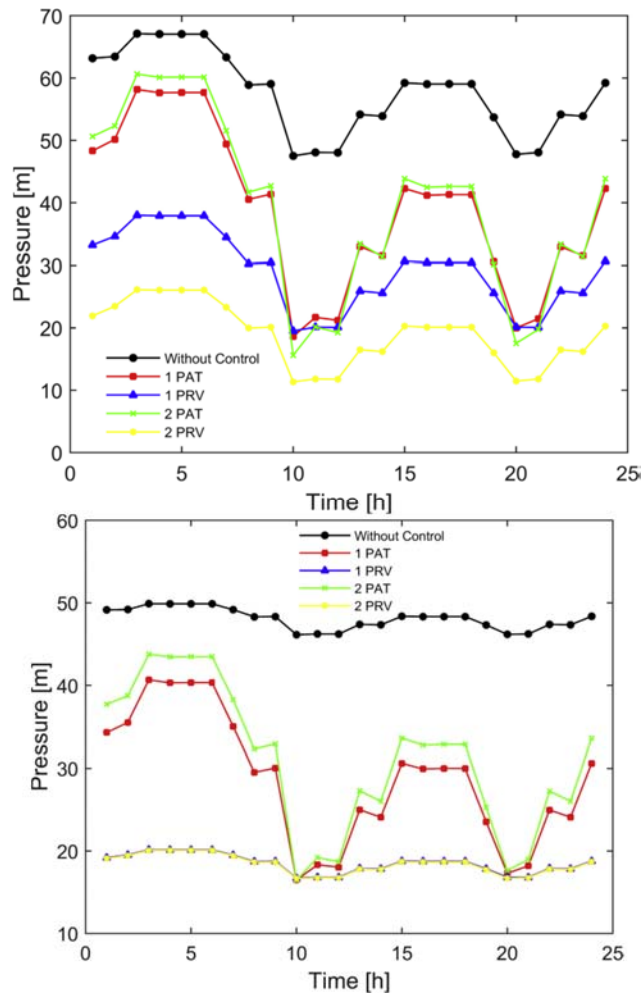


Figure 5-10 Critical node pressure for Example 3: a) Node 11; b) Node 53. [65]

### 5.1.5 Conclusion

An innovative method for PAT selection was presented, considering the dynamic operation of water supply networks and establishing the best location for its installation at the same time. The method shows that the maximum consumption period is used to define the BEP of the machine. Despite the reduced pressure drop during this period, the high flow maximizes energy production and leakage reduction. In addition, the method could identify the best location for installation of multiple PATs, optimizing the combined operation. However, Examples 2 and 3 show that the addition of a small PAT is not always a good strategy, since such PATs can affect the operation of the principal machines, reducing the benefits of energy production and leakage reduction.

Due to the complexity of the problem, a high number of particles in the PSO optimization algorithm must be used to avoid premature convergence in local minimums. This characteristic confirms that PSO is well suited to this problem, since the results obtained are good responses to the problem. PSO according its original purpose cannot manage the constraints of the problem, requiring the use of a penalty function, which distorts the search space and makes the search process more difficult. Future research should study penalty functions and methodologies to address the constraints, to improve the efficiency of the method.

Considering the maximum consumption period, PAT and PRV show similar performance. However, during low consumption periods, PAT cannot maintain adequate outlet pressure, yielding high leakage rates. Thus, control mechanisms should be developed to solve this problem. Attractiveness of the investment will depend on the local electricity tariff, which should be higher than water production costs, enabling the micro central installations described herein. However, it is necessary to highlight the uncertainties of the proposed method. The characteristic curves used are estimated, based on available dimensionless curves, which can differ from real PAT performance curves. Therefore, performance tests are highly recommended when possible. Another source of uncertainty is leakage modeling, which cannot represent the real scenario, due to its dynamic behavior and undefined location. The optimization procedure also carries uncertainty, since bio-inspired algorithms cannot guarantee achievement of the best solution. Finally, the hydraulic models also carry uncertainty in their results, since their stopping criteria is based on an acceptable error, which is very small, contributing to the total uncertainty. nevertheless, the method presented is fundamental to obtaining the best solution in exercising pressure control and generating electricity in a water supply network [65].

## 5.2 Environmental impacts of electricity generation

### 5.2.1 Introduction

The water industry is the 4th largest energy intensive sector in both the UK and Ireland [73]. Most of the electricity used to treat and supply water is sourced from fossil fuels, with an average carbon footprint of 483 g CO<sub>2</sub> equivalent per kWh (g CO<sub>2</sub> eq./kWh) consumed [74]. Overall, the UK water industry is responsible for 5 million tons of CO<sub>2</sub> emissions annually [74], and reducing the

demand for fossil-based electricity is a key sustainability objective in terms of economics, resource efficiency and environmental responsibility.

Water companies often have to respond to government regulations that state that utility suppliers must monitor and reduce greenhouse gas (GHG) emissions [75]. For example, [76] are targeting a 25% reduction of their GHG emissions by 2015, and 50% by 2035. Renewable energy can provide one solution to help water companies meet their GHG emission targets and provide long-term sources of energy for water treatment and supply. In Europe, hydropower is considered the most suitable technology for the water sector to adopt for generating electricity.

Micro-hydropower (MHP) installations have recently been identified as an area of growing interest for water companies as they consider energy recovery from within water infrastructure [77]. These sites are located throughout the water infrastructure where excess pressure exists and sites can generate between 5 and 300 kW. Life cycle assessment (LCA) has previously been used to assess the environmental impacts of renewable energy systems [78].

## 5.2.2 Methods

### a) Goal and scope definitions

The objective of this study is to calculate the life cycle environmental balance of electricity generated by three micro hydropower installations in the water supply infrastructure. Five relevant environmental impact categories were selected from CML [80].

*Table 5-4 Life cycle assessment impact categories selected to compare micro-hydropower projects with marginal UK grid electricity generation, descriptions provided [79].*

Impact category	Abbrev	Units	Information
Global warming potential	GWP	kg CO <sub>2</sub> eq.	GHG emissions contributing to climate change and their effects on ecosystem health, human health and material welfare (measured in equivalents kg CO <sub>2</sub> eq./kWh).
Abiotic resource depletion potential	ARDP	kg Sb eq.	Protection of human welfare, human health and ecosystem health (measurement based on quantity of minerals extracted as a fraction of concentration of global reserves).
Acidification potential	AP	kg SO <sub>2</sub> eq.	Impacts of acidifying substances on soil, surface water, groundwater, organisms, ecosystems and building materials (expressed as equivalent sulphur dioxide concentrations).
Human toxicity potential	HTP	kg 1,4-DCBe eq.	Substances that are toxic to human health, calculated with USES-LCA, describing fate, exposure and effects of these substances (equivalent 1,4-dichlorobenzene).
Fossil resource depletion potential	FRDP	kg kJ eq.	Depletion of energy as fossil fuel deposits used to generate electricity (measured in equivalent kg kilojoules)

**Table 5-4**, These categories were chosen as they represent the direct environmental impacts (human health, ecosystem quality and resources) associated with the hydro projects and have been previously presented in literature for renewable projects and water infrastructure projects.

The functional unit was 1 kWh of electricity generated, for comparison with marginal UK grid electricity generation via a natural gas combined cycle turbine (NG-CCT) power station [81]. The system boundaries included raw material extraction, processing, transport and all installation operations, followed by electricity generation over the lifetime of the turbines [Figure 5-11](#)

*J. Gallagher et al. / Journal of Cleaner Production 99 (2015) 152–159*

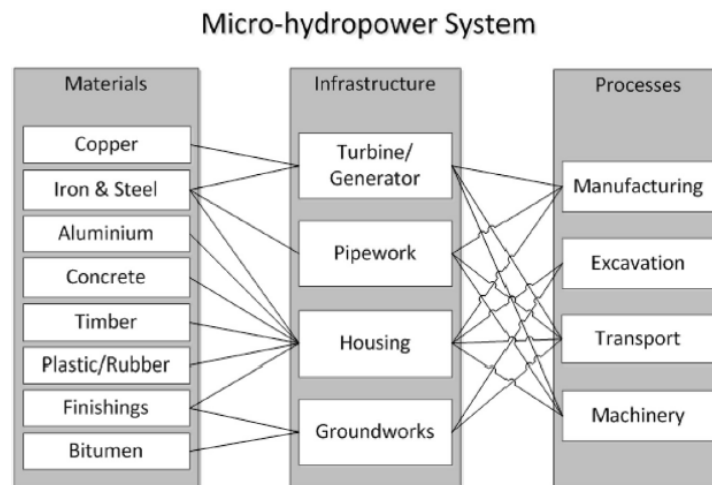




*Figure 5-11 Primary materials and processes considered within the system boundaries for MHP. [79]*

### b) Case study descriptions

Details relating to the three case studies examined in this paper are outlined in [Table 5-5](#). The three MHP projects selected represent a broad range of typical installations that can take place in water infrastructure: a 15-kW installation to control water flow into a new water treatment works, a 90-kW new build installation to replace a dated turbine at a water treatment works, and a 140-kW installation as part of a new water treatment works project.

Table 5-5 Description of MHP case studies for LCA [79]

15 kW Pen y Cefn Water Treatment Works	90 kW Vartry Reservoir & Water Treatment Works	140 kW Strata Florida Water Treatment Works
		
<ul style="list-style-type: none"> <li>• Location: Gwynedd, Wales</li> <li>• Dŵr Cymru Welsh Water</li> <li>• Design capacity: 15 kW</li> <li>• Power output: 12.5 kW</li> <li>• Turbine: Zeropex Difgen</li> <li>• Head: 90–105 m</li> <li>• Flow: 10–30 l/s</li> <li>• Existing housing in place</li> <li>• Gravity fed by Llyn Cynwch reservoir</li> <li>• New installation, flow control from Difgen turbine to DAF treatments system</li> </ul>	<ul style="list-style-type: none"> <li>• Location: Wicklow, Ireland</li> <li>• Dublin City Council</li> <li>• Design capacity: 90 kW</li> <li>• Power output: 78 kW</li> <li>• Turbine: Kaplan</li> <li>• Head: 7–16 m</li> <li>• Flow: 580–1200 l/s</li> <li>• Concrete housing constructed</li> <li>• Gravity fed from nearby Vartry reservoir</li> <li>• Replacing outdated Pelton wheel turbine which generated electricity for site since 1940's</li> </ul>	<ul style="list-style-type: none"> <li>• Location: Ceredigion, Wales</li> <li>• Dŵr Cymru Welsh Water</li> <li>• Design capacity: 140 kW</li> <li>• Power output: 110 kW</li> <li>• Turbine: Pelton twin jet</li> <li>• Head: 183–195.5 m</li> <li>• Flow: 100 l/s</li> <li>• GRP kiosk constructed</li> <li>• Fed by Llyn Teifi and Llyn Egnant raw water reservoirs</li> <li>• New installation, existing DAF system on site, 250–300 kW energy consumption on site</li> </ul>

A conservative nominal turbine and generator lifespan of 30 years was applied. Turbine lifespan values cited in the literature vary considerably, from 20 to 100 years [78].

A number of assumptions were made during the LCA study in order to define comparable system boundaries and account for all important contributory processes. These included aspects related to materials used, products, manufacturing processes, transportation contributions, operations/maintenance and decommissioning, Table 5-6.

Table 5-6 Assumptions made for LCA of MHP Projects. [79]

Assumptions	Details
Boundary conditions	Grid losses and some external infrastructure details omitted in calculations of carbon payback for MHP installations.
Project lifespan	30-year lifespan for turbines <sup>a</sup> , 100-year lifespan for housing, 10-year lifespan for paint (further details in <a href="#">Supplementary information</a> ).
Raw materials, manufacturing & transportation	Impact category data for raw materials (e.g. steel, concrete, etc.), manufacturing (e.g. steel product manufacturing) and transportation (e.g. freight transport) were sourced from Ecoinvent v.3 database via SimaPro8 (Ecoinvent, 2014). The environmental impact of soil excavation was omitted.
Products	Estimations for the mass of raw materials contained in turbines and generators were based on consultation with manufacturers (Dublin City Council, 2013; Dŵr Cymru Welsh Water, 2013).
Electricity generation	The power generated by the turbines is based on several years of historical data and the average power generated is assumed to be maintained over the 30-year project lifespan.
Operations & maintenance, decommissioning	Few data exist on turbine and generator maintenance burdens, which are considered trivial compared with manufacturing and installation burdens and therefore omitted from the LCA process, as for similar renewable generation LCA studies (D'Souza et al., 2011).

<sup>a</sup> Conservative nominal lifespan used as it varies in literature: 20 years (Guezuraga et al., 2012; Pascale et al., 2011), 25–30 years (Varun et al., 2009), 50 years (Suwanit and Gheewala, 2011), 100 years (Rule et al., 2009).

**c) Inventory for LCA case studies**

To undertake a detailed LCA of the three case studies, data were collected from water suppliers and/or turbine manufacturers [79]. The data included the size and capacity of the turbine and generator units, the materials and construction details, including information of on-site plant and machinery. This information was extracted from a combination of sources for the purpose of the LCA, project reports, quantities spreadsheets and project design drawings. This study followed ISO 14040 standards for LCA, and as such accounted for at least 95% of the total mass and 90% of the total energy inputs for each MHP project [85].

**d) Reference system and carbon payback time**

NG-CCT power stations operating at 50% conversion efficiency represent marginal electricity generation in the UK that is avoided by energy saving and renewable energy measures. Therefore, 1 kWh of NG-CCT-generated electricity was taken as the reference system for comparison with 1 kWh MHP-generated electricity. The carbon payback time was calculated as the operational time required for the MHP to offset a quantity of marginal grid electricity GHG emissions equivalent to GHG emissions arising over the life cycle of MHP system manufacture, installation and operation. However, [83] outlined how LCA results may not truly reflect the environmental balance of a product over its lifetime, owing to temporal trends in the environmental burdens of contributory or counterfactual processes. A dynamic analysis was therefore applied to forecast the potential cumulative GHG mitigation potential of MHP installations based on future emission projections for marginal grid electricity generation.

**e) Interpretation and sensitivity analysis**

To enable a comparison of relative contributions to the five environmental burdens considered at the European scale, EU25 annual loading data for those impact categories were taken from [80]. and expressed per capita, assuming a population of 465 million people. Environmental burdens per kWh were then divided by per capita loading, enabling a visual comparison of impact category contributions. Sensitivity analyses were undertaken in relation to manufacturing and transport for each MHP installation, as the most substantial level of uncertainty was noted for these project components. The following scenarios were assessed in which the environmental burdens attributable to uncertain components were varied by  $\pm 50\%$ .

- Scenario 1 Manufacturing of turbine/generator
- Scenario 2 Manufacturing of pipework
- Scenario 3 Manufacturing & construction of housing
- Scenario 4 Transportation of materials

### 5.2.3 Results & discussion

The results of the LCA are presented in [Table 5-7](#) as the total environmental burdens per kWh of electricity generated over the 30-year lifespan by the three MHP turbines. The table also shows the carbon payback time in relation to offset grid electricity generation.

*Table 5-7 Total environmental impacts of MHP projects for different impact categories and carbon payback time (expressed per kWh generated over project 30-year lifespan). [79]*

Case study	Impact categories <sup>a</sup>					Carbon payback (years)
	GWP (g CO <sub>2</sub> )	ARDP (g Sb)	AP (g SO <sub>2</sub> )	HTP (g 1,4DCBe)	FRDP (MJ)	
15 kW	2.14	1.4E-04	4.0E-02	10.05	2.7E-02	0.16
90 kW	4.36	1.1E-04	4.3E-02	9.17	1.1E-01	0.31
140 kW	2.78	9.4E-05	3.3E-02	8.91	6.1E-02	0.21

<sup>a</sup> GWP, global warming potential; ARDP, abiotic resource depletion potential; AP, acidification potential; HTP, human toxicity potential; FRDP, fossil resource depletion potential.

The total GWP impact associated with the three MHP installations over the lifespan of the project ranged from 2.14 to 4.36 g CO<sub>2</sub> eq./kWh. These results are comparable to previous results from LCA studies of hydropower projects: 5.6 g CO<sub>2</sub> eq./kWh for a 116MW project [84], a conservative 15 g CO<sub>2</sub> eq./kWh by [74], and a range from 0.3 to 13 g CO<sub>2</sub> eq./kWh for 11 run-of-river hydro projects [84].

[Figure 5-12](#) displays the contribution of major components towards the environmental burdens per kWh of electricity generated for each of the turbines. The figure displays the core components (turbine/generator and pipework) and variable components (ancillary metals, concrete and other) as block and hatched sections, respectively.

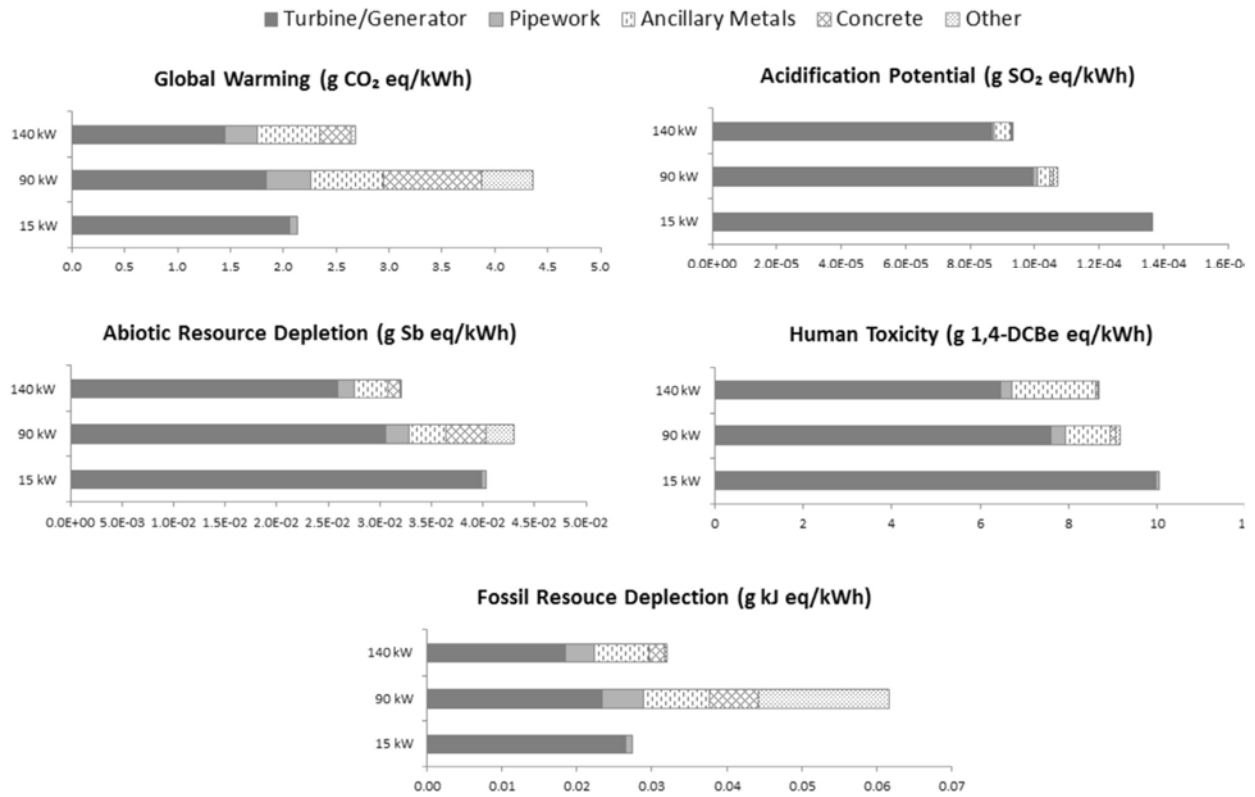


Figure 5-12 Breakdown of environmental impacts of MHP case studies expressed per kWh generated over project 30-year lifespan (solid blocks represents core components and hatched blocks represent variable components). [J. Gallagher et al. / Journal of Cleaner Production 99 (2015) 152e159

The turbine/generator and pipework (solid blocks) are considered as the only two core components across each of the three projects. Turbine housing and ancillaries varied significantly between the projects. Examining all five impact categories in Figure 5-12 shows an incremental pattern for the turbine/generator, as a reduction in the capacity of the turbine related to an increase in the environmental impact of each category.

The three projects examined in this study have been constructed, yet there is the potential for a large number of additional MHP installations in the water infrastructure. The power generated from the MHP installations can reduce GHG emissions from electricity and offset the carbon footprint of the water industry, but this carbon offset potential will decline over time as the carbon intensity of marginal grid electricity declines, as projected by. Table 5-8 summarizes the evolution of cumulative GHG mitigation for the three case studies up to 2050, making the assumption that the MHP projects are all constructed in 2014 and GHG emissions are offset from 2015. The



calculations account for a reduction in the GHG emissions through offsetting electricity generated from a gas power plant.

MHP installation	Cumulative GHG emissions offset (t CO <sub>2</sub> eq.)					
	Decline of marginal grid electricity					No change
	2014 <sup>a</sup>	2015	2025	2045 <sup>b</sup>	2050	2050
15 kW	-7	36	450	1206	1379	1873
90 kW	-86	173	2658	7191	8233	11195
140 kW	-80	300	3944	10592	12121	16465

<sup>a</sup> Assuming MHP installations constructed by the end of 2014.

<sup>b</sup> Signifies GHG emissions produced over the 30-year lifespan.

Table 5-8 Mitigation forecasting for total GHG emissions offset by MHP installations between 2015 and 2050 (displacements of CO<sub>2</sub> emissions associated with gas power plant). [79]

#### 5.2.4 Conclusion

Micro-hydropower is a growing area of interest to water companies as potential energy recovery sites can capture excess energy within water infrastructure and can generate between 5 and 300 kW. This study quantifies the environmental impacts of electricity generation from three MHP case studies in the water industry, using a life cycle assessment approach.

Sites may present different technical challenges to other MHP sites. Environmental burdens were therefore calculated per kWh electricity generated over nominal turbine operational lifespans. Compared with marginal UK grid electricity generation in combined cycle turbine natural gas power plants, normalized life cycle environmental burdens for MHP electricity were reduced by: >99% for global warming potential (GWP); >98% for fossil resource depletion potential; >93% for acidification potential; >50-62% for human toxicity potential. However, the burden for abiotic resource depletion potential was 251-353% higher for MHP than marginal grid-electricity.

Different quantities of raw materials and installation practices led to a range in GWP burdens from 2.14 to 4.36 g CO<sub>2</sub> eq./kWh. One case benefitted from very low site preparation requirements while others required substantial excavation works and material quantities. Carbon payback times

ranged from 0.16 to 0.31 years, extending to 0.19-0.40 years for worst-case scenarios examined as part of a sensitivity analysis.

The carbon payback period for future MHP installations was estimated to increase by 1% annually, as the carbon intensity of marginal grid electricity is predicted to decline. This study demonstrates that MHP installations in the water industry have a strongly positive environmental balance [79].

## Conclusion

The substantial portion of this study consists of an investigation of renewable energy generation regarding to micro hydro-power technology and selection of a pump working as turbine.

Very general observation has been provided in the early stage of this study to illustrate a better understanding of the functioning of turbines and pumps. The multi-stage design of a Francis turbine has been proposed. The system analysis with common requirements of all applications for centrifugal pumps has been developed. Energy efficiency indicator, in respect to the growing attention to water-energy nexus, has been presented. A State-of-the-Art review of PAT, where pump-turbine performance prediction, theoretical studies, experimental studies, numerical studies and pump-turbines stability aspects have been broadly discussed. Other features such as flow instability-related hydraulic phenomena, rotating stall, cavitation, rotor-stator interactions (RSI), pump-turbine improvement attempts, misaligned guide vanes (MGV), case-sensitive attempts and inlet valve throttling have been suggested to be carried out through further researches.

The most challenging criteria of PAT, which is selecting the appropriate machinery, has been investigated subsequently. Various researchers have theoretically and practically presented solutions to select a proper PAT for known hydraulic data. Corresponding with previous studies, an estimation of the characteristic curve in regard to dimensionless head and the power curve of PAT has been shown. To predict the operation of a PAT outside the BEP, other experimental reports have been obtained from tests carried out on the seven types of pumps. For evaluating the performance, stability and suitable machinery, six centrifugal pumps measured at the DIMEG of the University of Calabria, at the CNPM in Milan and at the University of Trento, have been further examined. A numerical model, to foresee the performances of centrifugal pumps used as turbines, has been proposed. Using the experimental test on six centrifugal pumps with specific speed between nine and sixty-five, the model has been validated by comparing the head and efficiency foreseen with the measured ones. The next step of this research would be to find the best measurement strategies for improving the model estimations and its reliability despite the good level achieved so far.

Using PAT substituting PRV as an interesting PAT application has been reviewed. Selecting and locating the PAT based on maximizing the benefit has been considered. An objective function,

together with three different scenarios provided a proper range of certainty. The penalty function, which distorts the search space and makes the search process more difficult, is to be developed by means of further research to achieving accurate result with bio-inspired algorithm. Three fictitious case studies demonstrated that considering the maximum consumption period, PAT and PRV show similar performance. However, during low consumption periods, PAT cannot maintain adequate outlet pressure.

Three micro hydro-power installations in the water supply infrastructure in the UK have been reviewed. The life-cycle environmental balance of electricity generation has been observed and it has been demonstrated that MHP installation in the water industry have a strongly positive environmental balance.



## 6 References

- [1] Anthony Couzinet, Laurent Gros, and Daniel Pierrat “*Characteristics of Centrifugal Pumps Working in Direct or Reverse Mode: Focus on the Unsteady Radial Thrust*”. Cetim, 74 route de la Joneli`ere, 44326 antes, France. International Journal of Rotating Machinery, Volume 2013,
- [2] Armando Carravetta • Shahram Derakhshan Houreh Helena M. Ramos, “*Pump as Turbine Fundamentals and Applications*”, Springer, New York, NY, USA, ISBN 978-3-319-67506-0
- [3] Val S. Lobanoff, Robert R. Ross “*Centrifugal Pumps, design and application*”, Second edition. Butterworth-Heimann 1992, ISBN 0-87201-200-X
- [4] A. Nourbakhsh, S. Derakhshan, E. Javidpour, A. Riasi, *Centrifugal & axial pumps used as turbines in small hydropower stations*. Hydroenergia 2010 International Congress on Small Hydropower International Conference and Exhibition on Small Hydropower, pp. 16–19 (2010)
- [5] K.R. Sharma, Small Hydroelectric Project-Use of Centrifugal Pumps as Turbines. Technical Report, India (Kirloskar Electr. Co, Bangalore, 1985)
- [6] A.A. Williams, Pumps as turbines used with induction generators for stand-alone micro-hydroelectric power plants, Doctoral dissertation, Nottingham Trent University (1992) URL: <http://ethos.bl.uk/OrderDetails.do?uin=uk.bl.ethos.262127>
- [7] C. Alatorre-Frenk, Cost minimisation in micro-hydro systems using pumps-as-turbines, Doctoral dissertation, University of Warwick (1994) URL: [http://wrap.warwick.ac.uk/36099/1/WRAP\\_THESIS\\_Alatorre-Frenk\\_1994.pdf](http://wrap.warwick.ac.uk/36099/1/WRAP_THESIS_Alatorre-Frenk_1994.pdf)
- [8] H. Ramos, A. Borga, Pumps as turbines: an unconventional solution to energy production. Urban Water 1(3), 261–263 (1999)
- [9] H. Ramos, A. Borga, Pumps yielding power. Dam Eng. 10(4), 197–217 (2000)
- [10] M. Valadas, H. Ramos, Use of pumps as turbines to profit the available energy in irrigation system. Water Resour. J. APRH. 24(3), 63–76 (2003)
- [11] P. Singh, Establishment of a test-rig for turbine for micro hydro and detailed testing of a pump as turbine, Centre for Energy Studies, Indian Institute of Technology, New Delhi, India (2000)
- [12] P. Singh, Optimization of the internal hydraulic and of system design in pumps as turbines with field implementation and evaluation, Doctoral dissertation, University of Fridericana, Karlsruhe, Germany (2005)
- [13] S.-S. Yang, S. Derakhshan, F.-Y. Kong, Theoretical, numerical and experimental prediction of pump as turbine performance. Renew. Energy 48, 507–513 (2012)

- [14] S. Derakhshan, A. Nourbakhsh, Experimental study of characteristic curves of centrifugal pumps working as turbines in different specific speeds. *Exp. Therm. Fluid Sci.* 32(3), 800–807 (2008)
- [15] J.F. Gülich, *Centrifugal Pumps* (Springer, Berlin, 2008)
- [16] <http://www.ksb.com/pa>
- [17] Balkhair KS, Ur Rahman K. Sustainable and economical small-scale and low-head hydropower generation: A promising alternative potential solution for energy generation at local and regional scale. *Appl Energy* 2017; 188:378–91.
- [18] Khan R. Small hydro power in india: is it sustainable business? *Appl Energy* 2015; 152:207–16.
- [19] Carravetta A, Del Giudice G, Fecarotta O, Ramos H. Energy production in water distribution networks: A PAT design strategy. *Water Resour Manage* 2012; 26:3947–59.
- [20] Derakhshan S, Nourbakhsh A. Experimental study of characteristic curves of centrifugal pumps working as turbines in different specific speeds. *Exp Therm Fluid Sci* 2008; 32:800–7.
- [21] Derakhshan S, Nourbakhsh A. Theoretical, numerical and experimental investigation of centrifugal pumps in reverse operation. *Exp Therm Fluid Sci* 2008; 32:1620–7.
- [22] Derakhshan S, Kasaeian N. Optimization, numerical, and experimental study of a propeller pump as turbine. *Energy Resour Technol* 2014;136(1):012005.
- [23] Barbarelli S, Amelio M, Florio G. Predictive model estimating the performances of centrifugal pumps used as turbines. *Energy* 2016; 107:103–21.
- [24] Barbarelli S, Amelio M, Florio G. Experimental activity at test rig validating correlations to select pumps running as turbines in microhydro plants. *Energy Convers Manage* 2017; 149:781–97.
- [25] D. Novara, A. Carravetta, S. Derakhshan, A. McNabola, H. Ramos, A cost model for pumps as turbines and a comparison of design strategies for their use as energy recovery devices in Water Supply Systems, in EEMODS'17, Rome (eemods17.org), Energy Efficiency in Motor Driven Systems (2017)
- [26] D. Novara, A. Carravetta, S. Derakhshan, A.M. Nabola, H. Ramos, Centrifugal pumps as turbines cost determination and feasibility study for pressure reducing valve substitution in a water supply system, *Submitt. to Renew. Energy* (2017)
- [27] J.M. Chapallaz, P. Eichenberger, G. Fischer, in *A Manual on Pumps Used as Turbines* (Vieweg, 1992)
- [28] D. Novara, A. Carravetta, S. Derakhshan, A. McNabola, H. Ramos, A cost model for pumps as turbines and a comparison of design strategies for their use as energy recovery devices in Water Supply Systems, in EEMODS'17, Rome (eemods17.org), Energy Efficiency in Motor Driven Systems (2017)

- 
- [29] A.Bolognesi ,C.Bragalli C.Lenzi ,S.Artinaa Energy efficiency optimization in water distribution systems 12th International Conference on Computing and Control for the Water Industry, CCWI2013.
- [30] S.-S. Yang, F.-Y. Kong, W.-M. Jiang, X.-Y. Qu, Effects of impeller trimming influencing pump as turbine. *Comput. Fluids* 67, 72–78 (2012)
- [31] A. Carravetta, G. del Giudice, O. Fecarotta, H. Ramos, PAT design strategy for energy recovery in water distribution networks by electrical regulation. *Energies* 6(1), 411–424 (2013)
- [32] A. Carravetta, L. Antipodi, U. Golia, O. Fecarotta, Energy saving in a water supply network by coupling a pump and a pump as turbine (PAT) in a turbopump. *Water* 9(1), 62 (2017)
- [33] D. Novara, S. Derakhshan, A. McNabola, H. Ramos, Estimation of unit cost and maximum efficiency for Pumps as Turbines, in *Young Water Professionals* (2017)
- [34] O. Fecarotta, A. Carravetta, H. Ramos, R. Martino, an improved affinity model to enhance variable operating strategy for pumps used as turbines. *J. Hydraul. Res.* 54(3), 332–341 (2016)
- [35] Barbarelli S. *Analisi Teorico-Sperimentale del Funzionamento di PompeCentrifughe Utilizzate come Turbine* [Doctoral thesis]. Italy: Polytechnic of Bari; March 2000.
- [36] Amelio M, Barbarelli S. A one-dimensional numerical model for calculating the efficiency of pumps as turbines for implementation in micro-hydro power plants. In: *Proceedings of “7th Biennial ASME conference engineering systems design and analysis”*, Manchester, UK, 19-22 July, 2004; 2004.
- [37] Antonini A, Pinamonti P. Pressure distribution in centrifugal pump volutes: numerical and experimental calculations. In: *Proceedings from 15th symposium section on hydraulic machinery and cavitation*, 14 September 1990, Belgrade; 1990.
- [38] Neumann B. *The interaction between geometry and performance of a centrifugal pump*. London: Mechanical Engineering Publications Limited; 1991.
- [39] Aungier RH. Mean streamline aerodynamic performance analysis of centrifugal compressors. *J Turbomachinery* 1995; 117:360.
- [40] Ito H. Friction factors for turbulent flow in curved pipes. *J Basic Eng* 1959: 123e34.
- [41] Childs SM. Convert pumps to turbines and recover HP. *Hydrocarbon Process Petrol Refin* 1962;41(10):173e4.
- [42] Lewinsky-Kesslitz HP. Pumpen als Turbinen fur Kleinkraftwerke. *Wasserwirtschaft* 1987;77(10):531e7 [in German].
- [43] Jain Sanjay V, Swarnkar Abhishek, Motwani Karan H, Patel Rajesh N. Effects of impeller diameter and rotational speed on performance of pump running in turbine mode. *Energy Convers Manag* 1 January 2015; 89:808e24.
- [44] Hancock JW. Centrifugal pumps or water turbine. *Pipe Line News*. June 1963. p. 25e7.



- [45] Stepanoff AJ. Centrifugal and Axial flowpumps. New York: JohnWiley; 1957. p. 276.
- [46] Sharma KR. Small hydroelectric project-use of centrifugal pumps as turbines. Bangalore, India: Kirloskar Electric Co.; 1985.
- [47] Alatorre-Frenk C, Thomas TH. The pumps as Turbines approach to small hydropower. In: Word congress on renewable energy, reading; 1990. [9] Stepanoff AJ. Centrifugal and Axial flowpumps. New York: JohnWiley; 1957. p. 276.
- [48] Schmiel E. Serien-Kreiselpumpen im Turbinenbetrieb. 1988. Pumpentagung Karlsruhe, Sec. A6 [in German].
- [50] Grover KM. Conversion of pump to turbines. Katonah, New York: GSA Inter Corp; 1980.
- [51] ABNT e Brazilian Association of Technical Standards. NBR 12218-Project of Water Distribution Network for Public Supply, 1994. Technical report (in Portuguese).
- [52] C.F. Calvillo, A. S\_anchez-Miralles, J. Villar, Energy management and planning in smart cities, *Renew. Sustain. Energy Rev.* 55 (2016) 273e287.
- [53] L.S. Araújo, H. Ramos, T. Coelho, Pressure control for leakage mnimisation in water distribution systems management, *Water Resour. Manag.* 20 (2006) 133e149.
- [54] R. Wright, E. Abraham, P. Parpas, I. Stoianov, Optimized control of pressure reducing valves in water distribution networks with dynamic topology, *Procedia Eng.* 119 (2015) 1003e1011.
- [55] J. Chen, H.X. Yang, C.P. Liu, C.H. Lau, M. Lo, A novel vertical axis water turbine for power generation from water pipelines, *Energy* 54 (2013) 184e193
- [56] S. Malavasi, M.M.A. Rossi, G. Ferrarese, GreenValve: hydrodynamics and applications of the control valve for energy harvesting, *Urban Water J.* (2016) 1e10.
- [57] I. Samora, V. Hasmatuchi, C. Münch-Allign\_e, M.J. Franca, A.J. Schleiss, H.M. Ramos, Experimental characterization of a five-blade tubular propeller turbine for pipe inline installation, *Renew. Energy* 95 (2016) 356e366
- [58] H.M. Ramos, A. Borga, M. Sim~ao, New design solutions for low-power energy production in water pipe systems, *Water Sci. Eng.* 2 (4) (2009) 69e84.
- [59] N. Fontana, M. Giugni, D. Portolano, Losses reduction and energy production in water-distribution networks, *J. Water Resour. Plan. Manag.* 138 (3) (2012) 237e244.
- [60] M. Marchis, G. Freni, Pump as turbine implementation in a dynamic numerical model: cost analysis for energy recovery in water distribution network, *J. Hydroinformatics* 16 (1) (2015) 347e361.
- [61] R. Jafari, M.J. Khanjani, H.R. Esmaeilian, Pressure management and electric power production using pumps as turbines, *J. Am. Water Works Assoc.* 107 (7) (2015) 351e363.

- [62] A.R.D. Torley, M.H. Chaudhry, Pump characteristics for transient flow analysis, in: BHR Group Conference Series Publication, vol. 19, Mechanical Engineering Publications Limited, Bedford, 1996, pp. 461e476.
- [63] R.J. Gomes, A.S. Marques, J. Sousa, Estimation of the benefits yielded by pressure management in water distribution systems, *Urban Water J.* 8 (2) (2011) 65e77.
- [64] R.J. Gomes, A.S. Marques, J. Sousa, Identification of the optimal entry points at District Metered Areas and implementation of pressure management, *Urban Water J.* 9 (6) (2012) 365e384.
- [65] Gustavo Meirelles Lima, Msc \*, Edevar Luvizotto Junior, PhD, Bruno M. Brentan, Msc, Selection and location of Pumps as Turbines substituting pressure reducing valves.
- [66] E. Luvizotto Junior, E.K. Koelle, J.G.P. Andrade, Personality investigation of hydraulic networks using the MOC - method of characteristics, in: In: 7<sup>th</sup> International Conference on Pressure Surges and Fluid Transients in Pipelines and Open Channels, Harrogate, UK, 1996.
- [67] J. Izquierdo, P. Iglesias, Mathematical modelling of hydraulic transients in complex systems, *Math. Comput. Model.* 39 (4/5) (2004) 529e540.
- [68] E.B. Wylie, V.L. Streeter, *Fluid Transients*, Thomson-Shore, Michigan, United.
- [69] Z.Y. Wu, A.R. Simpson, A self-adaptive boundary search genetic algorithm and its application to water distribution systems, *J. Hydraulic Res.* 40 (2) (2002) 191e203.
- [70] O. Piller, J.E. van Zyl, Incorporating the FAVAD leakage equation into water distribution system analysis, *Procedia Eng.* 89 (2014) 613e617.
- [71] ABNT e Brazilian Association of Technical Standards. NBR 12218-Project of Water Distribution Network for Public Supply, 1994. Technical report (in Portuguese).
- [72] SNIS e National System of Sanitation Information. Diagnosis of Water and Sewage Servicese2014, 2014. Technical Report (in Portuguese).
- [73] Gallagher, J., Harris, I.M., Packwood, A.J., McNabola, A., Williams, A.P., unpublished work. A strategic assessment of micro-hydropower in the UK and Irish water industry: identifying technical and economic constraints.
- [74] Gallagher, J., Harris, I.M., Packwood, A.J., McNabola, A., Williams, A.P., unpublished work. A strategic assessment of micro-hydropower in the UK and Irish water industry: identifying technical and economic constraints.
- [75] Rothausen, S.G.S.A., Conway, D., 2011. Greenhouse-gas emissions from energy use in the water sector. *Nat. Clim. Change* 1, 210e219.
- [76] D ^ wr Cymru Welsh Water, 2007. D ^ wr Cymru Welsh Water: Our Sustainable Future. D ^ wr Cymru Welsh Water.
- [77] McNabola, A., Coughlan, P., Williams, A.P., 2014b. Energy recovery in the water industry: an assessment of the potential of micro-hydropower. *Water Environ. J.* 28, 294e304.

- [78] Guezuraga, B., Zauner, R., Pöölz, W., 2012. Life cycle assessment of two different 2 MW class wind turbines. *Renew. Energy* 37, 37e44.
- [79] John Gallagher a, \*, David Styles a, Aonghus McNabola b, A. Prysor Williams, Life cycle environmental balance and greenhouse gas mitigation potential of micro-hydropower energy recovery in the water industry.
- [80] CML, 2010. Characterization Factors Database Available Online from Institute of Environmental Sciences (CML). Universiteit Leiden, Leiden.
- [81] DECC, 2012. Electricity Generation Costs. Department of Energy & Climate Change.
- [82] ISO, 2006. ISO 14040: Environmental Management e Life Cycle Assessment e Principles and Framework. ISO, Geneva.
- [83] Sleeswijk, A.W., van Oers, L.F.C.M., Guinée, J.B., Struijs, J., Huijbregts, M.A.J., 2008. Normalization in product life cycle assessment: an LCA of the global and European economic systems in the year 2000. *Sci. Total Environ.* 390, 227e240.
- [84] Rule, B.M., Worth, Z.J., Boyle, C.A., 2009. Comparison of life cycle carbon dioxide emissions and embodied energy in four renewable electricity generation technologies in New Zealand. *Environ. Sci. Technol.* 43, 6406e6413.
- [85] Maxime Binamaa, Wen-Tao Sua,\*, Xiao-Bin Lia, Feng-Chen Lia,\*, Xian-Zhu Weia,b, Shi Anc Investigation on pump as turbine (PAT) technical aspects for micro hydropower schemes: A state-of-the-art review 79 (2017) 148–179.
- [86] Brown A, Müller S, Dobrotkova Z. Renewable energy: markets and prospects by technology. IEA Inf Pap 2011.
- [87] Electricity Generation. 2016. ([https://en.wikipedia.org/wiki/Electricity\\_generation](https://en.wikipedia.org/wiki/Electricity_generation)).
- [88] Saxena P. Overview of small hydro power development in India. Himalayan small Hydro Power Summit, Dehradun; 2006.
- [89] Ismail MA, Othman AK, Islam S, Zen H. End suction centrifugal pump operating in turbine mode for microhydro applications. *Adv Mech Eng* 2014; 6:139868.
- [90] Kaunda CS, Kimambo CZ, Nielsen TK. A technical discussion on micro hydropower technology and its turbines. *Renew Sustain Energy Rev* 2014; 35:445–59.
- [91] Jain SV, Patel RN. Investigations on pump running in turbine mode: a review of the state-of-the-art. *Renew Sustain Energy Rev* 2014; 30:841–68.
- [92] Prasad V, Shukla S, Joshi S. Performance characteristics of pump as turbine. *Indian Pumps* 2006:5–9.
- [93] Williams A. Pumps as turbines for low cost micro hydro power. *Renew Energy* 1996; 9:1227–34.

- [94] Orchard B, Klos S. Pumps as turbines for water industry. *World Pumps* 2009; 2009:22–3.
- [95] Ramos H, Borga A. Pumps as turbines: an unconventional solution to energy production. *Urban Water* 1999; 1:261–3.
- [96] Arriaga M. Pump as turbine – a pico-hydro alternative in Lao People's Democratic Republic. *Renew Energy* 2010; 35:1109–15.
- [97] Williams A. *Pumps as turbines: a user's guide*. London: Intermediate Technology Publications; 1995.
- [98] Paish O. Micro-hydropower: status and prospects. *Proc Inst Mech Eng, Part A: J Power Energy* 2002;216:31–40.
- [99] Franc J-P. *La cavitation: mécanismes physiques et aspects industriels*. France: EDP Sciences; 1995.
- [100] Chapallaz J-M, Eichenberger P, Fischer G. *Manual on pumps used as turbines*. Vieweg; 1992.
- [101] Fraenkel P, Paish O, Bokalders V, Harvey A, Brown A, Edwards R. *Micro-hydro power, a guide for development workers*. London, UK: Intermediate Technology Publications Ltd; 1991.
- [102] Coutu A, Monette C, Gagnon M. Life assessment of francis runners using strain gage site measurements. Chattanooga, TN: *Waterpower XV*; 2007.
- [103] Avellan F. *Course of hydraulic turbomachines-2010*. Switzerland: Ecole Polytechnique federale de Lausanne; 2010.
- [104] 3 kW pump as turbine micro hydro at Mae Wei village. Tak province; 2008. (<http://palangthai.blogspot.de/2008/02/3-kw-pump-as-turbine-microhydro-atmae.html>).
- [105] Nautiyal H, Varun V, Kumar A, Yadav SYS. Experimental investigation of centrifugal pump working as turbine for small hydropower systems. *Energy Sci Technol* 2011; 1:79–86.
- [106] Stepanoff AJ. *Centrifugal and axial flow pumps, design and applications*. New York: John Wiley and Sons, Inc; 1957.
- [107] Childs S. Convert pumps to turbines and recover HP. *Hydrocarb Process Pet Refin* 1962; 41:173–4.
- [108] Gopalakrishnan S. Power recovery turbines for the process industry. Proceedings of the third international pump symposium [Houston]. Texas A & M University; 1986. p. 3–11.
- [109] Diederich H. Verwendung von kreiselpumpen als turbinen. Frankenthal, Germany: KSB Techn Ber; 1967. p. 30–6.
- [110] Grover K. *Conversion of pumps to turbines*. Katonah, New York: GSA Inter corp; 1982.
- [111] Nautiyal H, Kumar A. Reverse running pumps analytical, experimental and computational study: a review. *Renew Sustain Energy Rev* 2010; 14:2059–67.

- [112] Yang S-S, Derakhshan S, Kong F-Y. Theoretical, numerical and experimental prediction of pump as turbine performance. *Renew Energy* 2012; 48:507–13.
- [113] Ventrone G, Ardizzon G, Pavesi G. Direct and reverse flow conditions in radial flow hydraulic turbomachines. *Proc Inst Mech Eng Part A: J Power Energy* 2000; 214:635–44.
- [114] Nourbakhsh A, Derakhshan Sh. Investigation of Pump as Turbine Performance in Small Hydropower Stations; 2004. (<http://www.wseas.us/e-library/conferences/corfu2004/papers/488-431.doc>).
- [115] Hossain IM, Ferdous S, Salehin S, Saleque AM, Jamal T. Pump-as-turbine (PAT) for small scale power generation: a comparative analysis. *Developments in renewable energy technology (ICDRET), 2014 3rd international conference on the: IEEE; 2014.* p. 1–5.
- [116] Williams A. The turbine performance of centrifugal pumps: a comparison of prediction methods. *Proc Inst Mech Eng, Part A: J Power Energy* 1994; 208:59–66.
- [117] Fernandez J, Blanco E, Parrondo J, Stickland M, Scanlon T. Performance of a centrifugal pump running in inverse mode. *Proc Inst Mech Eng Part A: J Power Energy* 2004; 218:265–71.
- [118] Carravetta A, Conte M, Fecarotta O, Ramos H. Evaluation of PAT performances by modified affinity law. *Procedia Eng* 2014; 89:581–7.
- [119] Singh P, Rao A, Ramasubramaniam V, Kumar A. Performance evaluation of the ‘pump as turbine’ based micro hydro project in Kinko village, Tanzania. *Himalaya small hydropower summit; 2006,* 156–7.
- [120] Raman N, Hussein I, Palanisamy K, Foo B. An experimental investigation of pump as turbine for micro hydro application. *IOP conference series: earth and environmental science.* IOP Publishing; 2013. p. 012064.
- [121] Raman N, Hussein I. Reconnaissance study to identify micro hydro potential sites in Malaysia. *Eur J Sci Res* 2010; 41:354–72.
- [122] Daniela Popescu AD, Rusinaru Denisa. Study of centrifugal pump operating as turbine in small hydropower plants. *wseas conference: recent researches of electric power and energy systems; 2013.* p. 285–8.
- [123] Suarda MSN, Adnyana WB. Assessment performance of pumps as hydro-turbines. *International conference on energy and environment 2006 (ICEE 2006).* Kajang, Malaysia; 2006.
- [124] Singh P, Kshirsagar J, Caglar S, Nestmann F. Experimental and computational studies of the effect of ‘casing eye rib’ on the swirl flow at the exit of a pump as turbine. *ASME 2004 heat transfer/fluids engineering summer conference.* American Society of Mechanical Engineers; 2004. p. 85–93.
- [125] Singh P, Nestmann F. A consolidated model for the turbine operation of centrifugal pumps. *J Eng Gas Turbines Power* 2011; 133:063002.

- [126] Yang S, Kong F, Jiang W, Qu X. Research on rotational speed to the influence of pump as turbine. IOP conference series: earth and environmental science. IOP Publishing; 2012. p. 042023.
- [127] Carravetta A, Fecarotta O, Ramos H. Numerical simulation on pump as turbine: mesh reliability and performance concerns. Clean electrical power (ICCEP), 2011 international conference on: IEEE; 2011. p. 169–74.
- [128] Ismail MA, Othman AK, Zen H. Numerical simulation on end suction centrifugal pump running in inverse flow for microhydro applications. Appl Mech Mater: Trans Tech Publ 2015:358–62.
- [129] Fernández J, Barrio R, Blanco E, Parrondo J, Marcos A. Numerical investigation of a centrifugal pump running in reverse mode. Proc Inst Mech Eng Part A: J Power Energy 2010; 224:373–81.
- [130] Páscoa J, Silva F, Pinheiro J, Martins D. A new approach for predicting PAT pumps operating point from direct pumping mode characteristics. J Sci Ind Res 2012; 71:144–8.
- [131] Hlbocan P, Varchola M. Numerical simulation on a mixed-flow pump operating in a turbine mode. Eng Mech 2013; 20:97–105.
- [132] Nautiyal H, Kumar V, Thakur A. CFD analysis on pumps working as turbines. Hydro Nepal: J Water Energy Environ 2010; 6:35–7.
- [133] Rawal S, Kshirsagar J. Numerical simulation on a pump operating in a turbine mode. Proceedings of the 23rd international pump user's symposium. Texas A & M University; 2007. p. 21–7.
- [134] Baburaj RS E, Manikandan C, Sudha K. CFD analysis of pump as turbine for micro-hydro schemes. Int J Innov Res Sci Eng Technol 2013:2.
- [135] Bogdanović-Jovanović JB, Milenković DR, Svrkota DM, Bogdanović B, Spasić ŽT. Pumps used as turbines power recovery, energy efficiency, CFD analysis. Therm Sci 2014; 18:1029–40.
- [136] Sedlář M, Šoukal J, Komárek M. CFD analysis of middle stage of multistage pump operating in turbine regime. Eng Mech 2009; 16:413–21.
- [137] Greitzer EM. The stability of pumping systems—the 1980 Freeman Scholar Lecture. J Fluids Eng 1981; 103:193–242.
- [138] Martin C. Stability of pump-turbines during transient operation. 5th Conference on pressure surges BHRA. Hannover, Germany; 1986.
- [139] Amblard H, Henry P, Borciani G, Martin G, Guiton P, Thalmann R. Behavior of Francis turbines and pump-turbines at partial flow. La Houille Blanc 1985; 5:435–40.
- [140] Pérez-Díaz JI, Cavazzini, G, Blázquez, F, Platero, C, Fraile-Ardanuy, J, Sánchez, JA, et al. Technological developments for pumped-hydro energy storage, Technical Report. Mechanical Storage Subprogramme, Joint Programme on Energy Storage, European Energy Research Alliance; 2014.

- [141] Gentner C, Sallaberger M, Widmer C, Braun O, Staubli T. Numerical and experimental analysis of instability phenomena in pump turbines. IOP conference series: earth and environmental science. IOP Publishing; 2012. p. 032042.
- [142] IEA. Key World Energy Statistics; 2012.
- [143] Zuyan M. Pumped storage technology [M]. Beijing: Tsinghua University Press; 1986.
- [144] Sun H, Xiao R, Wang F, Xiao Y, Liu W. Analysis of the pump-turbine S characteristics using the detached eddy simulation method. Chin J Mech Eng 2015; 28:115–22.
- [145] Zhou J, Karney B, Hu M, Xu J. Analytical study on possible self-excited oscillation in S-shaped regions of pump-turbines. Proc Inst Mech Eng Part A: J Power Energy 2011; 225:1132–42.
- [146] Coutu A. Francis runner reliability. Johannesburg, South Africa: Hydro Power Africa; 2008.
- [147] Seidel U, Koutnik J, Martin G. S-curve characteristic of pump-turbines. HYDRO 2012 innovative approaches to global challenges. Bilbao, Spain; 2012.
- [148] Hasmatuchi V, Farhat M, Maruzewski P, Avellan F. Experimental investigation of a pump-turbine at off-design operating conditions. Proceedings of the 3<sup>rd</sup> international meeting of the workgroup on cavitation and dynamic problems in hydraulic machinery and systems. Brno University of Technology; 2009. p. 339–47.
- [149] Houdeline J-B, Liu J, Lavigne S, Laurant Y, Balara L. Start-up improvement in turbine mode for high head PSP machine. IOP conference series: earth and environmental science. IOP Publishing; 2012. p. 042022.
- [150] Wang L, Yin J, Jiao L, Wu D, Qin D. Numerical investigation on the “S” characteristics of a reduced pump turbine model. Sci China Technol Sci 2011; 54:1259–66.
- [151] Sun H, Xiao R, Liu W, Wang F. Analysis of S characteristics and pressure pulsations in a pump-turbine with misaligned guide vanes. J Fluids Eng 2013; 135:051101.
- [152] Li J, Hu Q, Yu J, Li Q. Study on S-shaped characteristic of Francis reversible unit by on-site test and CFD simulation. Sci China Technol Sci 2013; 56:2163–9.
- [153] Cavazzini AC G, Pavesi G, Ardizzon G. Numerical analysis of the s-shape characteristic in a pump-turbine. Proceedings of 11th European conference on turbomachinery fluid dynamics & thermodynamics ETC11. Madrid-Spain; 2015.
- [154] Yin J, Wang D, Walters DK, Wei X. Investigation of the unstable flow phenomenon in a pump turbine. Sci China Phys Mech Astron 2014; 57:1119–27.
- [155] Guggenberger MFS, Jürgen S, Helmut J, Manfred S, Widmer C. Investigating the dynamic aspects of the turbine instability of a pump turbine model. 6th IAHR international meeting of the workgroup on cavitation and dynamic problems in hydraulic machinery and systems. Ljubljana, Slovenia; 2015.

- [156] Zhang S, Shi Q, Zhang K. Flow behaviour analysis of reversible pump-turbine in " S" characteristic operating zone. IOP conference series: earth and environmental science. IOP Publishing; 2012. p. 032045.
- [157] Casartelli E, Mangani L, Romanelli G, Staubli T. Transient simulation of speed-no load conditions with an open-source based c++ code. IOP conference series: earth and environmental science. IOP Publishing; 2014. p. 032029.
- [158] Billdal J, Wedmark A. Recent experiences with single stage reversible pump turbines in GE energy's hydro business. *Hydro* 2007; 2007:15–7.
- [159] Chen T, Luo X, Guo P, Wu Y. 3-D Simulation of a prototype pump-turbine during starting period in turbine model. IOP conference series: materials science and engineering. IOP Publishing; 2013. p. 052028.
- [160] Edinger G, Erne S, Doujak E, Bauer C. Flow determination of a pump-turbine at zero discharge. IOP conference series: earth and environmental science. IOP Publishing; 2014. p. 032051.
- [161] Gong R, Li D, Wang H, Wei X, Qin D. Investigation into the flow details of runner region in a pump turbine at off-design conditions. *Adv Mech Eng* 2016;8, [1687814016630727].
- [162] Stens C, Riedelbauch Stefan. CFD simulation of the flow through a pump turbine during a fast transition from pump to generating mode. 6th IAHR international meeting of the workgroup on cavitation and dynamic problems in hydraulic machinery and systems. Ljubljana, Slovenia; 2015.
- [163] Liu J, Liu S, Sun Y, Wu Y, Wang L. Numerical study of vortex rope during load rejection of a prototype pump-turbine. IOP conference series: earth and environmental science. IOP Publishing; 2012. p. 032044.
- [164] Dörfler P, Sick M, Coutu A. Flow-induced pulsation and vibration in hydroelectric machinery: engineer's guidebook for planning, design and troubleshooting. London, UK: Springer Science & Business Media; 2012.
- [165] Mei Z. Generation technology of pumped storage power. Beijing, China: Machinery Industry Press; 2000.
- [166] Ješe U, Fortes-Patella R, Dular M. Numerical study of pump-turbine instabilities under pumping mode off-design conditions. ASME/JSME/KSME 2015 joint fluids engineering conference: american society of mechanical engineers; 2015. p.V001T33A18-VT33A18.
- [167] Yangyang Y, Yexiang X, Wei Z, Liming Z, Hwang AS, Zhengwei W. Numerical analysis of a model pump-turbine internal flow behavior in pump hump district. IOP conference series: earth and environmental science. IOP Publishing; 2014. p.032040.
- [168] Li D-y, Gong R-z, Wang H-j, Fu W-w, Wei X-z, Liu Z-s. Fluid flow analysis of drooping phenomena in pump mode for a given guide vane setting of a pumpturbine model. *J Zhejiang Univ Sci* 2015:1.



- [169] Liu D, Zhao Y, Liu X, Ma Y, Wang W. Pump hump characteristic research based on mass transfer equation. IOP conference series: materials science and engineering. IOP Publishing; 2015. p. 032016.
- [170] Deyou L, Hongjie W, Gaoming X, Ruzhi G, Xianzhu W, Zhansheng L. Unsteady simulation and analysis for hump characteristics of a pump turbine model. *Renew Energy* 2015; 77:32–42.
- [171] Braun O, Kueny J-L, Avellan F. Numerical analysis of flow phenomena related to the unstable energy-discharge characteristic of a pump-turbine in pump mode. *ASME 2005 Fluids Eng Div Summer Meet: Am Soc Mech Eng* 2005:1075–80.
- [172] Liu J, Liu S, Wu Y, Jiao L, Wang L, Sun Y. Numerical investigation of the hump characteristic of a pump-turbine based on an improved cavitation model. *Comput Fluids* 2012; 68:105–11.
- [173] <https://water.usgs.gov/edu/wuhy.html>
- [174] <https://www.worldenergy.org/data/resources/resource/hydropower/>
- [175] [https://www.mpoweruk.com/hydro\\_power.htm](https://www.mpoweruk.com/hydro_power.htm)
- [176] <http://www.diyplumbingadvice.com/waterpressure.shtml>
- [177] <https://www.townoflyons.com/DocumentCenter/View/350/Pressure-Reducing-Valve-Information-PDF>
- [178] [https://en.wikipedia.org/wiki/Water\\_turbine](https://en.wikipedia.org/wiki/Water_turbine)
- [179] <https://www.energy.gov/eere/water/types-hydropower-turbines>
- [180] [https://mitt.uib.no/courses/4050/pages/4-dot-3-water?module\\_item\\_id=8361](https://mitt.uib.no/courses/4050/pages/4-dot-3-water?module_item_id=8361)
- [181] [https://en.wikipedia.org/wiki/Water\\_wheel](https://en.wikipedia.org/wiki/Water_wheel)
- [182] [https://en.wikipedia.org/wiki/Reverse\\_overshot\\_water-wheel](https://en.wikipedia.org/wiki/Reverse_overshot_water-wheel)
- [183] <https://www.energy.gov/eere/water/types-hydropower-turbines>
- [184] [https://en.wikipedia.org/wiki/Turgo\\_turbine](https://en.wikipedia.org/wiki/Turgo_turbine)
- [185] <https://boilerproperty.com/hydropower-plants-and-types-of-turbines>

- [186] [https://en.wikipedia.org/wiki/Jonval\\_turbine](https://en.wikipedia.org/wiki/Jonval_turbine)
- [187] [https://en.wikipedia.org/wiki/Screw\\_turbine](https://en.wikipedia.org/wiki/Screw_turbine)
- [188] <https://boilerproperty.com/hydropower-plants-and-types-of-turbines/>
- [189] A Review on Micro Hydro Gravitational Vortex Power and Turbine Systems, July 2014-Jurnal Teknologi 69(7) DOI:10.11113/jt.v69.3259
- [190] Flow Investigation in a Francis Draft Tube : the Flindt Project January 2000, François Avellan
- [191] PRESENTED BY ❧ TAMOOR KHALIL UW-14-MET-BSC-011 ❧ M ZUBAIR UW-14-MET-BSC-032 ❧ MATTI ULLAH UW-14-MET-BSC-018 FRANCIS TURBINE SUBMITTED TO Mr. Umer Sohail
- [192] <https://nptel.ac.in/courses/112104117/28>
- [193] [https://petrowiki.org/Centrifugal\\_pumps](https://petrowiki.org/Centrifugal_pumps)
- [194] <http://nuclearpowertraining.tpub.com/h1018v1/css/Centrifugal-Pump-Classification-By-Flow-98.htm>
- [195] <http://www.aga-tech.at/assets/uploads/2016/09/Datenheft-KPL.pdf>
- [196] <https://maintenanceskill.com/how-horizontal-multistage-centrifugal-pump-works/>
- [197] <http://www.microhydropower.net/basics/intro.php>
- [198] [https://energyeducation.ca/encyclopedia/Energy\\_from\\_water](https://energyeducation.ca/encyclopedia/Energy_from_water)
- [199] <https://www.worldpumps.com/waste-wastewater/features/pumps-as-turbines-in-the-water-industry/>
- [200] © Springer International Publishing AG 2018 A. Carravetta et al., Pumps as Turbines, Springer Tracts in Mechanical Engineering, [https://doi.org/10.1007/978-3-319-67507-7\\_2](https://doi.org/10.1007/978-3-319-67507-7_2)

## 7 Tables & Figures

### 7.1 Figures

Figure 1-1 Hydro Electric Power Generation[175].....	8
Figure 1-2 Euler Turbine Equation [175] .....	9
Figure 1-3 Turbine [178] .....	10
Figure 1-4 Water wheel .....	12
Figure 1-5 Reverse overshot water-wheel .....	12
Figure 1-6 Pelton [183].....	13
Figure 1-7 Turgo [184] .....	14
Figure 1-8 Cross-Flow[185] .....	14
Figure 1-9 Jonval [186].....	15
Figure 1-10 Screw [187].....	15
Figure 1-11 Bulb turbine.....	16
Figure 1-12 Straflo.....	17
Figure 1-13 Tube turbine .....	17
Figure 1-14 Kaplan .....	17
Figure 1-15 Francis Turbine .....	18
Figure 1-16 Draft Tube [190].....	19
Figure 1-17 A Francis turbine [192] .....	20
Figure 1-18 Spiral Casing [192].....	21
Figure 1-19 Guide vane .....	22
Figure 1-20 Draft tube .....	22
Figure 1-21 Complete Assembly (Without draft tube) .....	22
Figure 1-22 Spiral casing .....	23
Figure 1-23 Head across a reaction turbine [192].....	24
Figure 1-24 Velocity triangle for a Francis runner [192].....	26
Figure 1-25 instalation of a Francis turbine [192].....	29
Figure 2-1 Multi stage centrifugal pump[196].....	31
Figure 2-2 System head curve[3] .....	33
Figure 2-3 The system head curve establishes pump conditions[3].....	33
Figure 2-4 Continuously rising head capacity curve[3].....	34

Figure 2-5 Unstable or hooked head capacity curve.[3] .....	35
Figure 2-6 poorly planned performance chart [3] .....	37
Figure 2-7 recommended performance chart [3] .....	38
Figure 3-1 [198] .....	44
Figure 3-2 Typical performance curves for PAT for various rotational speeds [2] .....	47
Figure 3-3 A centrifugal PAT-based pico hydropower station, installed in the West of Iran [4] .....	48
Figure 3-4 Application of various pumps as turbines [4] .....	48
Figure 3-5 An axial PAT based micro hydropower station, installed in the North of Iran [2] .....	48
Figure 3-6 PAT components (www.processindustryforum.com) .....	50
Figure 3-7 Plan view of PAT [15] .....	50
Figure 3-8 Impeller and details of a blade [15] .....	51
Figure 3-9 Draft tube of a PAT [15] .....	52
Figure 3-10 Cost distribution for large and micro hydropower plants.[92] .....	53
Figure 3-11 Head-flowrate selection chart [104] .....	55
Figure 3-12 Head-Specific speed selection chart [104] .....	56
Figure 3-13 Turbine selection flow chart for micro hydropower schemes [90] .....	56
Figure 3-14 Comparison between Pump (a) and PAT (b) experimental and numerical results. [85] .....	59
Figure 3-15 Performance characteristics for pump and reverse modes [111] .....	65
Figure 3-16 Karlsruhe University-based testing facility [96]. .....	67
Figure 3-17 Four quadrant characteristics of a reversible pump turbine a) Flow-speed curve [139] .....	69
Figure 3-18 S-shape characteristics of a pump turbine [140]. .....	70
Figure 3-19 turbine instability conditions for both reverse (b, c) and conventional (a) modes [141]. .....	70
Figure 4-1 Head ratios of the tested PATs with various pump specific speeds [20] .....	74
Figure 4-2 Discharge ratios of the tested PATs with various pump specific speeds [21] .....	74
Figure 4-3 PAT maximum efficiency ranges against the H-Q space [25,26] .....	76
Figure 4-4 Proposed 3D representation for PAT efficiency estimation against the real efficiency of selected machines [28] .....	76
Figure 4-5 2D contours of the proposed function for PAT efficiency plotted against the nominal flow rate and specific speed of selected machines [28] .....	77
Figure 4-6 Head ratios of tested PATs with various pump maximum efficiencies [20] .....	77
Figure 4-7 Discharge ratios of tested PATs with various pump maximum efficiencies [20] .....	77
Figure 4-8 Turbine specific speed versus pump specific speed [20] .....	78

Figure 4-9 h of the tested PATs with various pump maximum efficiencies [20] .....	79
Figure 4-10 q of the tested PATs with various pump maximum efficiencies [20] .....	80
Figure 4-11 Geometrical parameters of a semi-axial PAT [34].....	83
Figure 4-12 Generalized characteristic and efficiency curves by RAE [34].....	84
Figure 4-13 Reference geometry. [23].....	86
Figure 4-14 Flow chart of the geometry modelling. [23].....	88
Figure 4-15 Geometry of the sector j [23]. .....	90
Figure 4-16 Outline of the volute geometry. [23].....	91
Figure 4-17 Head calculus flow chart. [23] .....	92
Figure 4-18 Leakage path. [23].....	93
Figure 4-19 Head (a) and efficiency (b) for the PAT 40-335 ( $ns = 9.1$ ) - design mode. [23].....	95
Figure 4-20 Head (a) and efficiency (b) for the PAT 40-250 ( $ns = 12.5$ ) – design mode. [23] .....	95
Figure 4-21 Head (a) and efficiency (b) for the PAT 50-160 ( $ns = 28.7$ ) – design mode. [23] .....	96
Figure 4-22 Head (a) and efficiency (b) for the PAT 80-220 ( $ns = 30.3$ ) – design mode. [23] .....	96
Figure 4-23 Head (a) and efficiency (b) for the PAT 80-200 ( $ns = 34.1$ ) – design mode. [23] .....	96
Figure 4-24 Head (a) and efficiency (b) for the PAT 100-160 ( $ns = 64$ ) e design mode. [23].....	97
Figure 4-25 Head (a) and efficiency (b) for the PAT 40-335 $ns = (9.1)$ e geometry known mode. [23] ..	97
Figure 4-26 Head (a) and efficiency (b) for the PAT at 40-250 ( $ns = 12.5$ ) e geometry known mode. [23] .....	97
Figure 4-27 Head (a) and efficiency (b) for the PAT 50-160 ( $ns = 28.7$ ) e geometry known mode. [23]	98
Figure 4-28 Head (a) and efficiency (b) for the PAT 80-220 ( $ns = 30.3$ ) e geometry known mode. [23]	98
Figure 4-29 Head (a) and efficiency (b) for the PAT 80-200 ( $ns = 34.1$ ) e geometry known mode. [23]	98
Figure 4-30 Head (a) and efficiency (b) for the PAT 100-160 ( $ns = 64$ ) e geometry known mode. [23] .	99
Figure 4-31 Comparison, for the PATs 40e250 (left side) and 50e160 (right side), between experimental data and numerical simulations (new model e dashed line e and old model [23].....	99
Figure 4-32 Losses distribution at BEP e PAT 40-335 $ns = 9.08$ . [23].....	101
Figure 4-33 Losses distribution at BEP e PAT 40-250 $ns = 12.80$ . [23].....	101
Figure 4-34 Losses distribution at BEP e PAT 50-160 $ns = 28.70$ . [23].....	101
Figure 4-35 Losses distribution at BEP e PAT 80-220 $ns = 30.31$ . [23].....	102
Figure 4-36 Losses distribution at BEP e PAT 80-200 $ns = 34.11$ . [23].....	102
Figure 4-37 Losses distribution at BEP e PAT 100-160 $ns = 64.07$ . [23].....	102
Figure 4-38 Predictions comparison in the Williams plane for the PAT 40-335. [23] .....	104

Figure 4-39 Predictions comparison in the Williams plane for the PAT 40-250. [23] .....	105
Figure 4-40 Predictions comparison in the Williams plane for the PAT 50-160. [23] .....	105
Figure 4-41 Predictions comparison in the Williams plane for the PAT 80-220. [23] .....	106
Figure 4-42 Predictions comparison in the Williams plane for the PAT 80-200. [23] .....	106
Figure 4-43 Conceptual sketch of PAT system .....	113
Figure 4-44 Pump-as-turbine range chart [16].....	114
Figure 4-45 Hydraulic diagram of a PAT system [16] .....	115
Figure 4-46 system diagram of a constant-speed PAT [16].....	117
Figure 4-47 Four of eight parallel PATs in service at the water utility authority (Zweckverband Landeswasserversorgung, Stittgart, Germany) [16].....	118
Figure 4-48 Direct coupling[16] .....	119
Figure 5-1Connections in a generic node. [65].....	126
Figure 5-2 Non-pipe element “Pipe þ PAT00. [65] .....	127
Figure 5-3 a) Head and torque curves in Suter plan; b) Dimensionless curves in turbine mode.[65] .....	128
Figure 5-4 Layout of network 1 and PAT location. [65] .....	131
Figure 5-5 Critical node pressure for Example 1. [65] .....	132
Figure 5-6 Layout of network 2 and PAT location. [65] .....	133
Figure 5-7 Critical nodes pressure for Example 2: a) Node 8; b) Node 17. [65].....	135
Figure 5-8 Layout of network 3 and PAT location. [65] .....	136
Figure 5-9 Pressure zones of network 3 for maximum consumption. [65].....	136
Figure 5-10 Critical node pressure for Example 3: a) Node 11; b) Node 53. [65] .....	138
Figure 5-11 Primary materials and processes considered within the system boundaries for MHP. [79]..	141
Figure 5-12 Breakdown of environmental impacts of MHP case studies expressed per kWh generated over project 30-year lifespan (solid blocks represents core components and hatched blocks represent variable components). [J. Gallagher et al. / Journal of Cleaner Production 99 (2015) 152e159 .....	145

## 7.2 Tables

Table 3-1 Hydropower installations [197] .....	45
Table 3-2 Source: Moreire, J.R. & Poole, A.D. (1993) Hydropower and its constraints. In: Johansson T.B. et al, (1993) Renewable energy: sources for fuels and electricity (ISBN 1-85383-155-7).....	45
Table 3-3 Hydropower scheme classification. [85] .....	53
Table 3-4 PAT installations [85].....	54

Table 3-5 Performance prediction methods for pump-turbines. [85].....	57
Table 3-6 BEP predictions by various methods.[85] .....	59
Table 4-1 Review of methods to determine non-dimensional head and flow parameters (adapted from [30]) .....	79
Table 4-2 Machine data set .....	82
Table 4-3 Hydraulic losses. [23] .....	91
Table 4-4 Main parameters of the six pumps. [23] .....	94
Table 4-5 Head and flow rate data at BEP: computed by model (_calc) and experimental (_meas) e model operating in “design mode”. The highest errors are highlighted with gray shade. [23].....	103
Table 4-6 Head and flow rate data at BEP: experimental (_meas) and computed by model (_calc) e model operating in “geometry known mode”. The highest errors are highlighted with gray shade. [23] .....	103
Table 4-7 Efficiency at BEP: computed by model (_calc) and experimental (_meas) e model operating in “design mode”. The highest errors are highlighted with gray shade. ....	107
Table 4-8 Efficiency at BEP: experimental (_meas) and computed by model (_calc) e model operating in “geometry known mode”. The highest errors are highlighted with gray shade.....	107
Table 4-9 Required PAT system component [16] .....	116
Table 4-10 Feed-in tariffs for new facilities up to 5 MW [16] .....	119
Table 4-11 Feed-in tariffs acc. to the 2009 green electricity regulation 50%. [16] .....	120
Table 4-12 tariffs acc. to the 2009 green electricity regulation 15%. [16].....	120
Table 4-13 se-rate feed-in tariff in Switzerland acc. to power class [16] .....	121
Table 4-14 pressure class bonus in Switzerland acc. to head category [16] .....	122
Table 4-15 Hydraulic engineering bonus in Switzerland acc. to power class.....	122
Table 5-1 Results of PAT selection and location for Example 1[65] .....	131
Table 5-2 Results of PAT selection and location for Example 2.[65] .....	134
Table 5-3 Results of PAT selection and location for Example 3. [65] .....	137
Table 5-4 Life cycle assessment impact categories selected to compare micro-hydropower projects with marginal UK grid electricity generation, descriptions provided [79]. ....	140
Table 5-5 Description of MHP case studies for LCA [79] .....	142
Table 5-6 Assumptions made for LCA of MHP Projects. [79].....	142
Table 5-7 Total environmental impacts of MHP projects for different impact categories and carbon payback time (expressed per kWh generated over project 30-year lifespan). [79].....	144

Table 5-8 Mitigation forecasting for total GHG emissions offset by MHP installations between 2015 and 2050 (displacements of CO2 emissions associated with gas power plant). [79] ..... 146

### 7.3 Equations

Equation 1-1..... 19

Equation 1-2..... 19

Equation 1-3..... 19

Equation 1-4..... 19

Equation 1-5..... 23

Equation 1-6..... 24

Equation 1-7..... 24

Equation 1-8..... 26

Equation 1-9..... 26

Equation 1-10..... 26

Equation 1-11..... 26

Equation 1-12..... 27

Equation 1-13..... 27

Equation 1-14..... 27

Equation 1-15 [192]..... 27

Equation 1-16..... 28

Equation 1-17..... 28

Equation 1-18..... 28

Equation 1-19..... 28

Equation 1-20..... 28

Equation 1-21..... 29

Equation 1-22..... 29

Equation 1-23..... 29

Equation 2-1 [29]..... 40

Equation 2-2 [29]..... 40

Equation 2-3 [29]..... 41

Equation 3-1 The theoretical power..... 44

Equation 3-2 the gross power of the flow of water [197] ..... 45



Equation 3-3.....	55
Equation 3-4.....	55
Equation 3-5.....	60
Equation 3-6.....	63
Equation 3-7.....	71
Equation 4-1.....	75
Equation 4-2.....	75
Equation 4-3.....	78
Equation 4-4.....	78
Equation 4-5.....	78
Equation 4-6.....	78
Equation 4-7.....	80
Equation 4-8.....	80
Equation 4-9.....	81
Equation 4-10.....	81
Equation 4-11.....	81
Equation 4-12.....	83
Equation 4-13.....	83
Equation 4-14.....	87
Equation 4-15.....	88
Equation 4-16.....	89
Equation 4-17.....	89
Equation 4-18.....	89
Equation 4-19.....	89
Equation 4-20.....	90
Equation 4-21.....	92
Equation 4-22.....	93
Equation 4-23.....	93
Equation 4-24.....	94
Equation 4-25.....	104
Equation 5-1.....	126
Equation 5-2.....	127

Equation 5-3..... 128

Equation 5-4..... 129

Equation 5-5..... 129

Equation 5-6..... 130